

EXPERIMENTAL AND THEORETICAL STUDY OF
WATER SIDE FOULING THERMAL PERFORMANCE
OF REFRIGERANT TO WATER CONDENSERS

By

XIAOXIAO WU

Bachelor of Science in HVAC
Donghua University
Shanghai, China
2007

Master of Engineering in HVAC
Donghua University
Shanghai, China
2010

Submitted to Faculty of
Mechanical and Aerospace Engineering
Oklahoma State University
In partial fulfillment of the requirements of
the Degree of
MASTER OF SCIENCE
December, 2013

EXPERIMENTAL AND THEORETICAL STUDY OF
WATER SIDE FOULING THERMAL PERFORMANCE
OF REFRIGERANT TO WATER CONDENSERS

Thesis Approved:

Dr. Lorenzo Cremaschi

Thesis Adviser

Dr. Daniel Fisher

Dr. Chad Penn

ACKNOWLEDGEMENT

Completing my Master's degree is probably one of the top 10 most challenging journeys of my life so far. The best and worst moments of this journey have been shared with many people, and the memories will always remain.

My first debt of gratitude would go to my advisor, Dr Lorenzo Cremaschi for his patience, motivation, immense knowledge, and encouragement. His continuous guidance helped me through all the ups and downs in the past three years, and I cannot have asked for a better advisor. Heartiest thanks to the committee members, Dr. Fisher, Dr. Penn and Dr. Spitler for their insightful comments and hard questions. Special thanks to Gary Thacker, the ATRC building manager, for spending time and effort in the electronic and safety connections.

My sincere appreciation also goes to my fellow lab partners in OSU HVAC group: Atharva Barve, Ardi Yatim, Jeremy Smith, Pratik Deokar, Auvi Biswas, Shanshan Cai, Weiwei Zhu, Pedro Perez, Ehsan Moallem, Kasey Worthington, Ozgur Aslan, etc. for helping me adjust to the new environment, for the troubleshooting discussions, for the sleepless nights working together before deadlines and for all the fun we had during the last three years.

Last but not least, I would like to thank my family for their unconditional love and support; I would not be able to make it without them.

Name: XIAOXIAO WU

Date of Degree: DECEMBER, 2013

Title of Study: EXPERIMENTAL AND THEORETICAL STUDY OF WATER SIDE
FOULING THERMAL PERFORMANCE OF REFRIGERANT TO
WATER CONDENSERS

Major Field: MECHANICAL & AEROSPACE ENGINEERING

Abstract:

Brazed plate heat exchangers (BPHEs) and tube-in-tube heat exchangers (TTHEs) are commonly used in the refrigeration, air conditioning, and food industry as refrigerant-to-water condensers, in which the refrigerant rejects heat to water circulating in cooling tower loops. These heat exchangers often suffer from severe fouling issues because as the water in the cooling tower evaporates, the mineral concentration in the remaining water increases. Once the solubility limits are reached, the minerals precipitate and a layer of fouling formed on the heat transfer surfaces. Due to the fouling deposit, the thermal resistance between refrigerant and water gradually increases. The fouling formation penalizes the overall effectiveness of the refrigerant condensers, and thus, must be properly accounted for during the equipment design.

This thesis focuses on fouling effects on the thermal and hydraulic performance of condensers in cooling tower systems. Two braze plate heat exchangers and a smooth tube-in-tube heat exchanger was experimentally investigated under fouling operating conditions by using a new experimental facility at Oklahoma State University. The aim was to measure the fouling resistance in real time and correlate the data with the heat exchanger internal geometry, water quality, and refrigerant saturation temperature. The fouling resistance in the TTHE was observed to have asymptotic trend, and the asymptotic limit was lower than that for BPHEs with soft corrugation angles and higher than that of BPHEs with hard corrugation angles operating at similar conditions. The hydraulic performance was similar to BPHEs with hard corrugation angles. Both refrigerant saturation temperature and water fouling potential increase would lead to a measurable increase in the fouling resistance inside the refrigerant to water condenser. A model for the mineral species dissociation and mineral precipitation on the heat transfer surfaces was verified. By considering a semi-empirical relation for the fouling deposition strength factor, the simulation results predicted the fouling thermal resistance with an error of 30%. Model limitations and research needs for potential improvements are discussed.

TABLE OF CONTENTS

Chapter	page
1 INTRODUCTION.....	1
1.1 Introduction.....	1
1.2 Thesis organization	2
2 LITERATURE REVIEW.....	3
2.1 Fouling formation	3
2.2 Parameters influencing fouling	5
2.3 Fouling model	10
2.4 Conclusion from the literature review	12
3 OBJECTIVE	14
3.1 Objectives	14
3.2 Research approach	14
3.3 Scope of this thesis work	17
4 EXPERIMENTAL METHODOLOGY	22
4.1 Description of test set up.....	22
4.2 Experimental apparatus.....	22
4.2.1 Cooling tower water loop.....	22
4.2.2 Refrigerant loop	23
4.2.3 Auxiliary loops and safety devices	24
4.3 Instrumentation and data acquisition system	26
4.3.1 Pressure measurement.....	26
4.3.2 Temperature measurement.....	27
4.3.3 Mass flow rate measurement.....	28
4.3.4 Pump control and heater control	28
4.3.5 Data acquisition system	29

Chapter	page
5 DATA REDUCTION AND UNCERTAINTY ANALYSIS	31
5.1 Test procedure.....	31
5.2 Data reduction.....	37
5.3 Uncertainty analysis.....	41
6 RESULTS AND DISCUSSION	45
6.1 Fouling deposit chemical analysis	45
6.2 Fouling heat transfer analysis	49
6.2.1 Fouling formation in BPHEs and TTHE.....	49
6.2.2 Impacts of condensation temperature and water quality on fouling formation.....	54
6.3 Water loss in cooling tower due to fouling	65
6.4 Application and improvement of existing fouling model	67
7 CONCLUSION.....	77
7.1 Conclusion from this thesis work.....	77
7.2 Recommendations for future work	79
REFERENCE.....	83
APPENDICES	87
Appendix A Fouling tests results summary	87
Appendix B water sample report	88
Appendix C LSI computation	92

LIST OF TABLES

Table	page
Table 3-1 Summary of the condensers tested for the fouling study	18
Table 3-2 Test conditions for fouling tests	19
Table 3-3 Summary of test matrix for the fouling tests	20
Table 4-1 Fouling tests facility application.....	25
Table 4-2 BPHE application in auxiliary loops	26
Table 4-3 Differential pressure transducer calibration from Validyne	27
Table 5-1 Typical chemistry analysis for water quality	36
Table 5-2 Specifications of the key instrumentation for the fouling experiments	41
Table 6-1 comparison of measured fouling from approximated LMDT and comprehensive LMDT method	58
Table 6-2 Effect of refrigerant saturation temperature on asymptotic fouling resistance.....	63
Table 6-3 Effects of water quality on asymptotic fouling resistance.....	65
Table 6-4 Fouling model verification of linear correlation.....	68
Table 6-5 Sensitivity analysis of R_f with respect to Ψ	71
Appendix A	
Figure A - 1 Summary of fouling tests results	87
Appendix B	
Table B - 1 Water sample report for Test No. 1 (A1-105F)	88
Table B - 2 Water sample report for Test No. 2 (A2-105F)	88
Table B - 3 Water sample report for Test No. 3 (A2-120F)	89
Table B - 4 Water sample report for Test No. 4 (A1-120F)	89
Table B - 5 Water sample report for Test No. 5 (A1-105F-med)	90
Table B - 6 Water sample report for Test No. 6 (A2-105F-med)	90
Table B - 7 Water sample report for Test No. 7 (A1-105F-repeat)	91
Table B - 8 Water sample report for Test No. 8 (tube-in-tube)	91
Appendix C	
Table C - 1 LSI computation for Test No. 1 (A1-105F)	92
Table C - 2 LSI computation for Test No. 2 (A2-105F)	93
Table C - 3 LSI computation for Test No. 3 (A2-120F)	94
Table C - 4 LSI computation for Test No. 4 (A1-120F)	95
Table C - 5 LSI computation for Test No. 5 (A1-105F-med FP)	96
Table C - 6 LSI computation for Test No. 6 (A2-105F-med FP)	97
Table C - 7 LSI computation for Test No. 7 (A1-105F-repeat)	98
Table C - 8 LSI computation for Test No. 8 (Tube-in-tube).....	99

LIST OF FIGURES

Figure	page
Figure 2-1 Illustration of fouling formation on a simple flat plate	5
Figure 3-1 Main geometric parameters of BPHEs [from (Cremaschi, <i>et al.</i> , 2011)].....	18
Figure 3-2 Schematic and dimensions of tube-in-tube heat exchanger	19
Figure 4-1 Principles of the cooling tower water loop.....	23
Figure 4-2 Principle of refrigerant loop	24
Figure 5-1 Langelier Saturation Index (LSI) during the fouling tests	34
Figure 5-2 Schematic of temperature distribution of refrigerant R134a and water	37
Figure 5-3 Fouling resistance uncertainty analysis.....	44
Figure 6-1 Fouling sample from TTHE condenser.....	47
Figure 6-2 Solubility of CaCO ₃ [adapted from (Flynn & Nalco, 2009)]	47
Figure 6-3 Image of fouling deposit inside smooth tubes.....	48
Figure 6-4 Images of fouling deposit inside a BPHE	49
Figure 6-5 Measured fouling factor for TTHE and BPHEs.....	50
Figure 6-6 Measured water temperature difference for TTHE and BPHEs.....	52
Figure 6-7 Measured pressure drop penalty factor for TTHE and BPHEs	53
Figure 6-8 Effect of refrigerant temperature and water quality on fouling resistance.....	55
Figure 6-9 Degree of sub-cooling of the refrigerant for the BPHEs in fouling tests	58
Figure 6-10 Effect of refrigerant temperature and water quality on pressure drop.....	60
Figure 6-11 Reduction of water leaving temperature in the condenser due to fouling.....	61
Figure 6-12 Effect of refrigerant saturation temperature on asymptotic fouling resistance (high water fouling potential LSI 2.1 to 3.5).....	62
Figure 6-13 Effect of water quality on asymptotic fouling resistance with refrigerant saturation temperature of 1.5.5 °F(41°C)	64
Figure 6-14 Summary of water losses in cooling tower	67
Figure 6-15 Ca ²⁺ accumulate due to water loss in smooth tubes	67
Figure 6-16 Fouling model verification in a smooth tube-in-tube heat exchanger.....	71
Figure 6-17 Fouling model verification in BPHE ($\phi=63^\circ$)	73
Figure 6-18 Fouling model verification in BPHE ($\phi=30^\circ$)	74
Figure 6-19 Fouling model verification in BPHE ($\phi=30^\circ$) from literature	74
Figure 6-20 Fouling model verification with experimental data	75

NOMENCLATURE

A	area	ft ² or m ²
BPHE	brazed plate heat exchanger	
[Ca ²⁺]	calcium concentration	ppm
[Cl ⁻]	chloride concentration	ppm
[CO ₃ ²⁻]	carbonate concentration	ppm
c _r	removal coefficient	dimensionless
cycle	concentration cycle	dimensionless
d _e	equivalent diameter	in or m
f	friction factor	dimensionless
FP	fouling potential	
G	mass flux	lb _m /ft ² -s or kg/m ² -s
k _D	convective diffusion coefficient	dimensionless
k _R	precipitation rate coefficient	dimensionless
k _{SP}	solubility product	mol ² /L ²
L	length	in or m
LMTD	Logarithm mean temperature difference	°F or °C
LSI	Langelier Saturation Index	dimensionless
\dot{m}	Mass flow rate	lbm/min or kg/s
m	mass	lbm/in ² -min or g/m ² -s
M _{alklinity}	“M” alkalinity	ppm
med	medium	
p	corrugation depth	in or m
ΔP	pressure drop	kPa
PDPF	pressure drop penalty factor	dimensionless
\dot{Q}	heat transfer rate	Btu/hr or W
R	thermal resistance	hr-°F –ft/Btu or m ² -K/W
Re	Reynolds number	dimensionless
R _g	universal gas constant	cal/K-mol
RTD	resistance temperature detector	
t	time	hours or days
T	temperature	°F or °C or K
TDS	total dissolved solid	ppm
TTHE	tube-in-tube heat exchanger	
UA	Overall heat transfer coefficient	Btu/hr-°F or W/°C
\dot{V}	volume flow rate	gpm or m ³ /s
v	velocity	m/s
w	width	in or m
Subscript		
c	clean	
circulate	Circulate water	
d	deposit	

EWT	entering water temperature
f	fouled or fouling
ht	heat transfer
k	conduction
LWT	leaving water temperature
makeup	makeup water
r	removal
ref	refrigerant
s	surface
sat	saturated
SH	superheat
tot	total
w	water
∞	asymptotic

Greek symbols

ϕ	corrugation angle (degree from flow direction)	degree
λ	corrugation pitch or thermal conductivity	in or W/m-K
ρ	density	lbm/ft ³ kg/m ³
δ	fouling thickness	in or m
ψ	deposition strength factor	dimensionless
τ_c	time constant	day

CHAPTER I

1 INTRODUCTION

1.1 Introduction

Tubular heat exchanger was commonly applied in industry for heat transfer purposes due to its high flow velocity and high capacity, not sensitive to particle clogging and easy for maintenance. Recently, Braze plate heat exchangers (BPHEs) have been introduced in the air conditioning industry as refrigerant to water condensers because they provide higher heat transfer coefficients and are more compact than conventional tube-and-shell heat exchangers. The performance of BPHEs relies on the internal geometry of their corrugated plates, which often incorporate a herringbone pattern. This type of pattern is designed to maximize effective surface area of the plates, promote turbulence, and distribute the fluid flow. Depending on the internal geometry of the plates, the flow pattern could either be in the form of “zigzag” or “double-cross” flow (Luan *et al.*, 2008). In both flow patterns, the fluid streams flows to each other at the intersection, which induces turbulent flow and at the same time increases pressure drop inside the BPHE (Focke *et al.*, 1985) The stacked plates are assembled with thin copper sheets between the plates before the unit enters a furnace. The melted copper acts as a brazing agent to seal the edges of the BPHE plates and also bonds the meeting points of the corrugation ridges to provide pressure retention strength.

In refrigerant to water condensers, heat is rejected from the refrigerant side to the water side, which often circulates in cooling tower loops. Since large amount of inversely-soluble minerals, such as calcium carbonate and magnesium carbonate contained in the water loop, due to the evaporation

process, water became concentrated. When the concentrated water is heated up by the refrigerant inside condensers, the solubility of the minerals decrease, and precipitation occurs (Cho *et al.*, 2003). Mineral fouling, the deposition of this unwanted layer of material on the heat transfer surface, reduces the overall heat transfer coefficient and increases the resistance to the fluid flow (Muller-Steinhagen & Branch, 1988).

The performance of BPHEs under clean conditions is well understood; however, the impact of fouling on the thermal and hydraulic performance of BPHEs is difficult to quantify because it is a function of multiple variables of water chemistry, suspended particles, temperature, pH, operating conditions of the condenser, and chemical cleaning procedures.

1.2 Thesis organization

The focuses of this master thesis is to investigate the thermal and hydraulic performance of refrigerant to water condensers under fouling conditions experimentally and theoretically. This thesis is divided into seven chapters. The first chapter is the introduction. The second chapter summarizes the recent literature on fouling formation, driving factors leading to fouling in heat exchangers, and fouling models in the literature. The third chapter presents the objectives and the scope of work in this thesis.

Chapter four introduces the experimental apparatus developed to measure the thermal and hydraulic performance of test condensers in cooling tower applications. The test equipment and instrumentation are described. In chapter five, test procedure, data reduction and uncertainty analysis are included.

Chapter six presents the chemical and thermal analysis of the fouling study, and fouling model verification. Chapter eight summarizes the main findings in this thesis.

CHAPTER II

2 LITERATURE REVIEW

2.1 Fouling formation

Fouling has been an unavoidable problem since the cooking pot was invented (Somerscales, 1990). The first reference in history appeared in 1756; it was reported that a layer of deposit, the inverse solubility salt, which was the component of hard water, was left on the heated surface after water evaporated. Because of this layer of deposit, fouling, thermal efficiency of the equipment was reduced. From 1850 to 1900, disputes regarding the significance of fouling effects were aroused. In order to quell the controversy, experiments were conducted at the University of Illinois in 1898. Clean and fouled boilers were tested, results shown that the former evaporated 13% more steam than the latter.

Since the influence of fouling was agreed, heat transfer surface cleaning became necessary. Due to the potential corrosive nature and difficulties of using acid solution, hand washing using untreated or poorly treated water to clean fouling deposit on the heat transfer surface was prevailed in nineteenth century. By the early 1920s, people tended to apply phosphate treatment in boilers, which was confirmed suitability. Since 1920, measurement and representation of fouling became more systematic. The heat transfer coefficient, thermal resistance, cleanliness factor and fouling resistance were formulated to present empirical results in structural and machine design. In 1959, Kern and Seaton proposed a time related model to describe fouling formation, which was regarded as a landmark of the fouling study. Their study changed the original way people look at fouling, which took no account of the time dependent nature of fouling.

According to Kern and Seaton, fouling formation is a continuous deposition and removal process, and the fouling resistance is proportional to the net fouling deposition rate per unit area, \dot{m}_f , which depends on the rates of this process (Kern & Seaton, 1959):

$$\dot{m}_f = \frac{d}{dt}(m_f) = \dot{m}_d - \dot{m}_r \quad (2-1)$$

where \dot{m}_d , and \dot{m}_r are the deposition and removal rate per unit area, respectively. An illustration of this theory for a simple heated flat plate is shown in Figure 2-1. Fluid with fouling agent flows across the heated surface with velocity v and fluid temperature at wall surface T_s , as indicated in Figure 2-1(a). Fluid is heated up and an increase of fluid temperature leads to a drop of local solubility; thus previously dissolved calcium carbonate in the fluid begins to precipitate and a layer of fouling deposit begins to form on the heat transfer surface, shown in Figure 2-1 (b). The layer of fouling increases the thermal resistance between the heated surface and fluid, leading to the reduction of fluid film temperature on the top of the surface. Since the solubility of calcium carbonate increases with decreasing temperature (Flynn & Nalco, 2009), then the fouling precipitation rate decreases due to lower T_s , see Figure 2-1 (c). Meanwhile, due to the flow barrier caused by the fouling deposit, the local fluid velocity and shear stress increase accordingly. A removal process of clusters of fouling deposit might occur if the shear stress is high enough to carry particles away from the fouling layer, in Figure 2-1 (d). The removal of fouling reduces the thermal resistance of the heat transfer surface, thus the fouling precipitation restarts due to higher local water film temperature T_s near the plate. The local water temperature and mineral concentration drive the precipitation process. The thickness of fouling inside the condensers is expected to reach a limiting threshold in which the process of fouling deposition and fouling removal are in equilibrium. If the particles do not obstruct the flow, particle precipitation and removal process would recur, and Figure 2-1 (c) and (d) show this situation; and the thermal resistance offered by the mineral deposition layer on the heat transfer surface approaches an asymptotic value, referred to as the asymptotic fouling resistance.

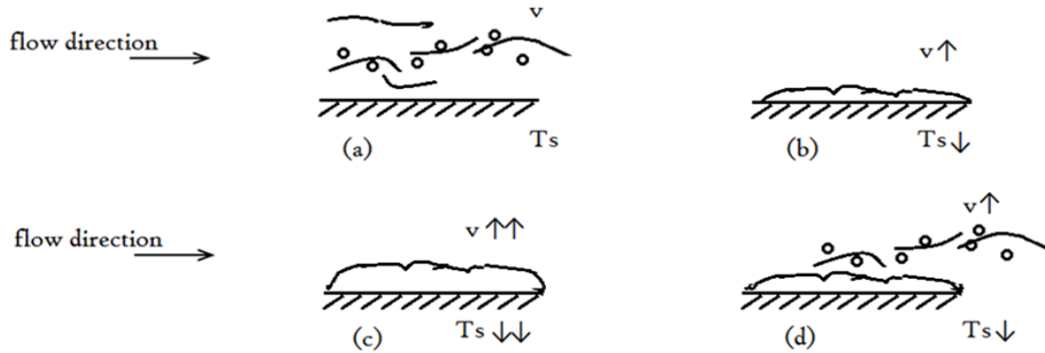


Figure 2-1 Illustration of fouling formation on a simple flat plate

Design and manufactory procedures based on this theory were applied in industry after the theory was published. In 1963, Heat Transfer Research Inc (HTRI) investigated the fouling problem on the cooling water side of shell-and-tube heat exchangers; they developed Kern and Seaton's model by including more fouling related factors of a cooling water stream. Later, this theory was applied in fouling studies in BPHEs.

Aside from precipitation, other fouling mechanisms are particulate fouling, biological fouling and corrosion fouling (Haider *et al.*, 1991). Since cooling tower water is often pre-treated with biological and corrosion inhibitors, the last two types of fouling mechanism can be more or less controlled (Walker, 1976). However, the actual fouling problem depends on the water quality, operating conditions, monitoring system, and maintenance practices. The same fouling resistances are recommended for plate type and tube-type heat exchangers, which are summarized in the AHRI Guideline E (AHRI, 1997). Further and detailed guidance to the industry were provided by AHRI Standard 450 (AHRI, 2007) and Tubular Exchanger Manufacturers' Association (TEMA, 2007).

2.2 Parameters influencing fouling

One of the main driving potentials for the fouling deposition is the concentration of the minerals within the water stream. Although there are several inversely-soluble minerals found in typical cooling tower water, calcium carbonate (CaCO_3) seemed to be the predominant one. Hence, fouling of heat

exchangers by precipitation of CaCO_3 has been the main focus of many researchers for the past two decades. The first study performed regarding precipitation fouling was done by Langelier (1936). He proposed the “Langelier Index” now commonly known as Langelier Saturation Index or LSI. This parameter is used to predict solubility of CaCO_3 in water. The parameters used to determine the LSI are the amount of total dissolved solids, calcium hardness, total alkalinity, fluid temperature, and actual pH of the water. LSI is defined as the algebraic difference between actual pH of the water sample and its computed saturation pH, pH_{sat} , which is the pH at which the calcium concentration in a given water sample is in equilibrium with the total alkalinity. In the current work, the saturation pH values are approximated using the following equations from (Pearson, 2003).

$$LSI = pH_{actual} - pH_{sat} \quad (2-2)$$

$$pH_{sat} = 12.18 + 0.1 \log_{10}(TDS) - 0.0084 (T_w) - \log_{10} (Ca) - \log_{10} (M_{alkalinity}) \quad (2-3)$$

Where: TDS = Total Dissolved Solid (ppm)

T_{water} = water temperature in ($^{\circ}\text{F}$)

Ca = calcium concentration (ppm as CaCO_3)

$M_{alkalinity}$ = “M” alkalinity (ppm as CaCO_3)

If the index equals zero, the water is in equilibrium state; a plus sign of the index means a tendency of precipitation and a minus sign indicating a tendency of dissolving. However, the quality of cooling tower water varies geographically. In order to determine the typical water qualities applied in actual cooling towers, Zdaniuk & Chamra (2008) established a database according to the survey of cooling tower water applications collected from 19 sites across the United States. Chemical analysis results showed that water qualities can be grouped in three levels: low, average and severe, in terms of fouling potential. Tap water quality was also assessed and inversely-soluble elemental ions such as calcium

ions and magnesium ions was found in city water sources (Al-Rawajfeh & Al-Shamaileh, 2007). According to solubility, elemental ions can be described as directly-soluble ions and inversely-soluble ions. The former includes NaCl and NaNO₃, its solubility increases with solution temperature. However, for inversely-soluble ions, like CaCO₃, MgCO₃, and CaSO₄, their solubility do not always increase with temperature, beyond some certain temperature, their solubility decreases and minerals precipitate. Besides temperature, the solubility of inversely-soluble ions is also affected by the pH of the solution. E.g., CaCO₃ is more dissolvable in acidic solution than basic solution (Grace, 2007).

The definition of “water fouling potential” was adopted by Cremaschi *et al.* (2011), to describe the scaling conditions of the water inside heat exchangers cooled by cooling tower water, and the evaluation of water fouling potential was based on LSI and other minerals. LSI lower than 1 was defined as low fouling potential water, where slight and low scaling formation were expected. LSI between 1 and 2 were for medium fouling potential water, and moderate scaling formations were expected. Any LSI higher than 2 was grouped in the high fouling potential water category, which represents very aggressive water in terms of mineral precipitation. Our previous work, Cremaschi *et al.*, (2012) presented the impact of water quality and refrigerant condensation temperature on the fouling performance of BPHEs for building air conditioning applications. In another work, Chamra (2007) focused on fouling inside smooth and enhanced shell-and-tube refrigerant condensers by using copper alloy tubes. In his work, a water loop and a refrigerant loop were connected through the test section, which consisted of a shell-and-tube heat exchanger with refrigerant flowing through the shell and water flowing through the inner tube. Chamra investigated the waterside fouling performance using only water with a very low concentration of minerals, resulting in an LSI less than 0.3. In these conditions, measurements suggested that low fouling potential water did not produce any measurable fouling effects.

Awad *et al.* (2009) also investigated at different surface temperatures of the tubular heat exchanger and asymptotic values of fouling resistance were estimated. Their results suggested that the surface temperature had a significant effect on the particulate fouling resistance but a small effect on the precipitation fouling. They concluded that particulate fouling is of the asymptotic type while precipitation fouling is of the linear type. As the surface temperature increased, the particulate fouling resistance decreased while the precipitation fouling resistance increased. Thus, depending of the local water quality, the authors recommended operation of the heat transfer equipment at the highest possible temperature if particulate fouling needed to be minimized and vice versa if hindering precipitation fouling was the critical factor to improve the performance of the heat exchanger. Xu and Knudsen (1986) analyzed experimental data of fouling resistance and change in overall heat transfer coefficients for cooling tower applications. They suggested the idea that at constant fluid velocity, the shear stress responsible for interference in the fouling process would also be constant. Their study indicated that deposit strength, in terms of adherence and toughness, increased with an augment of the surface temperature of the heat exchanger.

Several researchers worked on evaluating the impact of geometry on fouling formation in heat exchangers. Karabelas *et al.* (1997) conducted experiments to reveal that internal geometry of BPHEs would impact the fouling resistance, plates with corrugation angle of 30° had more tendencies to foul than ones with corrugation angle of 60°. Similar observation was reported by (Grandgeorge *et al.*, 1998), (Thonon *et al.*, 1999), and our previous work (Cremaschi, *et al.*, 2011) and (Wu & Cremaschi, 2012). Webb & Li (2000) evaluated the impact of internal geometry on fouling formation in tubular heat exchangers. In their work, the fouling mechanism is a combination of precipitation and particulate fouling, which was similar as our work, and the fouling tests in the Webb and Li study were conducted with water velocity of 3.5 ft/s (1.1 m/s) and Reynolds number of about 16,000. The total hardness of cooling tower water was approximately 800 ppm CaCO₃, electrical conductivity of 1600 to 1800 μΩ, and pH = 8.5. They observed that more minerals would precipitate in enhanced tubes than smooth tubes,

indicating that the asymptotic fouling resistance has a strong dependence on internal geometry of the tubular heat exchangers.

Flow velocity and particle type are also believed to be parameters impacting fouling deposit. Bansal & Mueller-Steinhagen (1993) proposed that, due to mineral fouling, the free flow area inside the heat exchanger channels decreased, resulting in the growth of the flow velocity and a drop on the surface temperature, hence the fouling deposition rate was decreased accordingly. Similar phenomenon was also reported by Thonon *et al.* (1999), who investigated in the influence of flow velocity on fouling formation in plate heat exchangers experimentally. They claimed that the asymptotic fouling resistance was inversely proportional to the flow velocity. In their experiments, TiO_2 , CaCO_3 and clay were applied as fouling agents and the fouling rate was significantly affected by the particle type. For similar particle size and concentration, fouling rates with TiO_2 were much lower than with CaCO_3 . Bansal *et al.* (1997) further investigated the impact of suspended particles on crystallization fouling and they observed that the presence of calcium sulfate particles created extra nucleation sites for crystallization, resulting in significant increase in the fouling rate; however, the presence of alumina particles reduced the crystallization rate because they acted as distorting agents, leading to a reduction of crystal growth rate and an increase of fouling removal rates. In another work, Noda *et al.* (2013) proposed that a trace amount of phosphate in water solution would also slow down the calcium carbonate precipitation rate.

Bansal & Mueller-Steinhagen (1993) proposed that, most crystal formation was initiated near the contact points inside the plate type of heat exchangers, because the temperature profile in this part is different from the flow channels, since the liquid was heated up from several directions. Also, the scanning electron microscope micrograph of fouling crystals suggested that crystals can be divided into two different size categories, that is, homogeneous small cubic crystals directly on the plate surface and needle shape crystals on the top of this initial layer. Researchers also proposed that the precipitation fouling has an induction period of 3-4 days, in which crystal nucleation sites start developing before

mineral precipitation (Webb & Li, 2000; Zan *et al.*, 2009). However, the induction period was not observed in the appearance of particulate fouling (Chamra & Webb, 1994; Kim & Webb, 1991). Hasson (1997) proposed that, longer induction period can be expected for surfaces with higher roughness because the surface roughness increases the contact surface area. An increase in the surface roughness promotes the mineral precipitation because the local valley of the surface profile provides a shelter from the main water stream velocity. Thus lower fouling removal rate can be expected for rough surfaces with respect to smooth surfaces. Benzinger *et al.* (2007) and Geddert *et al.* (2009) studied the impacts of different surface materials on the induction period and fouling formation. Their tested surface materials included stainless steel, fluorinated ethylene propylene (FEP), diamond like carbon (DLC), and others. They reported that no major influence of the tested surface materials on the induction period and on the fouling formation was observed for calcium carbonate precipitation. However, in the case of calcium sulfate precipitation, the DLC coated surface showed less fouling tendency compared to the uncoated surface.

2.3 Fouling model

Analytical and numerical analysis was also developed to describe fouling characteristic of heat transfer surfaces. In 1959, Kern and Seaton (1959) proposed a time related model to describe fouling formation. Their asymptotic fouling model indicates, once the heat transfer surface is exposed to the fouling fluid, the fouling formation is a combination of fouling deposit and fouling removal. As reported by Webb (1994), there are three possible fouling curve trends: linear, falling and asymptotic. A linear growth rate occurs either when the removal rate is negligible or when the deposition rate is constantly greater than the removal rate. The fouling resistance will attain an asymptotic value only when the deposition rate equals the removal rate. If the fouling removal rate is greater than the precipitation rate, a falling fouling curve could be expected. Most fouling studies report the measured fouling resistance with respect to time, for example, the study of effects of alkalinity on fouling in simulated cooling tower

water by Morse & Knudsen (1977); the investigation of the impacts of surface temperature, flow rate and water quality on fouling characteristics by Knudsen & Story (1978) and the work on particulate fouling by Chamra and Webb (1993) in enhanced tubes. Assuming deposition on the heat exchanger surface is uniform, the fouling resistance R_f , can be expressed as a function of net fouling deposition rate, \dot{m}_f as follows:

$$\frac{dR_f}{dt} = \frac{1}{\rho \cdot k_f} \frac{dm_f}{dt} \quad (2-4)$$

Where ρ is the density of fouling deposit and k_f is the thermal conductivity of the deposit material. From equation (2-4), it is clear that the fouling phenomenon depends on physical properties of the deposit material and fouling mechanisms. Hasson and Zahavi (1970) presented a scaling thickness model to predict the deposition rate of CaCO_3 in tube-type heat exchangers using ionic diffusion theory; this model was further improved to a deposition rate model to predict CaCO_3 fouling rate in acid and basic solution by Hasson *et al.* (1978). Taborek *et al.* (1972b) made a comparison of fouling models in the literature, and the characteristics of fouling type were discussed for each of them, as well as the parameters might impact the deposition and removal term. Then, based on the massive data bank accumulated with the HTRI fouling tests, they proposed a semi-theoretical model to predict fouling formation. Particularly, they included two processes in the deposition term: diffusion of the potential depositing substance to the surface and bonding at the surface; and the removal rate is proportional to the ratio of the fluid shear stress to the bonding resistance of the fouling layer. Chamra & Webb (1994) proposed a semi-theoretical model to predict the asymptotic fouling resistance in enhanced tubes, which considered solution concentration, velocity and particle size.

Models were also developed to predict fouling phenomenon in plate heat exchangers. Mueller-Steinhagen and Bloechl (1988) investigated the impacts of particle size, particle concentration and particle/fluid combination on fouling in plate heat exchangers experimentally; they also applied the experimental data to verify a fouling model from the literature. Grandgeorge *et al.* (1998) studied the

impacts of flow velocity on fouling formation in corrugated BPHEs and a fouling rate global model was proposed to predict the asymptotic deposit on the heat transfer surface.

More recent work on fouling model development includes logistic fouling model proposed by Mwaba *et al.* (2006a) which can be applied to predict the evolution of the fouling scale layers in heat exchangers. Quan *et al.* (2008) developed a heat mass transfer model based on kern-Seaton model to predict fouling formation of CaCO_3 in tube-type heat exchangers. Xu *et al.* (2011) investigated the impacts of water quality in a river on fouling formation in plate heat exchangers experimentally and a partial least squares regression (PLS) model was proposed to predict the fouling characteristics. The model applied a set of input variables, including mineral concentration, pH, dissolved oxygen, turbidity, conductivity, and etc. Ojamiemi *et al.*, (2013) investigated on the impact of turbulence on the particulate fouling by comparing LES (Large Eddy Simulations) and standard k- ϵ model numerically, and the author reported that the resulting profile for the deposition distribution were markedly different and LES result seemed to be more close to experimental results.

2.4 Conclusion from the literature review

Brazed plate heat exchanges (BPHEs) and tube-in-tube heat exchangers (TTHEs) were adopted in refrigeration, air conditioning and food industry as condensers, in which refrigerant rejects heat to water circulating in cooling tower loops. These heat exchangers often suffer from severe fouling because as the water evaporates, the mineral concentration increases and once the solubility limits are reached, the minerals precipitate and might stick to the heat transfer surfaces. Due to the layers of fouling deposit on the heat transfer surfaces, the thermal resistance between refrigerant and water gradually increases. The fouling resistance, or sometimes referred to as fouling allowance, depends on several factors such as heat exchanger geometry, heat flux, water quality, and water flow rates. The fouling resistance penalizes the overall effectiveness of the refrigerant condensers, and thus, must be properly accounted for during the equipment design. Work has been conducted to study the parameters that affect fouling

mechanisms in both BPHEs and TTHERs, and some correlations to predict the long term fouling allowances exist in open literature.

CHAPTER III

3 OBJECTIVE

3.1 Objectives

The main purpose of this work is to study the impacts of water fouling on refrigerant to water condensers thermal and hydraulic performance experimentally and theoretically. The overall objectives were:

1. Determine the key parameters that affect water-side fouling formation inside heat exchangers.
2. Isolate and possibly quantify the effects of these parameters on the thermal and hydraulic performance of refrigerant condensers under fouling conditions.
3. Verify and possibly improve the fouling models in the literature.

Based on the overall objectives of this thesis work, specific objectives in the experimental part and the theoretical part were made and the research approach was discussed in detail.

3.2 Research approach

Researchers have conducted experiments to investigate parameters affecting fouling formation inside the heat exchangers and it is proposed that one of these parameters is heat exchanger internal geometry. In this master thesis, we want to clarify that, the internal geometry of BPHEs (braze plate heat exchangers) mainly referred to the corrugation angle. Since the refrigerant condensers were cooled by cooling tower water, the impact of refrigerant saturation temperature and water quality of the cooling water was also investigated.

Fouling studies have been conducted by people in different place and most of them tested heat exchangers with different type and geometry with local water sources with particular chemistry, which make generalization and comparison difficult. In this thesis, we want to provide a baseline in the investigation of thermal and hydraulic performance of BPHEs, to make it comparable with traditional tubular heat exchangers.

Considering fouling is a very slow process that requires months, investigations showed that the long term fouling performance can be inferred from the accelerated fouling experiments (Webb & Li, 2000). With the above mentioned consideration, accelerated-type of fouling tests were developed in our laboratory and the specific objectives for the experiments were given below:

- 1) To measure fouling resistance of BPHEs with different corrugation angles under the same operating condition.
- 2) To investigate the impacts of water quality and refrigerant saturation temperature on fouling formation inside BPHEs.
- 3) To test a TTHE (tube-in-tube heat exchanger) under the same operating condition and identify any similarities and differences of fouling performance between BPHE and TTHE.

Several steps were taken in the theoretical study of fouling formation to verify and possibly improve the fouling models in the literature. Firstly, among the different fouling model approaches in the open literature, a common linear correlation with the format of $R_f = a_0 + a_1x_1 + a_2x_2 + a_3x_3 + \dots + a_nx_n$ was proposed to predict fouling resistance inside heat exchangers (Wen *et al.*, 2013; Xu, *et al.*, 2011; Zhang & Wang, 2010). In the linear fouling correlation, $x_1, x_2, x_3 \dots x_n$ represent parameters such as water chemistry, water velocity, water temperature, etc. The linear correlation proposed in the literature was verified against the experimental work presented in this thesis. The linear approach tended to overestimate the fouling resistance significantly and it would not capture the asymptotic trend of the fouling formation inside heat exchangers. So the author speculated that, the linear correlation does not represent the

fouling formation in the general case. Secondly, another type of semi-empirical fouling model in the literature which considered the chemical dissociation, heat and mass transfer by applying the first principle equations in fouling formation (Quan, *et al.*, 2008) was further verified against our experimental work. It should be noted that, water pH affects minerals solubility and precipitation rate, thus the proper chemical reaction equation should be incorporated into the model. Thirdly, the difficulty in applying the semi-empirical fouling model in engineering application is that, it included a parameter, deposition strength factor, to describe the fouling removal rates. Since little information was in the literature to compute this parameter, a sensitivity analysis was conducted based on one of the experiments in this thesis, and a correlation was proposed to estimate the value of this parameter. The same correlation was applied in the semi-empirical model to verify against our other fouling tests conducted in this thesis and in the literature. The modified semi-empirical model would somewhat predict the fouling resistance both from our experiments and from the literature. Detailed discussion about this modified semi-empirical model was given in chapter 6.

According to the semi-empirical fouling model, water chemistry, local velocity inside the heat exchanger, and deposition factor are considered as important parameters in computing fouling resistance. We monitored water chemistry information in our fouling experiments in an interval of once every week and we assumed the mineral concentration contained in the water had a linear change between each sampling rate. As discussed in detail in chapter 6, it turns out that, this assumption was not accurate enough in fouling resistance prediction and more intensive monitoring on the water chemistry is required. We would not be able to monitor the deposition strength factor and local water velocity directly in our fouling tests. However, research have proposed that the deposition strength factor is affected by fluid shear stress, surface material and structure (Taborek *et al.*, 1972a; Webb *et al.*, 2000) as well as the type and shape of the fouling particles (Andritsos & Karabelas, 2003).

CFD (Computation Fluid Dynamic) simulation is also a prevalent approach in fouling model development. For a given 3D geometry of the heat exchanger, CFD simulation would help to compute the local flow velocity and temperature profile inside the heat exchanger, but it cannot simulate the fouling process and crystal growth on heat transfer surface (Brahi *et al.*, 2003). In order to simulate the fouling formation process in CFD software, additional fouling models are needed in the form of user defined subroutines. Among the existing CFD simulation in the literature, the following assumptions were commonly applied to simplify the fouling process (Izadi, 2011), (Mwaba *et al.*, 2006b): (1) All particles are assumed to be spherical. (2) Any chemical reaction between the particles and water is neglected. (3) The wall of the heat exchanger is assumed to be a trap for the particles and particle detachment from the surface is neglected. These assumptions overlooked the impact of particle shape on deposition strength factor, and furthermore, it would not be able to capture the nature of mineral solubility change with water pH nor the particulate fouling phenomenon. Thus the CFD approach was not applied in the theoretical study of fouling formation in this thesis.

It should be noted that the purpose of verifying and improving the semi-empirical fouling model investigated in this thesis was to provide a simple but accurate enough fouling model in engineering application. However, this semi-empirical fouling model was not verified against fouling experiments conducted on enhanced tubes since that type of geometry was missing in our fouling experiments.

3.3 Scope of this thesis work

To fulfill the experimental objectives, two BPHEs (A1 and A2) and a smooth TTHE that were commonly applied in industry were selected and the geometries of the tested condensers were summarized in Table 3-1.

Inside a BPHE, alternating plates are stacked together to form a network of contact points. These contact points support the two plates and increase the intensity of turbulence. Figure 3-1 shows the plate geometric parameters that contribute to the heat transfer process, such as aspect ratio L/W , corrugation

angle ϕ , corrugation depth p , and corrugation pitch λ . The corrugation angle is considered as one of the key variables that control the heat transfer enhancement and the fouling resistance of a BPHE. In the current work, the two BPHEs selected had the same geometry, aspect ratio, number of plates and heat transfer area; the only difference was they had different corrugation angles.

Table 3-1 Summary of the condensers tested for the fouling study

	Dimensions, L x W [inch x inch] (cm x cm)	Aspect Ratio L/W	Number of Plates/tubes	Heat transfer area [ft ²] (m ²)	Corrugation angle	Calculated water velocity [ft/s] (m/s)
BPHE-A1	13.3 x 5.1 (33.8 x 12.9)	2.6	14	4.6 (0.43)	30° soft angle	0.6 (0.19)
BPHE-A2	13.3 x 5.1 (33.8 x 12.9)	2.6	14	4.6 (0.43)	63° hard angle	0.6 (0.19)
Tube*	31.34 x 1.38 (79.6 x 3.5)	--	10	4.54 (0.42)	Smooth tube	3.28 (1)

*Total length of the tube-in-tube heat exchanger is 297.96in (756.8cm), with diameter of 7/8 in (2.22cm), these dimensions were taken from a small sample of measurements at OSU laboratory on a commercially available off-the-shelf tube-in-tube refrigerant condenser. They were not given by the manufacturer.

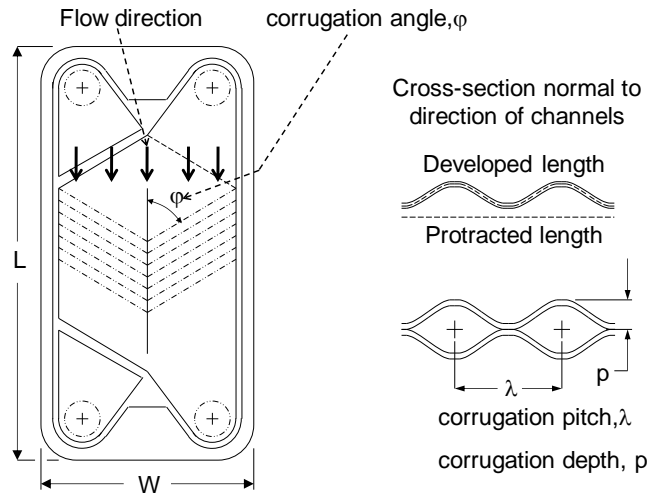


Figure 3-1 Main geometric parameters of BPHEs [used by permission (Cremaschi, *et al.*, 2011)]

As indicated in the research objective, a smooth tube-in-tube heat exchanger with counter-flow design was tested for comparison purpose. It had similar nominal heat transfer area as the A1 and A2 BPHEs; since it had larger cross sectional free-flow area, the tube was not sensitive to particle clogging.

mineral precipitation was promoted due to a local sudden drop of solubility. The operating conditions for the fouling tests were shown in Table 3-2.

The operating conditions during the fouling measurements were carefully selected, so that the tested condensers would operate in similar conditions as cooling tower applications in industry. Test conditions were also in agreement with the recommendations given in the AHRI 450 guidelines (AHRI, 2007). Table 3-2 provides the list of independent variables that were fixed and accurately controlled during the fouling experiments in this thesis. Since this work is part of a broad research project supported by ASHRAE, the American Society of Heating, Refrigeration and Air Conditioning Engineers, the degree of superheat and the water flow rate were selected from typical range of brazed plate-type condensers and within the scope expressed by the request for proposal RF-1345 (ASHRAE, 2007).

Table 3-3 Summary of test matrix for the fouling tests

Test No	Plate type	Ref T _{sat} [°F] (°C)	Water fouling potential	Ref P _{sat} [psi] (kpa)	Water pressure drop in clean condition	Δ(ΔT _{water}) from clean to fouled
1*	A1	105(41)	High FP	150 ±1 (1034±6.9)	1.0psi (6.9kpa)	1.7°F (0.94°C)
2*	A2	105(41)	High FP	150 ±1 (1034±6.9)	1.2psi (8.3kpa)	0.3°F (0.17°C)
3	A2	120(49)	High FP	186 ±0.7 (1282±4.8)	0.9psi (6.2kpa)	0.4°F (0.22°C)
4	A1	120(49)	High FP	186 ±0.8 (1282±5.5)	0.96psi (6.6kpa)	1.5°F (0.83°C)
5	A1	105(41)	Med FP	150 ±0.5 (1034±3.4)	--	0.3°F (0.17°C)
6	A2	105(41)	Med FP	150 ±0.8 (1034±5.5)	1.2psi (8.3kpa)	0.3°F (0.17°C)
7	A1-repeat	105(41)	High FP	150 ±1.5 (1034±11)	1.0psi (6.9kpa)	1.1°F (0.61°C)
8	Tube	105(41)	High FP	150 ±1 (1034±6.9)	1.8psi (12.4kpa)	0.7°F (0.38°C)

*: Tests adapted from (Lim, 2010)

Table 3-3 shows the test matrix for the experimental work. For instance, test No 2 was conducted on A2 plate in high fouling potential water with refrigerant saturation temperature 105°F (41 °C); during the test the refrigerant pressure ranged from 149 to 151 psi and by the end of the test, the temperature difference between water inlet and water outlet of the BPHE varied by 0.3°F (0.17°C). The water side pressure drop across the A2 plate was about 1.2 psi (8.3kpa) in clean conditions, which was the very beginning of this fouling test. The last column, ΔT_{water} refers to the water side temperature difference

across the test heat exchanger, that is $\Delta T_{\text{water}} = T_{\text{LWT}} - T_{\text{EWT}}$. $\Delta(\Delta T_{\text{water}})$ indicates the relative change of the water temperature from the beginning of the test until the last day of the fouling test period.

CHAPTER IV

4 EXPERIMENTAL METHODOLOGY

4.1 Description of test set up

A test set up was designed and built in laboratory to investigate the thermal and hydraulic performances of refrigerant to water condensers under fouling conditions. The overall dimension of the experimental apparatus was 10.5ft W \times 9.5ft H \times 4ft D (3.2m W \times 2.9m H \times 1.2m D). Large amounts of piping, heat exchangers, tanks and pumps were applied. The experimental apparatus mainly consisted of two loops: a simulated cooling tower water loop and a refrigerate loop. The two loops shared the test heat exchanger, functioned as refrigerant to water condenser. System construction detail was given in (Ramesh, 2010).

4.2 Experimental apparatus

4.2.1 Cooling tower water loop

The principle of the cooling tower water loop was shown in Figure 4-1, in which the facility application was labeled and the detail information was given in Table 4-1. The main components in the cooling tower water loop were a test heat exchanger functioned as refrigerant to water condenser, a cooling tower (item #7) used as a mineral concentrator, a water tank (item #4) with an electric heater (item #8) to control water entering temperature to the test condenser as desired and pumps (item #1) to circulate water in cooling tower water loop.

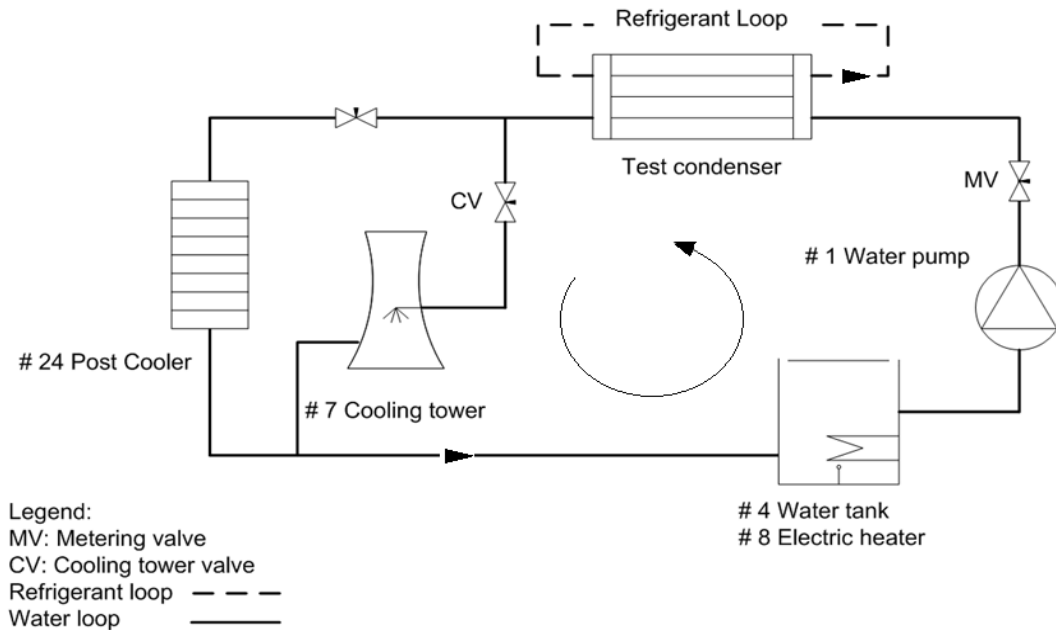


Figure 4-1 Principles of the cooling tower water loop

About 25% of the total flow rate was diverted to the cooling tower in order to evaporate the water at ambient temperature, and the rest of the load was shared by a post-cooler (item #24 in Figure 4-1) installed in parallel. In the current work, the cooling tower acted more as a mineral concentrator rather than a heat sink. The cooling tower progressively increased the concentration of the minerals in the water stream until saturated conditions were achieved. Low fouling potential water was applied as make up water to replace the amount of water evaporated in cooling tower water loop periodically. This concentration method was significant in preparing cooling tower water with desired fouling potential.

4.2.2 Refrigerant loop

As shown in Figure 4-2, the dashed line loop indicates the refrigerant loop, and solid line demonstrates auxiliary water loops; the facility application was labeled and the detailed information was given in Table 4-1. It consisted of a refrigerant gear pump (item #2), an evaporator (item #22), a super-heater (item #23), a test condenser, a sub-cooler (item #25) and a mass flow meter (MFM). In order to solve cavitations problem, a gear pump was selected. The revolution of the pump can be controlled by a VFD

(Variable Frequency Drive), which was used to set the RPM of the gear pump. The refrigerant was first evaporated in the evaporator and then further superheated in the super-heater before entering the test condenser. The pressure was taken at the inlet of the test condenser while temperature sensors were installed before and after the test condenser. The flow rate was measured by using a coriolis type flow meter (MFM), which was installed right after the sub-cooler.

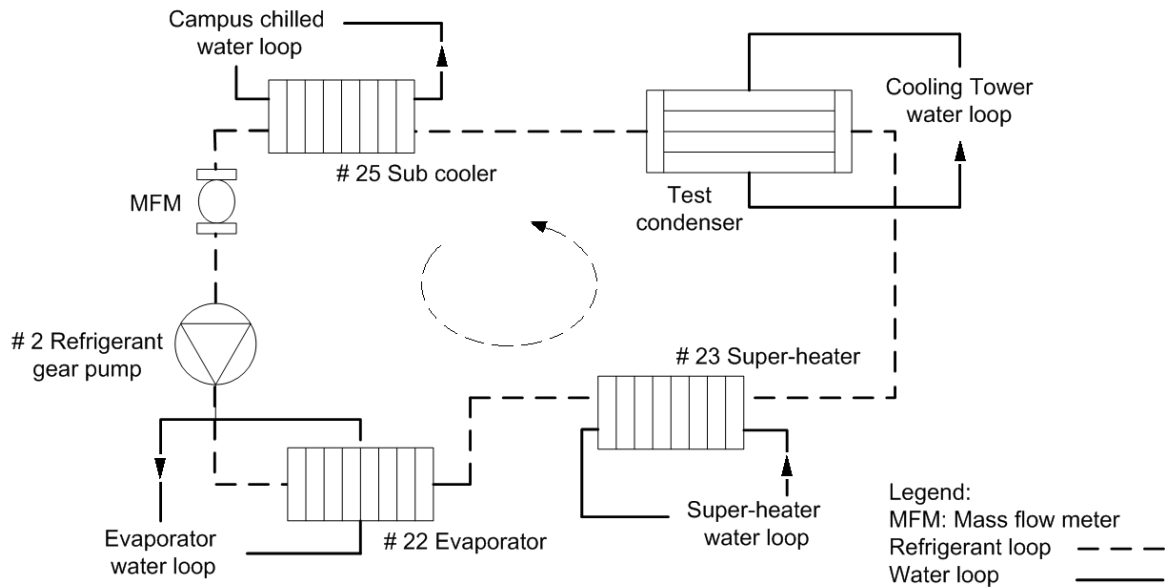


Figure 4-2 Principle of refrigerant loop

4.2.3 Auxiliary loops and safety devices

The saturation pressure of the refrigerant was controlled by the saturation temperature and the refrigerant charge in the system. In order to precisely control the refrigerant saturation temperature, three auxiliary loops: evaporator water loop, super-heater water loop and campus chilled water loop were designed to control the system at the specific conditions shown in Table 3-2. The description, function, manufacturers, models and specifications of the main components used in the experimental apparatus were summarized in Table 4-1 and heat exchangers application were listed in Table 4-2. And the detail description of the three auxiliary loops were given in (Ramesh, 2010) and (Lim, 2010).

Table 4-1 Fouling tests facility application

Item	Component	quantity	Manufacture	Description
1	Water pump	5	TACO	Model: 1400-50; 115V/5.0Amps; Located in water loop
2	Gear pump	1	Micro Pump	Model: GC-M25-JVSE; 230/460V, 2.8/1.4A, 1HP Located in refrigerant loop
3	Chiller pump	1	Dayton	Model: 6K581B; HP3/4, 3450RPM
4	makeup water tank	1	Ace Roto-Mold	Polyethylene tank, 170 gallon located in cooling tower water loop
5	Conical tank	1	Ace Roto-Mold	Polyethylene tank, 30 gallon, located in evaporator loop
6	Storage tank	1	Ace Roto-Mold	Polyethylene tank, 300 gallon, contain make-up water
7	Cooling tower	1	Ace Roto-Mold	Polyethylene tank, 105 gallon; 65”H×23”D,diameter 8” ¾”PVC pipe inserted through the sidewall, two flat nozzles are installed at the end of pipe to spray water downward
8	Electric heater in makeup water tank	1	Chromalox	Model: KTLS-390A-036; 480V/3PH/9KW Located in water loop
9	Electric heater in conical tank	1	Chromalox	Model: KTLS-330A-036; 480V/3PH/3KW Located in evaporator loop
10	column heater	1	Chromalox	Model: VTS-3-024P-E; 480V/24KW Located in super-heater loop
11	Cooling tower fan	1	EMS	Equip with a variable frequency drive, Model P5U-23P7, 240V/30A/50 Hz Mesh wire is installed to stop water droplets by mechanical filter
12	Cooling tower blower	1	Dayton	model 9KX03, 3 HP, RPM 3505
13	Cooling tower nozzle	2		¼” NPT male connection, 80° deflection angle
14	Flexible duct	1		Connect cooling tower and fan, diameter 8”
15	PVC pipes	30ft		Located in water loop, diameter ¾”
16	Electric fan	1	Lasko	Used to cool down the water pump in super-heater loop
17	Electric fan	1	Honeywell	Used to cool down the chiller pump in chiller loop
18	Expansion tank	1	Bell & Gossett	Model:HFT-15 located at the exit of electric heater in super-heater loop
19	Floating switch	2	SJE-Rhombus	120/230VAC, 5A, 50/60Hz
20	Liquid flow switch	1	McDonnell & Miller	FS4-3T general purpose liquid flow switches
21	Copper pipes	60ft		25ft used in water loop, 1” diameter; 15ft used in evaporator loop, 1” diameter; 20ft used in super-heater loop, ¾” diameter

For safety purposes, three flow switches were installed in cooling tower water loop, evaporator water loop and super heater water loop, respectively. The first two operated as floating valves in water tanks and they were activated when the water level in the tank was above the cut off limit. The third flow

switch was connected inside the pipes in super heater water loop and it was activated when certain amount of water flowing in the pipelines. These three flow switches were installed in parallel in the system, serving as primary safety devices. In case of water leakage, pipe bursts or dry outs in any of the three water loops, the flow switches would automatically stop the system to prevent further damage. Thermal fuses were installed on the outside surface of water tank and pipelines in evaporator loop and super heater loop to serve as secondary safety devices. The thermal fuses would stop the system if the water temperature in tanks or pipelines is above 165 °F.

Table 4-2 BPHE application in auxiliary loops

Item	Component name	Model	No of plates	Nominal heat transfer area (ft ²)	Overall dimension (in)
22	Evaporator	GB400H-14	14	4.6	13.3”H×5.1”W×1.6”D
23	Super-heater	GB400L-14	14	4.6	13.3”H×5.1”W×1.6”D
24	Post-cooler	GB400H-14	14	4.6	13.3”H×5.1”W×1.6”D
25	Sub-cooler	GB200H-10	10	1.5	8.9”H×3.4”W×1.3”D
26	Campus chiller	FP5x12-28	28	10	12.2”H×4.9”W×2.9”D

4.3 Instrumentation and data acquisition system

This section contains a brief description of the instrumentation, data acquisition system, various measurement and control devices installed in the test apparatus.

4.3.1 Pressure measurement

Refrigerant pressure at the inlet of the test heat exchanger was measured with an absolute pressure transducer from Setra, model 207. It can measure up to 250 psi with an accuracy of ± 0.13 %. The pressure transducer required a power excitation between 12-24 VDC and the output voltage ranges from 0.1-5.1V.

For the cooling tower water side, a differential pressure transducer from Validyne, with model P855 was applied to measure the pressure drop across the test condenser. It had a working range of 0-20 psi with an accuracy of 0.1% of full scale. It required an excitation of 7-55VDC and its output current ranged from 4-20mA. Five-point calibration was conducted by Validyne with ambient temperature of 68.8°F and the calibration results were given in Table 4-3.

Table 4-3 Differential pressure transducer calibration from Validyne

Pressure	Unit output
PSI	VDC
0.000	0.000
10.000	2.506
20.000	5.000
10.000	2.507
0.000	0.001

4.3.2 Temperature measurement

Resistance Temperature detectors (RTDs) and thermocouples were used to measure the temperatures in the experimental apparatus. Calibration was conducted to the RTDs for water temperature measurements, and the range and accuracy would be discussed in chapter 5, uncertainty analysis section.

Calibrations of the RTDs were conducted before each test and twice during preliminary calibration of the test apparatus. During the first calibration, the exact range of operating temperatures was unknown and the RTD's were calibrated within a large range. The second calibration was done after completion of the first two preliminary tests. At this point, a better idea of the operating temperatures was obtained and the RTDs were calibrated within a closer range of their expected operating temperature. This technique would improve the accuracy of the RTDs.

4.3.3 Mass flow rate measurement

Two Coriolis type mass flow meter from Micro Motion, were applied to measure the water and refrigerant mass flow rates. Each of them consisted of a sensor and a transmitter capable of measuring mass flow rate based on the coriolis force.

The refrigerant mass flow meter can measure flow rates up to 5 lb/min (0.04 kg/s), with an accuracy of $\pm 0.03\%$ and maximum measurable flow rate for the water mass flow meter was 55 lb/min (0.4 kg/s) with an accuracy of $\pm 0.03\%$. The transmitter current output ranged from 4-20mA, which was referred to no flow and maximum flow rate, respectively.

4.3.4 Pump control and heater control

A variable frequency drive (VFD) was used to control the speed of the refrigerant pump in order to maintain a constant flow rate of the refrigerant during the period at the fouling test. A Baldor VS1SP21-1B drive, with a 2 HP electric motor rating requiring 240V 3-phase, was used in this work. An input voltage ranging between 0-10V was supplied to the VFD drive by the LABVIEW control system. The speed varied linearly with the voltage and 10V enabled the pump to rotate with a maximum RPM of 3450.

Three heaters were installed in the system to heat up the water to a desired temperature in cooling tower water loop, super-heater water loop and evaporator water loop. Each of the heaters was controlled by a Mini Max controller. The controller received an input voltage from the LABVIEW program. The input voltage ranged between 0 and 10V, with 0 being no power supplied to the heater and 10V enables the heater to operate at its maximum capacity. A PID control determined the input voltage to the controller based on the difference between actual temperature and the set point temperature.

4.3.5 Data acquisition system

In this thesis, the measurements of the data were conducted using a data acquisition (DAQ) system from National Instrument. Each recorder file included quantities such as the entering/ leaving water temperature, water mass flow rate, refrigerant saturation pressure, refrigerant inlet/ outlet temperature, refrigerant flow rate and etc. Each quantity was sampled every 2 seconds for 3 hours for a total of 5400 data points. Averages were calculated for each quantity. The DAQ system consisted of three parts: a PXI, an SCXI and LABVIEW.

PXI is short for PCI Extensions for Instruments and was composed of three components, a chassis, a system controller and peripheral modules. The PXI applied here was from National Instruments with model NI PXI-1031.

SCXI (Signal Conditioning and Extension for Instrumentation) is a signal conditioning and switching platform for measurement and automation systems. SCXI chassis model 1000 was applied, which can power and control four modules. Three types of modules were installed in the SCXI; each type was designed for a specific task and connected to a terminal block, where all the measurement instruments, such as pressure transducers and thermocouples were connected to. All modules were located in an air-conditioned control room that was away from the test set up.

LABVIEW was the software used to communicate with the DAQ hardware. It was graphical programming software used to read, store and visualize the measurements. LABVIEW was selected for the data acquisition system because of the following merits: robustness during operation, high sample rate, easiness for code programming and maintaining, flexibility for modifications and expansion, and user-friendly graphic interfaces.

LABVIEW consisted of two windows, a front panel and a block diagram. The front panel contained controls and indicators, which allows the operator to control the inputs and visualize the measurements.

The block diagram contained all the actual programming code. The version of LABVIEW used in this thesis was LABVIEW Real Time 8.6.

CHAPTER V

5 DATA REDUCTION AND UNCERTAINTY ANALYSIS

5.1 Test procedure

The procedure for the fouling tests consisted of 10 main steps as follows:

- 1) Prepare 270 gallon (1.04 m³) of make-up water in storage tank. Magnesium Sulfate (93.7 grams or 0.2065 lb), Calcium Chloride (162.7 grams or 0.3587 lb) and Calcium Hydroxide (30.2 grams or 0.0666 lb) were added and mixed into the distilled water. Then Tolytriazole (344 ml or 330 ppm) and chlorine (about 198 ppm) were added to the solution to prevent corrosion (Rother *et al.*, 1985) and microbiology deposits (Flynn & Nalco, 2009). The make-up water had total hardness of about 180-358 ppm CaCO₃, electrical conductivity of 649-1359 μS/cm, M-alkalinity from 54 to 91 (ppm as CaCO₃), and pH ranging between 8.2 and 8.4. Chlorides and Sulfates were less than 260 ppm whereas the total dissolved solids ranged from 428 to 897 ppm. The calculated LSI of make-up water by applying Eq (2-2) and (2-3) is below 1, which could be grouped in low fouling potential water.
- 2) Turn on campus chilled water loop (shown in Figure 4-2) to pre-cool refrigerant sub-cooler (item #25 in Figure 4-2) for at least 20 minutes.
- 3) Turn on refrigerant gear pump (item #2 in Figure 4-2) at speed of 100 RPM to avoid vapor bubble entrainment into pump suction that could potentially cause pump cavitations.

- 4) Turn on two out of three water pumps (item #1 in Figure 4-1) in the cooling tower water loop and adjust metering valve (MV in Figure 4-1) to obtain desired flow rate of 4.6gpm. Turn on water pumps in evaporator and super-heater water loops.
- 5) Turn on heaters (item #8 in Figure 4-1 and heaters located in super-heater water loop and evaporator water loop) and increase RPM of the refrigerant pump (item #2 in Figure 4-2) to about 360-370 RPM in order to achieve refrigerant flow rate of 3.50 lb/min.
- 6) Adjust water/ refrigerant inlet temperature, water/ refrigerant mass flow rate and system pressure according to the test condition in Table 3-2, and wait 8-10 hours to reach thermal equilibrium of the set-up with the surrounding ambient.
- 7) Conduct calibration test to measure UA_{clean} within 24 hours once the system stabilized.
- 8) Open valve (CV in Figure 4-1) to divert water flow to the cooling tower (item #7 in Figure 4-1) and start cooling tower fan. At this point, measure the total volume of water in the system to determine LSI. Water evaporation was assumed to start once the cooling tower was on.
- 9) Adjust water pH according to the desired water fouling potential and calculate LSI. Sample the water from the water tank (item #4 in Figure 4-1) once every week to determine the concentration of the dissolved minerals.
- 10) Each day, record the data for about 2 to 3 hours. The period of recording start approximately at the same time of the day to avoid thermal difference between the test set-up and the surrounding ambient.

Tests were conducted until fouling resistance achieved the asymptotic fouling conditions or until the waterside pressure losses exceeded the maximum pumping head available in the water loop. Cleaning procedures were followed by the end of each test. For the cleaning procedures, we used Rydlyme and

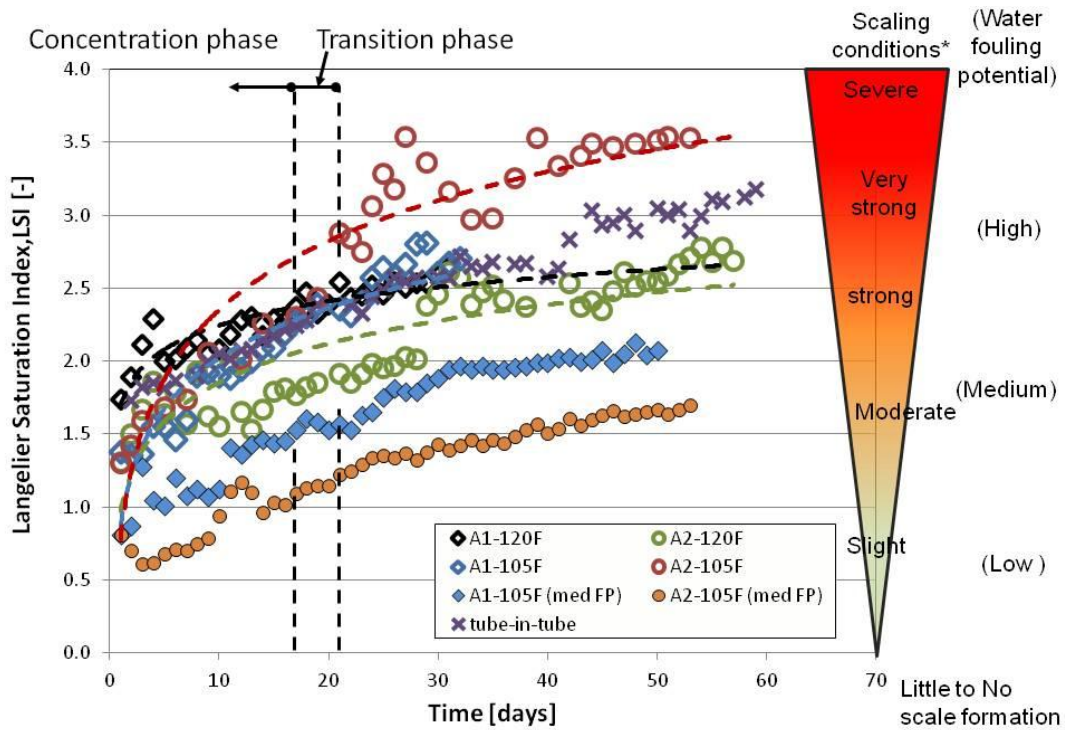
water mixture as cleanser. After using the cleanser, the system was flushed with clean water. The cleaning steps were as follows:

- a) Clean cooling tower water loop with cleanser and flush with clean water afterwards.
- b) Recover refrigerant in the system.
- c) Clean evaporator water loop and super-heater water loop.
- d) Clean the shafts of all the water pumps (item #1 in Figure 4-1) and cooling tower fan.
- e) Clean heat coils for electric heaters (item #8 in Figure 4-1) located in water tanks.
- f) Clean water tanks installed in cooling tower water loop (item #4 in Figure 4-1) and evaporator loop.
- g) Disconnect flexible duct from cooling tower (item #7 in Figure 4-1) and clean cooling tower nozzles.
- h) Recalibrate RTDs in temperature bath with thermo meter as reference
- i) Back up LABVIEW program and data files
- j) Install new condenser for next fouling test. Charge Nitrogen in the system to leak check.
- k) Charge 15 to 18 pounds of refrigerant R-134A in the system.

In each test, the low fouling potential water was circulated through the test heat exchangers and cycled through the cooling tower. The concentration of minerals in the cooling tower water was progressively increased by evaporating the water at a controlled rate of 10-15 gallons per day (38 - 57 liters per day) and the dissolved minerals quickly reached solubility limits. Make-up water was charged into the water tank in the cooling tower water loop periodically; if actual pH was below 8.6, Potassium Hydroxide

was added to adjust the pH to about 8.6 for medium fouling potential water and 9.3 for high fouling potential water. Then the water was circulated in the test condenser and the cooling tower.

To avoid sudden precipitation of the dissolved minerals, the evaporation in the cooling tower took place at ambient room temperature of about 79°F (26°C). Higher salt concentration can be expected when more water was evaporated in the cooling tower. Dissolved salts were kept in the remaining water stream and circulated in the cooling tower water loop. Mineral precipitation was further promoted within the close proximity of the heat transfer surfaces of the test condensers, where the water was heated by refrigerant, and the local concentration of the minerals was brought above the solubility limits. As make-up water was added to the simulated cooling tower water loop, the amount of salts dissolved in the cooling tower water loop was known. The LSI of the simulated cooling tower water during this process for each test is shown in Figure 5-1.



*Note: commonly used range adopted by laboratories specialized in industrial water treatment

Figure 5-1 Langelier Saturation Index (LSI) during the fouling tests

Figure 5-1 shows the change of water quality, evaluated by LSI of each fouling test. The mineral concentration in the cooling tower water was progressively increased due to water evaporation process and the dissolved minerals quickly reached solubility limits. During the period labeled “concentration phase”, the mineral concentrations continuously increased with time, and the LSI ranged from 0.8 to 2.5, and a 3-4 days of transition phase was followed before the desired water fouling potential was reached. The water scaling conditions are reported on the right side of the plots of Figure 5-1. The scaling conditions were defined from commonly used ranges adopted by laboratories specialized in industrial water treatment. At little to slight scaling conditions, the water was defined as “low fouling potential” and the LSI was lower than 1. At moderate to strong scaling conditions, the LSI was between 1.0 and 2.1 and these conditions are referred as “medium fouling potential water” (med FP). At LSI greater than 2.1, very strong to severe scaling conditions might occur and the fouling potential was defined as high. The data at medium fouling potential are shown by the solid points in Figure 5-1 and are marked as “med FP” in the legend. All the other data in this figure represent LSI values with high water fouling potential and the tested condition of each test was also given in the legend. For instance, A1-120F indicates the fouling test was conducted on A1 plate with a refrigerant saturation temperature of 120°F (49°C).

Table 5-1 provides the range of the amount of minerals and water properties measured at our water chemistry laboratory during the fouling tests. The minerals were measured from water samples taken at regular intervals from the cooling tower water loop. It should be noted that copper was not directly introduced in the water loop, but visible changes in water color from clear to yellow opaque and then to brown opaque were observed after 1 to 2 weeks from the beginning of each fouling test. The simulated cooling tower water was circulated in copper pipelines of approximately 22 feet (6.7m) of length and 1 inch (2.54 cm) nominal pipe size diameter. It is likely that small copper particles from the interior walls of the water pipelines were gradually entrained in the water stream causing the color to change during the fouling test. Another possibility is that the test condenser itself was corroded gradually during each

test, thus copper particles were detached from the test condenser and caused the water color change. It was observed that for the two tests conducted in medium fouling potential water, which is No. 5 and No. 6 in Table 3-3 test matrix, the water color in the simulated cooling tower loop was darker than the other tests. Since the difference between medium and high fouling potential water in water concentration was mainly the pH value, we speculate that water with lower pH value had more potential to corrode than water with higher pH. This hypothesis was supported by the corrosion phenomenon observed in super-heater and evaporator auxiliary water loops, in which tap water with pH 7 was used. The water circulating in these two loops was clear in color at the beginning of each test and it became turbid in two to three weeks. Internal leakages, most likely due to corrosion phenomena, were observed in the super-heater and in the evaporator BPHEs and they needed to be replaced every four to six months during the testing period.

Table 5-1 Typical chemistry analysis for water quality

Fouling Potential	Total Hardness	Calcium (as CaCO₃)	Magnesium (as CaCO₃)	M-Alkalinity (as CaCO₃)	P-Alkalinity (as CaCO₃)	Chloride (ppm)	Sulfate (ppm)
Low	180-358	13-92	16-53	54-91	4-15	102-258	64-133
Medium	345-533	18-265	28-109	106-289	6-77	208-884	139-603
High	557-1765	129-391	76-183	204-1813	58-417	491-1947	319-1947
Fouling Potential	Sodium (ppm)	Iron (ppm)	Copper* (ppm)	pH	Total Dissolved Solid (ppm)	EC (µS/cm)	LSI (-)
Low	43-93	<0.1	NA	8.2-8.4	428-897	649-1359	< 1.0
Medium	87-373	<0.1	NA	8.4-8.8	826-2896	1251-4360	1.1 – 2
High	192-741	<0.1	NA	9.0-9.6	2000-7971	3030-11690	2.1 – 3.8

*water is circulated in copper pipe of about 22 feet (6.7 m) of length and 1 inch (2.54 cm) nominal pipe size diameter. Copper particles were observed in the water changing its color after about 1-2 weeks

Minerals were present in the simulated cooling tower water in form of precipitate elements, deposit material, and dissolved compounds. The continuous evaporation process at the cooling tower guaranteed that the concentration of the minerals remained at the critical saturation limits. Supersaturated conditions occurred only in the close proximity of the heat transfer surface inside the

test condenser, where water was quickly heated up by the refrigerant and its local solubility limits suddenly decreased.

5.2 Data reduction

Heat transfer performance of the test heat exchanger was evaluated over a range of internal geometries, refrigerant saturation temperature and water qualities. In order to calculate the overall heat transfer coefficients, heat transfer rate on the water side of the test heat exchanger was computed as follows:

$$\dot{Q}_w = \dot{m}_w c_w \Delta T_w = \dot{m}_w c_w (T_{LWT} - T_{EWT}) \quad (5-1)$$

Water and refrigerant exchange heat inside the test condenser and a schematic of temperature distribution of these two fluids is shown in Figure 5-2(a). Super heated refrigerant entered the test condenser and was cooled to saturation status, then left the condenser as sub cooled liquid, which were indicated as stage 1, 2 and 3 in Figure 5-2(a).

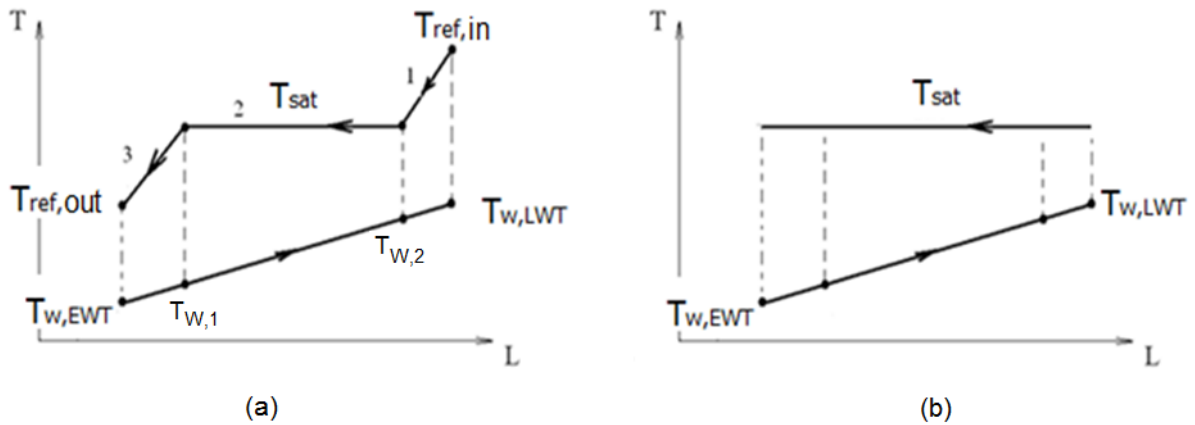


Figure 5-2 Schematic of temperature distribution of refrigerant R134a and water

Log mean temperature difference (LMTD) for a counter flow is defined as:

$$LMTD = \frac{(T_{ref,in} - T_{w,LWT}) - (T_{ref,out} - T_{w,EWT})}{\ln \frac{T_{ref,in} - T_{w,LWT}}{T_{ref,out} - T_{w,EWT}}} \quad (5-2)$$

However, according to AHRI standard 450, the LMTD for a water-cooled refrigerant condenser is computed with the following equation (AHRI, 2007):

$$LMTD = \frac{(T_{sat} - T_{w,LWT}) - (T_{sat} - T_{w,EWT})}{Ln \frac{T_{sat} - T_{w,LWT}}{T_{sat} - T_{w,EWT}}} \quad (5-3)$$

The corresponding temperature profiles are illustrated in Figure 5-2(b). The heat transfer coefficients reported here were obtained by applying the AHRI method. This method does not consider either the degree of superheat or the degree of sub-cooling on the refrigerant side of the test condenser. From the 8 tests conducted in this thesis, the degree of superheat was controlled to 65.0°F (36.1°C) in order to replicate operating conditions similar to the ones of actual condensers in cooling tower applications. However, the degree of sub-cooling of the refrigerant varied from test to test, depending on the refrigerant saturation temperature and fouled conditions. This observation had important impacts in the calculated fouling resistance as it will be discussed later.

As stated in (Cremaschi, *et al.*, 2011), the data reduction for calculating the fouling resistance in heat exchangers was carried out according to the following steps:

Step 1: At initial time $t=t_0$, measure the parameters, $\dot{m}_{w,c}$, $\dot{m}_{ref,c}$, $T_{EWT,c}$, $T_{LWT,c}$, $p_{sat,r,c}$

Perform a first test with refrigerant conditions as close as possible to their nominal values of Table 3-2. Calculate average values and standard deviation. For example

$$\dot{m}_{w,c} = 38.6 \pm 0.30 \text{ lb/min } (0.292 \pm 0.002 \text{ kg/s})$$

$$\dot{m}_{ref,c} = 3.5 \pm 0.02 \text{ lb/min } (0.0265 \pm 0.00015 \text{ kg/s})$$

$$p_{sat,r,c} = 149.7 \pm 1.0 \text{ psi } (1031.2 \pm 6.9 \text{ kpa})$$

$$T_{EWT} = 85.03 \pm 0.05^\circ\text{F } (29.46 \pm 0.03^\circ\text{C})$$

This preliminary test is needed to define the acceptable range of variability in the flow rates during the fouling period.

Step 2: Calculate the clean value of the heat transfer coefficient, $(UA)_c$ as below

$$\dot{Q}_w = \dot{m}_{w,c} c_w \Delta T_{w,c} = \dot{m}_{w,c} c_w (T_{LWT,c} - T_{EWT,c}) \quad (5-4)$$

$$LMTD_c = \frac{\Delta T_{w,c}}{\text{Ln} \frac{T_{\text{sat},r,c} - T_{EWT,c}}{T_{\text{sat},r,c} - T_{LWT,c}}} \quad (5-5)$$

$$(UA)_c = \dot{Q}_w / LMTD_c \quad (5-6)$$

where refrigerant saturation temperature $T_{\text{sat},r,c}$ is calculated from the saturation pressure $p_{\text{sat},r,c}$

Step 3: Perform step 2 at $p_{\text{sat},r,c}$ slightly above and below the nominal value.

For example, if the nominal $p_{\text{sat},r,c} = 149.7 \text{psi} (1032 \text{kpa})$, $T_{\text{sat},r,c} = 105^\circ \text{F} (40.5^\circ \text{C})$, we measured $(UA)_c$ coefficient at average refrigerant saturation pressures of about 148.5, 149.5, 150.0 and 150.7 psi (1024, 1031, 1034 and 1039 kpa). This would provide four values of $(UA)_c$ that are slightly different from each other.

Correlate the $(UA)_c$ coefficient with the values of $p_{\text{sat},r,c}$ and derive a linear trend of the type “ $(UA)_c = C_1 + C_2 \times p_{\text{sat},r,c}$ ” for the specific water flow rate, where C_1 and C_2 are two empirical constants obtained by linearly fitting of the $(UA)_c$ factors with the $p_{\text{sat},r,c}$

Step 4: Repeat step 2 and 3 for two water flow rates.

One flow rate is close to the highest limit and the other is close to the lowest limit of the fouling period. For instance, if the desired nominal flow rate of water is 4.65 gpm ($29.34 \times 10^{-5} \text{m}^3/\text{s}$), we measure $(UA)_c$ coefficient at about 4.63 and 4.67 gpm (29.21 and $29.46 \times 10^{-5} \text{m}^3/\text{s}$).

Plot all $(UA)_c$ coefficients versus saturation pressure and water flow rate. Derive the linear trend for each water flow rate as specified in step 3.

Step 5: Start fouling condition and at time t , measure parameters, $\dot{m}_{w,f}$, $\dot{m}_{ref,f}$, $T_{EWT,f}$, $T_{LWT,f}$, $P_{sat,r,f}$.

Verify that the entering water temperature to the test condenser in fouled and clean condition is the same, that is $|T_{EWT,f} - T_{EWT,c}| \leq 0.1^\circ\text{F}$ (0.05°C)

Verify that the refrigerant flow rate in fouled and clean conditions is also the same, that is

$$\left| \frac{\dot{m}_{ref,f} - \dot{m}_{ref,c}}{\dot{m}_{ref,f}} \right| \leq 0.6\%$$

Step 6: If the conditions in step 5 are satisfied, calculate the heat transfer coefficient in fouled conditions, $(UA)_f$

$$\dot{Q}_w = \dot{m}_{w,f} c_w \Delta T_{w,f} = \dot{m}_{w,f} c_w (T_{LWT,f} - T_{EWT,f}) \quad (5-7)$$

$$(LMTD)_f = \frac{\Delta T_{w,f}}{\text{Ln} \frac{T_{sat,r,f} - T_{EWT,f}}{T_{sat,r,f} - T_{LWT,f}}} \quad (5-8)$$

$$(UA)_f = \dot{Q}_w / LMTD_f \quad (5-9)$$

Step 7: Compute following resistance R_f as follows,

$$R_f = A_{ht} \cdot \left[\frac{1}{(UA)_f} - \frac{1}{(UA)_{c,corrected}} \right] \quad (5-10)$$

where, A_{ht} is the nominal heat transfer area; the $(UA)_{c,corrected}$ is the corrected clean $(UA)_c$ factor of the test condenser and it is obtained from double linear interpolation of the $(UA)_c$ coefficients recorded in step 4. The double interpolation is preferred using the actual saturation pressure and average water flow rate of the fouling experiment.

5.3 Uncertainty analysis

As introduced in chapter 4, measurement instruments were applied in the experimental apparatus. Resistance temperature detectors (RTDs) were installed at the inlet/outlet of the test condenser to read the water and refrigerant inlet/outlet temperatures while the refrigerant saturation temperature was obtained from the refrigerant pressure.

A data logger from National Instruments and LABVIEW Real Time data acquisition system were used to record and store the data. Operating conditions were closely monitored every 1 second at all times by the LABVIEW Real Time control module. 3 hours of data collection was applied each day with a sampling rate of 2s. The measurement samples were statistically large enough to reduce the error from noise, random fluctuations of the sensor output signals, and sensors response time. The sensors and corresponding accuracies are summarized in Table 5-2.

Table 5-2 Specifications of the key instrumentation for the fouling experiments

Sensor function	Type	calibration	Nominal range	Accuracy
Water mass flow meter	Coriolis	Manufac.	16 to 55 lb/min (0.1 to 0.4 kg/s)	±0.03% of flow rate
Ref mass flow meter	Coriolis	Manufac.	1 to 5 lb/min (0.01 to 0.04 kg/s)	±0.1% of flow rate
Water inlet temperature	In-stream Pt-RTD	In situ	83 to 87 °F (28 to 30 °C)	±0.09 °F (0.05°C) ⁺⁺
Water exit temperature	In-stream Pt-RTD	In situ	88 to 95 °F (31 to 35 °C)	±0.09 °F (0.05°C) ⁺⁺
Ref inlet temperature	In-stream Pt-RTD	In situ	68 to 173 °F (20 to 78 °C)	±0.09 °F (0.05°C) ⁺⁺
Refrigerant pressure	Piezo-transducer	Manufac.	2.2 to 251 psia (15 to 1,730 kPa)	±0.13% of full scale
Water side pressure drop	Piezo-transducer	Manufac.	0 to 20 psid (0 to 137 kPa)	±0.10% of full scale

⁺⁺Special limits from high accuracy in-house customized calibration with isothermal bath and precision thermometer

As indicated in the data reduction procedure, both UA values for fouled conditions and clean conditions were required to compute the fouling resistance values. Since the deviation of the average refrigerant

saturation pressure and water flow rates in both conditions was small, double interpolation correction for $(UA)_c$ was applied to reduce the systematic error, which was summarized in test procedure Step 7.

Refrigerant flow rate was observed to be another critical parameter and it was kept within 0.6% deviation during the whole test. By measuring $(UA)_f$ and evaluating the corresponding clean coefficient, $(UA)_{c,corrected}$, at the same refrigerant saturation pressure and water flow rate, the fouling resistance, R_f , was obtained from Eq (5-10). It represents the influence of fouling formation on the thermal resistance of the test condenser.

The water side pressure drop of the test condenser was measure by a differential pressure transducer, with $\Delta p_{w,c}$ for clean condition and $\Delta p_{w,f}$ for fouled condition. The water friction factor in clean ($f_{w,c}$) and fouled ($f_{w,f}$) conditions could be calculated according to the following definitions:

$$f_{w,c} = -\frac{1}{2} \frac{d_e}{L} \frac{\rho_w}{G_{w,c}^2} \Delta p_{w,c} \quad f_{w,f} = -\frac{1}{2} \frac{d_e}{L} \frac{\rho_w}{G_{w,f}^2} \Delta p_{w,f} \quad (5-11)$$

where d_e and L are the flow channel equivalent diameter and channel nominal length, respectively (Ayub, 2003). During the fouling tests the water mass flux and inlet temperature were constant, thus the fouling pressure drop penalty factor, $PDPF$, is reduced to:

$$PDPF = \Delta p_{w,f} / \Delta p_{w,c} \quad (5-12)$$

A complete and thorough uncertainty analysis was done by following the uncertainty propagation method suggested by Taylor (1994). The uncertainty of the fouling resistance is determined as below:

$$e_{R_f} = \pm \sqrt{\left(\frac{\partial R_f}{\partial T_{LWT}} e_{T_{LWT}}\right)^2 + \left(\frac{\partial R_f}{\partial T_{EWT}} e_{T_{EWT}}\right)^2 + \left(\frac{\partial R_f}{\partial m_{water}} e_{m_{water}}\right)^2 + \left(\frac{\partial R_f}{\partial P_{sat}} e_{P_{sat}}\right)^2} \quad (5-13)$$

where, $\frac{\partial R_f}{\partial T_{LWT}}$ Sensitivity coefficient due to leaving water temperature,

$\frac{\partial R_f}{\partial T_{EWT}}$ Sensitivity coefficient due to entering water temperature,

$\frac{\partial R_f}{\partial m_{water}}$ Sensitivity coefficient due to water mass flow rate,

$\frac{\partial R_f}{\partial P_{sat}}$ Sensitivity coefficient due to refrigerant saturation pressure,

$e_{T_{LWT}}, e_{T_{EWT}}$ Accuracy of RTD for leaving (LWT) and entering (EWT) water, °F or °C

$e_{P_{sat}}$ Accuracy of a pressure transducer, psi or kPa

Accuracies of each instrument were obtained by in-situ periodic calibration of the RTDs and from high precision certified calibration of the flow meter and pressure transducers by the manufacturer. Considering each measurement as uncorrelated and random, the uncertainty on the fouling resistance was estimated. The results showed that the uncertainty depended mainly on the difference between the leaving water temperatures in fouled condition compared to the one in clean condition; smaller uncertainty can be expected with greater leaving water temperature difference. From the experimental results of the 8 tests completed in this thesis, most of the measured fouling resistance of the test condenser was lower than $1 \times 10^{-3} \text{ hr} \cdot ^\circ\text{F} \cdot \text{ft}^2/\text{Btu}$ ($1.8 \times 10^{-4} \text{ }^\circ\text{C} \cdot \text{m}^2/\text{W}$), as shown in Figure 5-3.

In the test apparatus, the RTDs in the water stream were calibrated in situ to within 0.09°F (0.05°C). With some geometry tested in this thesis, the fouling resistance is on the order of 1×10^{-4} and $2 \times 10^{-4} \text{ hr} \cdot ^\circ\text{F} \cdot \text{ft}^2/\text{Btu}$ (1.8×10^{-5} to $3.5 \times 10^{-5} \text{ }^\circ\text{C} \cdot \text{m}^2/\text{W}$) and the corresponding uncertainty was estimated within $\pm 50\%$ to $\pm 25\%$, respectively. As shown in Figure 5-3, the sensitivity of the uncertainty was influenced by the leaving water temperature difference between clean condition and fouled condition, ΔT_{LWT} ; fouling resistance was still measurable if ΔT_{LWT} was less than 0.2°F , however the uncertainty would be more than 50%. The theoretical uncertainty in the pressure drop penalty factor depended mainly on the accuracy of the differential pressure transducer. For the range of experiments carried out in this thesis, the uncertainty in the pressure drop penalty factor was from ± 2.5 to $\pm 4\%$.

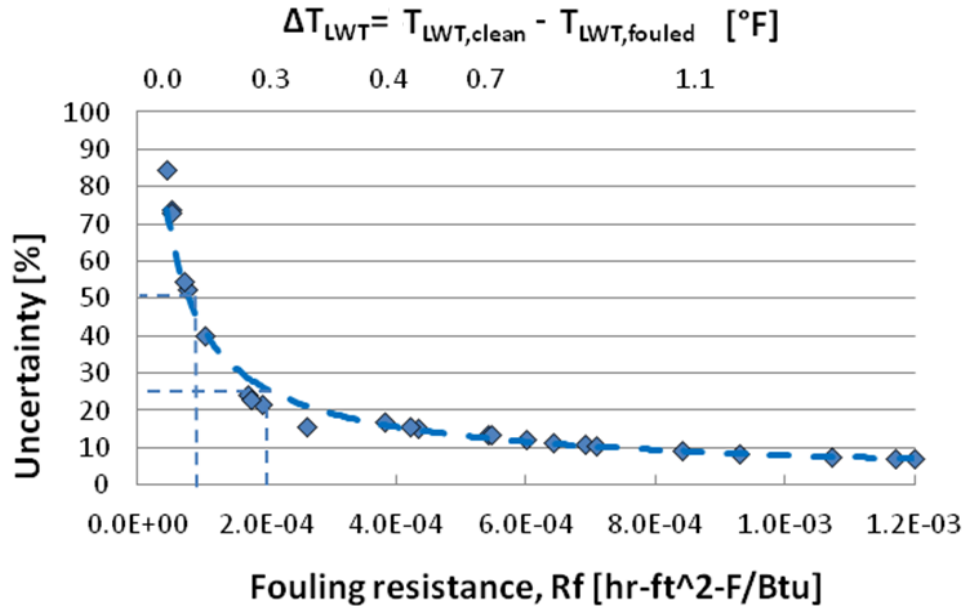


Figure 5-3 Fouling resistance uncertainty analysis

CHAPTER VI

6 RESULTS AND DISCUSSION

6.1 Fouling deposit chemical analysis

In each test, the low fouling potential water was circulated through the cooling tower, due to evaporation process, minerals contained in the cooling tower water was concentrated and quickly reached solubility limits. The concentrated water cycled through the test heat exchangers and heated up by refrigerant, precipitation occurred on the surface of the test condenser.

After two months of testing on the TTHE (tube-in-tube heat exchanger), the condenser was opened from the caps located at the end of each tube and a layer of light yellowish fouling deposit on the cap surface was visually observed, as shown in Figure 6-1(a). These images were taken by a conventional digital camera and it is evidence of mineral precipitation and that the heat exchanger experienced fouling.

The fouling deposit material was sampled, as shown in Figure 6-1(b), and chemical digestion analysis was conducted at Soil, Water and Forage Analytical Laboratory (SWFAL) at Oklahoma State University. Chemical analysis showed that more than 34% is calcium, the amount of Mg was less than 0.5%; and the amount of Fe, Cu, and Zn were within 5%. It is assumed that carbon dioxide from the air in the cooling tower was dissolved in the water stream and reacted with the calcium ions already present in the water, forming CaCO_3 . Since only certain specific amount of chemicals were added to distilled water in my tests to produce Calcium ions and no other anions were added, this is a reasonable assumption. By assessing the molecular weight of Ca and CaCO_3 , it was estimated that CaCO_3 was up to 85% of the fouling deposit.

However, when there are different types of anions coexisting in the water during the fouling operation, it is recommended to dissolve the fouling deposit in water and measure the balancing ions of both calcium and carbonate in order to estimate the chemical composition of the mineral fouling deposit.

During the fouling test, fouling deposited on every component throughout the entire water loop, including water tank, electric heater, cooling tower, water pumps, heat exchangers, and water pipes. By measuring the weight of fouling deposited on the surface of the eighteen caps located at the end of the smooth tube and the surface area of the caps, it was estimated that the precipitation mass flux in two months of continuous run was about 3.7×10^{-5} lb/in² (2.6 mg/cm²). When considering the total amount of calcium added to the water and its solubility, and the area of the entire test set up without the TTHE, the mineral precipitation mass flux in the rest of the system was about 4.4×10^{-5} lb/in² (3 mg/cm²) in two month of continuous run. Considering the measurement uncertainty in the fouling deposit mass sampled from the TTHE and the approximation for the effective area exposed to fouling in the water tank and in the cooling tower, the two precipitation mass flux were similar. In the TTHE the water had the highest bulk temperature but in the water tank, water reached the highest local temperature near the heating elements. Inside the cooling tower, due to aeration, the production of CaCO₃ is locally increased according to the reaction given in Eq (6-1):



These observations support the fact that the mineral precipitation mass flux was practically the same for the entire system and the analysis provide an order of magnitude of the mineral precipitation mass flux for the case of high water fouling potential.

In the process of sampling fouling deposit material from the tube caps, an observation was made that, the thickness of fouling varies according to the location of the cap. Thicker deposition appeared at the water outlet, where the water temperature was almost 10°F (5.56°C) higher than the water inlet. This phenomenon can be explained by the solubility of minerals in water since the solubility of CaCO₃

decrease with increasing temperature as shown in Figure 6-2. More minerals tend to precipitate at higher temperature resulting in a larger amount of fouling deposit at the outlet of water tube than the inlet. In order to verify this assumption, a CCD camera with an extended borescope probe was used to take digital images inside the smooth tube-in-tube heat exchanger, as shown in Figure 6-3. The CCD camera had a high resolution short focus charge-coupled device and a motorized 1 meter extended mini probe head, which was inserted in the condenser tubes.



(a) condenser caps with fouling deposit

(b) fouling deposit material sampled

Figure 6-1 Fouling sample from TTHE condenser

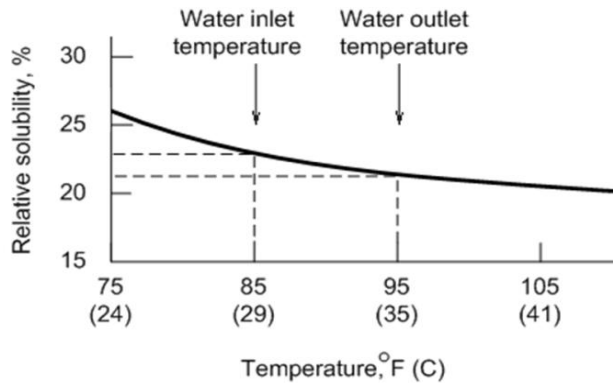


Figure 6-2 Solubility of CaCO₃ [adapted from (Flynn & Nalco, 2009)]

The borescope of the CCD camera was inserted inside the water inlet and outlet tubes of the TTHE and digital images were taken at various locations indicated as “a”, “b”, “c”, and “d” in Figure 3-2. The

corresponding images of the fouling deposit layers are shown in Figure 6-3; the top images are for the tube at the water inlet section while the bottom images are for the water outlet section. The four images are labeled (a), (b), (c) and (d) and they represent the fouling conditions at the entrance, in the first half, in the second half and at the end of each tube. In order to make a comparison of fouling appearance, the photos were taken at the same axial location inside the inlet and outlet tubes. Thicker layer of fouling was visually observed inside the outlet tube than the inlet tube and photo (d) in Figure 6-3 supports this observation.

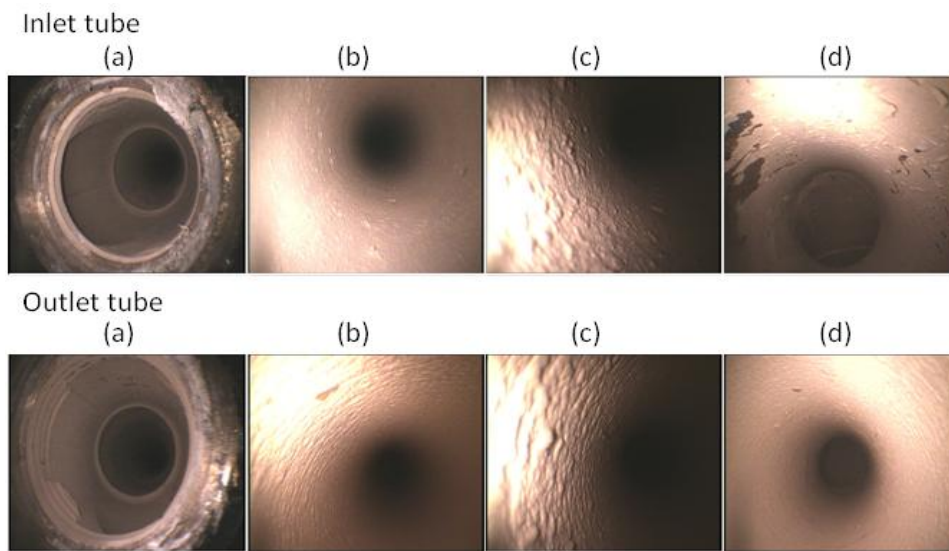


Figure 6-3 Image of fouling deposit inside smooth tubes

Attempts were also made to take fouling pictures inside the BPHEs, as shown in Figure 6-4. The authors cut the plate heat exchanger with a bench saw. It was observed that the thin metal plates plastically deformed due to the heat generated during the cutting process and the surfaces were contaminated by the cooling fluid of the saw. Inevitably some of the fouling deposit material was destroyed and removed. However, some fouling deposit was still visible inside the mini channels as shown in the circled region in Figure 6-4.

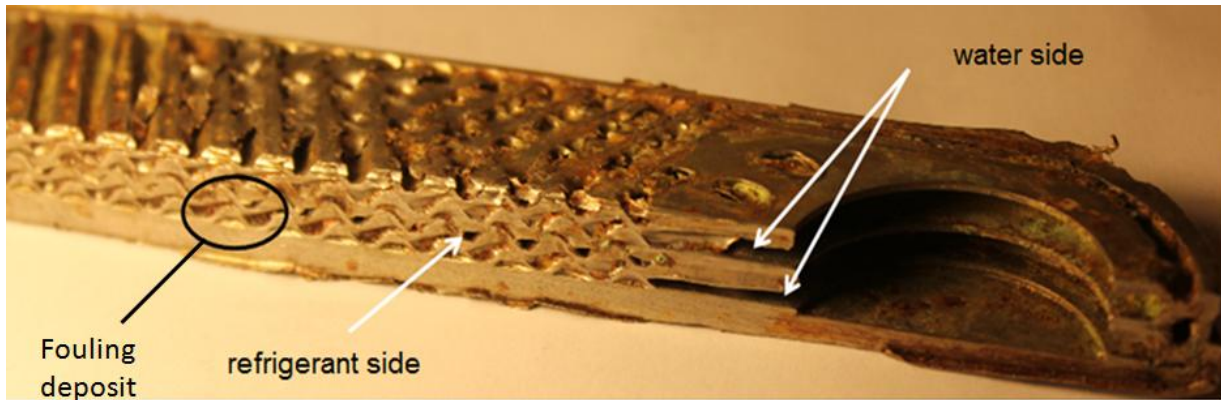


Figure 6-4 Images of fouling deposit inside a BPHE

6.2 Fouling heat transfer analysis

6.2.1 Fouling formation in BPHEs and TTHE

Figure 6-5 to Figure 6-7 shows a comparison of thermal and hydraulic performance between TTHE and two BPHEs under fouling conditions. The fouling tests were conducted with high fouling potential water and with the same refrigerant saturation temperature of 105°F (41°C). A1 indicates BPHE with soft corrugation angles of 30°, and A2 indicates BPHE with hard corrugation angle of 63°. The TTHE tested in the current work had the same nominal heat transfer area as A1 and A2 plates. Geometry information of the tested heat exchangers was given in Table 3-1. Detail information of test condition was given in Table 3-2.

In Figure 6-5, the A1 plate achieved a fouling resistance of about $1.0 \times 10^{-3} \text{ ft}^2 \cdot \text{°F} \cdot \text{hr} / \text{Btu}$ ($1.8 \times 10^{-4} \text{ m}^2 \cdot \text{°C} / \text{w}$) in 30 days, as shown in diamond points. A2 plate reached a fouling resistance of $1.3 \times 10^{-4} \text{ ft}^2 \cdot \text{°F} \cdot \text{hr} / \text{Btu}$ ($2.4 \times 10^{-5} \text{ m}^2 \cdot \text{°C} / \text{w}$) in 55 days, shown as square points. A1 and A2 plates had identical geometry; the only difference was that A1 had a soft corrugation angle while A2 had a hard angle. The experimental results clearly showed that the fouling resistance for A1 plate was almost one order of magnitude higher than A2 plate. Water in between the plates flows from the inlet to the outlet mainly in the mini-channels created by the corrugations on the plates, which are stacked on each other and rotated by 180°. Water also

crosses the ridges from one mini-channel to the adjacent one, thus moving in a zig-zag pattern. The extension of the angle of the zig-zag pattern depends on the corrugation angle and depth of the corrugations. Different local velocities and local turbulence intensity in between the plates are expected between the A1 plate and the A2 plate. The authors speculate that higher local velocity and higher degree of zig-zag were the A2 plate with respect to the A1 plate. Thus higher convective heat transfer coefficients and higher water side pressure drop in between the plates in BPHE A2 could be expected. This high level of local velocity and turbulence seems to promote the removal mechanism of the fouling deposit, resulting in a lower overall fouling resistance. Stasiak *et al.* (1996) investigated the influence of corrugation angles on flow and heat transfer phenomenon in plate heat exchangers. Their research revealed that the increase of corrugation angle would promote local Nusselt number and local turbulence, which is proportional to $Re^{2/3}$, which supported our speculation that higher local turbulence occurred in the A2 plate with hard corrugation angles. Similar observation was also reported by (Palm & Claesson, 2006).

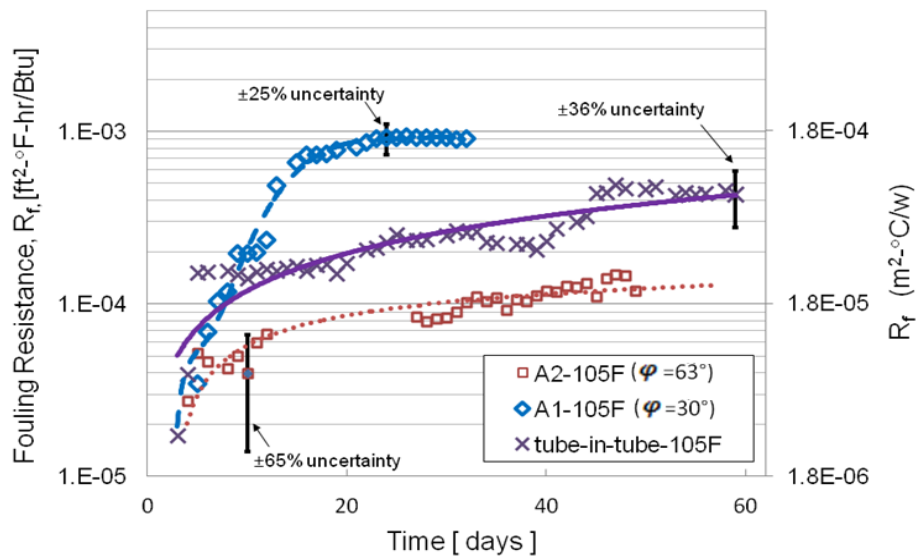


Figure 6-5 Measured fouling factor for TTHE and BPHEs

For the smooth tube-in-tube heat exchanger with same heat transfer area and same operating conditions, the measured fouling resistance data was shown as cross points in Figure 6-5. Since the TTHE had larger water flow cross-sectional area than the BPHEs, the local velocity was expected to be fairly low. The measured fouling resistance was in between A1 and A2 plate; after 60 days of operation, a fouling resistance of $4.8 \times 10^{-4} \text{ ft}^2 \cdot \text{°F} \cdot \text{hr} / \text{Btu}$ ($8.6 \times 10^{-5} \text{ m}^2 \cdot \text{°C} / \text{w}$) was obtained. The effects of geometry and local velocity were combined in this test, leading to a fouling behavior in between the A1 and A2 plate; similar phenomenon was reported by Bansal *et al.* (2001). However, more tests at different velocities and various tube diameters would be necessary for further investigation of the fouling behavior on plate and tube type condensers.

Figure 6-6 shows the water temperature difference between inlet and outlet of the test condenser. Three heat exchangers, A1, A2 and TTHE were compared. All of them were tested with same operating conditions. Since entering water temperature and the water flow rate were controlled to be constant for all the tests, the decrease of leaving water temperature has similar trend with the heat flux. A1 plate, shown as diamond points, had a sharp temperature drop of 1°F (0.56°C). The heat fluxes in clean conditions were about $3,001 \text{ Btu/hr} \cdot \text{ft}^2$ ($\sim 9.6 \text{ kW/m}^2$), and after 30 days of fouling test, the heat fluxes decreased by 15%. The A2 plate, with a hard corrugation angle of 63° , experienced a small decrease in the heat flux across the plate; the heat flux degradation was within 5% in 55 days with respect to heat flux in clean conditions. The trend of heat transfer degradation in TTHE was quite similar to the A2 plate. During 60 days of operation, a decrease of 8% in heat flux was observed, the water temperature difference across the test condenser for A2 plate and the TTHE had similar slope during first 40 days of operation. By the end of the fouling test, the temperature difference for the TTHE decreased by as much as 0.7°F ($\sim 0.4^\circ\text{C}$).

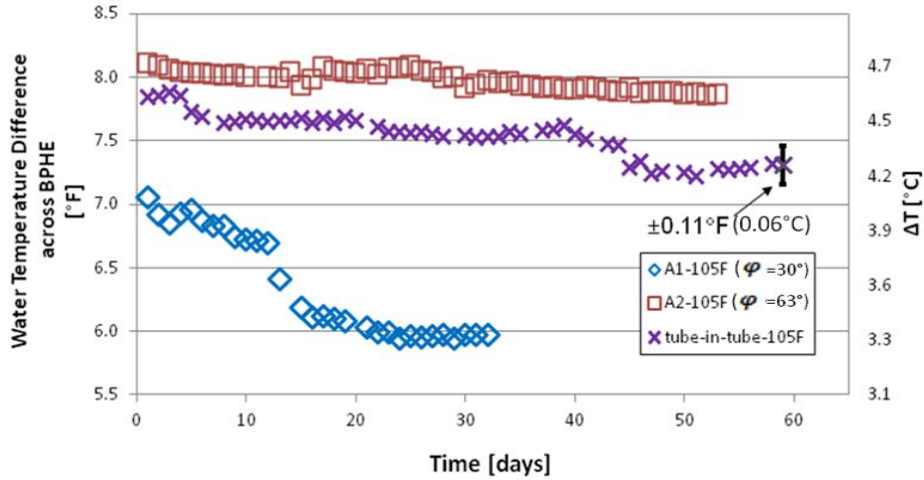


Figure 6-6 Measured water temperature difference for TTHE and BPHEs

The hydraulic performance of the test heat exchangers is presented in the form of pressure drop penalty factors (PDPF) in Figure 6-7, Pressure drop across the test condenser in clean conditions are also given in the legend. The pressure drop in clean condition was about 1.2 psi (8.3 kpa) on A2 plate and 1 psi (6.9 kpa) on A1 plate. This observation supports the expectation that hard corrugation angle in A2 would lead to higher local velocity and higher pressure drop. PDPF values for each test were calculated according to Eq. (5-12) and they represented the ratio of water side pressure drops measured in fouled conditions and the corresponding ones measured in clean conditions. For instance, A2 plate had a PDPF of 1.1 after 55 days of fouling tests, which means a 10% of pressure increase in fouled conditions was observed by the end of the test with respect to clean conditions. A1 plate experienced a localized blockage of the mini-channels and as a result, the pressure drop increased by 30%. The “×” points in Figure 6-7 indicate the pressure drop across the TTHE tested in this thesis. Since the TTHE had larger free flow cross sectional area than the plate-type heat exchangers, it was not subjected to severe clogging due to fouling.

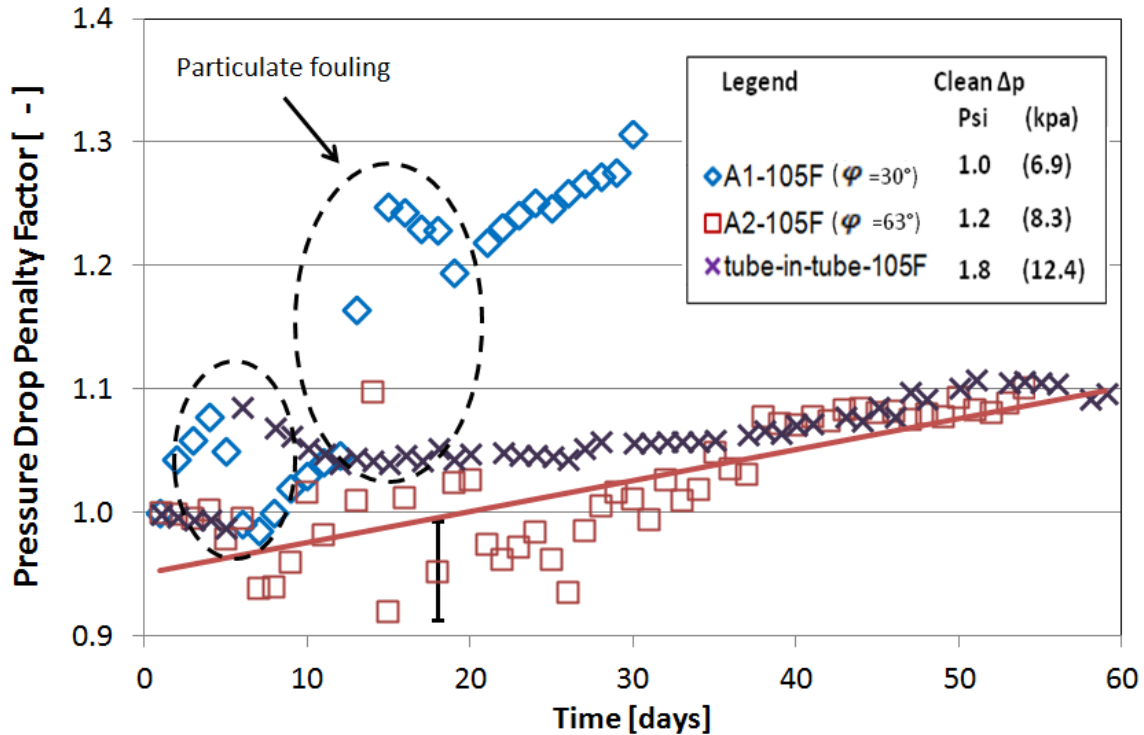


Figure 6-7 Measured pressure drop penalty factor for TTHE and BPHEs

As shown in Figure 6-7, the pressure drop for A1 plate showed scattered data, which are indicated with dashed line circle. A sudden increase in pressure drop was observed in day 3 and day 12, and this phenomenon might be due to localized flow blockage inside the mini channels from particulate fouling. Particles attached on the surface and trapped in the mini channels create a significant resistance to the water stream. This phenomenon suggested that the fouling mechanism in this test is a combination of precipitation and particulate fouling. Since part of the particles have a loose adherence on the surface, they were removed due to the increase of water velocity and shear stress, leading to a slight decrease in pressure drop right after the sudden increase, shown as pressure drop data in day 5 and day 17. Particulate fouling and localized particle blockage phenomenon was also observed for the smooth tube, at about day 5, the tube PDPF increased suddenly, and after that, the increase of the PDPF for the TTHE was minor and the pressure losses were about 10% higher than the initial pressure drop in clean conditions. The pressure drop for the A2 plate also showed a lot of scattered data during the first 20 days of operation

with high fouling potential water. Some PDPF values were even lower than initial values, which is an intriguing result but most likely due to a systematic error with the test apparatus at the beginning of this experimental campaign. This might be due to the uncertainty in the pressure measurements. In addition, it is also possible that the A2 plate have been contaminated with particles coming from the rest of the test set up at the beginning of the fouling test. Thus, the measured pressure drop in clean conditions might have been a worst case estimate. Comparing with the A1 plate, which is the lowest pressure drop BPHE by design, the pressure drop in clean conditions of the A2 plate could be 1.0 psi in the best case scenario. The measured value in clean conditions for this test was about 20% higher already. This observation could indicate some contamination of the A2 plate at the beginning of this test. To address this issue some recommendations are proposed in the future work section of the thesis.

6.2.2 Impacts of condensation temperature and water quality on fouling formation

Figure 6-8 to Figure 6-11 shows the experimental measurements of the fouling tests conducted on the BPHEs A1 and A2 at two refrigerant temperatures 105°F (41°C) and 120°F (49°C) and with high and medium water fouling potentials. Detailed information of the test conditions is given in Table 3-2. The data at medium fouling potential are shown by the solid points in Figure 6-8 to Figure 6-11 and are marked as “med FP” in the legend. All other data in these figures represent fouling tests with high water fouling potential and the notation of high fouling potential was omitted in the legend for clarity.

Figure 6-8 shows the measured fouling resistance data, after about 30 days of operation at refrigerant temperature at 105°F (41°C) with high fouling potential water, the fouling resistance of BPHE A1 was about 9.3×10^{-4} hr-°F-ft²/Btu (1.6×10^{-5} °C-m²/W), indicated as hollow diamond points; while the A2 plate, with hard corrugation angle of 63° had a fouling resistance of about 1.5×10^{-4} hr-°F-ft²/Btu (2.6×10^{-5} °C-m²/W) after 50 days, see hollow square points. Both BPHEs had same aspect ratio, identical geometry and heat transfer area. BPHE A1 had a soft corrugation angle of 30° and the experimental results clearly showed that its fouling resistance is one order of magnitude higher than the one experienced by BPHEs

with hard corrugation angles. These results are in agreement with the conclusions of Thonon *et al.* (1999) who reported that the asymptotic fouling resistance of a plate heat exchanger with a 30° corrugation angle was almost ten times higher compared to the one with 60° corrugation angle.

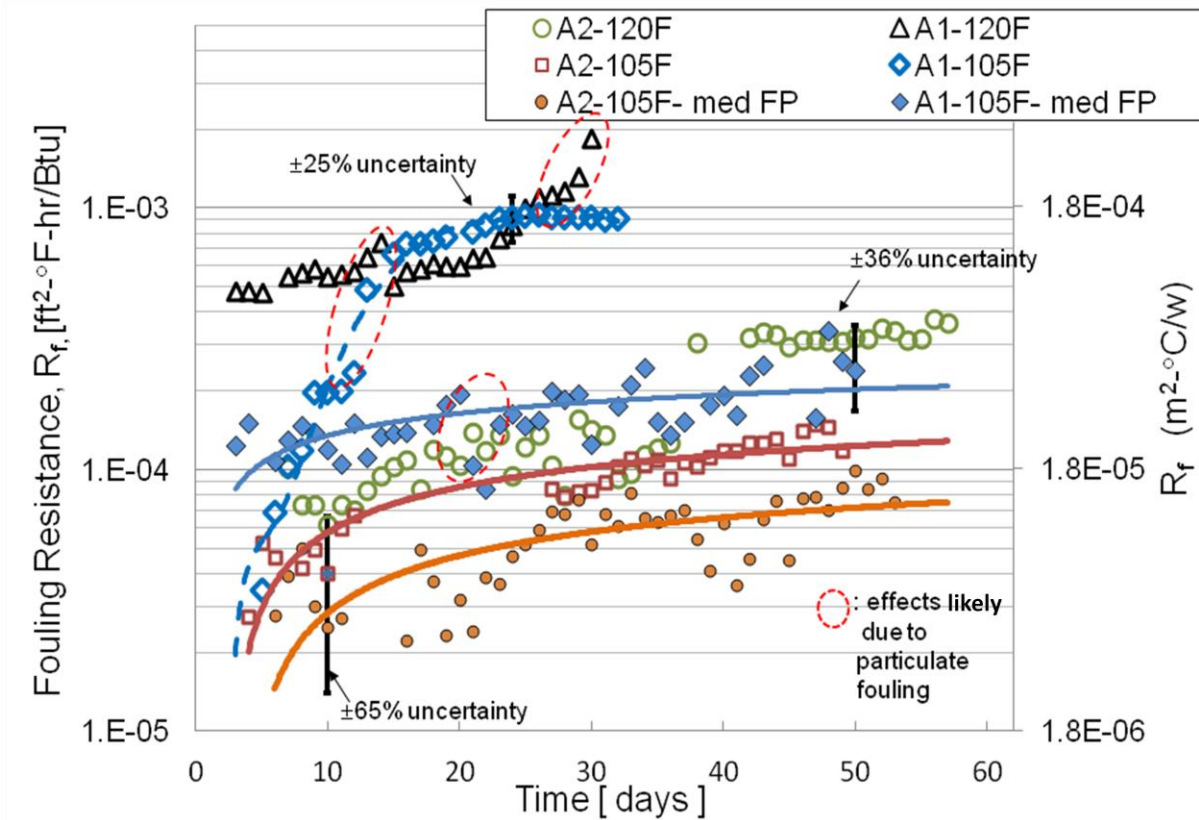


Figure 6-8 Effect of refrigerant temperature and water quality on fouling resistance

An increase of the refrigerant saturation temperature augmented the heat flux across the plates and a measurable increase of the fouling resistance was recorded for both BPHEs A1 and A2. The triangles data of Figure 6-8 showed some scattering during the first 20 days of the fouling test and a sharp increase of the fouling resistance occurred at about 30 days from the beginning of the fouling test. This phenomenon could be explained if one considers the effects due to flow blockage caused by particulate fouling, in which suspended particles might have been trapped in between the channels of the BPHE. Suspended solids are introduced into the water stream by precipitation within the water and/or removed particles from surface deposits. Suspended solids were evident in the system for this experiment, forming a soft

white-colored film on surfaces throughout the system wherever they settle out, including the BPHE. Thus, it seems inevitable that both precipitation fouling and particulate fouling occurred in the experiment. Suspended particles interfered with the water channel flow within the inlet and outlet regions of the plates, that is, between the BPHE water connecting ports and the central sections of the corrugated plates. For soft corrugation angle of 30° the suspended particles produced a blockage of the water flow within the plate channels more severe than the case of plates with a hard corrugation angle.

It should also be noted that, in our data analysis, we applied the LMTD method and only considered the saturation region as the reference parameter for the refrigerant operating conditions. With this approximation, the measured fouling resistance in Eq. (5-10) is an average value and the division among superheated region, two-phase region and sub-cooled region is not considered. This is reasonable if one considers that the two phase saturated region is the main contributor to the heat flux at the wall and to the wall surface temperature. Another reason to choose the approximated method is that, similar operating condition is required to compare the water fouling performance inside different heat exchangers, which means the same water quality, capacity and refrigerant temperature. Once the same water quality, heat exchanger capacity, refrigerant saturation temperature, and degree of superheat in the entering refrigerant were set, the refrigerant outlet temperature is not a controlled parameter but rather the result of the heat transfer process with fouled surfaces. On the contrary, if we test two heat exchangers with the same refrigerant entering and leaving temperature, we cannot guarantee they have the same refrigerant saturation temperature either. Moreover, the comprehensive method lacks the capability to capture the difference of fouling behavior for different saturation temperatures with the same refrigerant inlet and outlet temperatures. Taking the saturation temperatures in the approximated method would provide good trends when changing this parameter, shown in Figure 6-12. In our previous work, we conducted an assessment of the approximated method versus a comprehensive method that considers both superheat and sub-cooled regions, shown in Table 6-1. The fouling curve obtained from comprehensive method followed similar trend as the approximated method, but the fouling resistance values have been scaled up.

The scaling factors varied according to the type of the heat exchanger, it is about 8.5~14.6 for BPHEs with a corrugation angle of 63°, 2.4~6.2 for BPHEs with a corrugation angle of 30° and 2.4~4 for smooth tube. The variation of scaling factor might be due to the different degree of sub-cooling of the refrigerant at the heat exchanger outlet. Similar amount of sub-cooling was observed on BPHE A2 and the smooth tube, and they had similar scaling factors.

The calculated fouling resistance by applying the approximated method was in agreement with the procedures recommended by the standards and AHRI guidelines but, while the degree of superheat of the refrigerant at the inlet of the BPHEs A1 and A2 was kept constant to 65°F (~36°C) for all tests, the refrigerant outlet conditions varied a lot and was dependent on the corrugation angle, heat flux conditions, and fouled conditions of the plates. The degree of sub-cooling for the refrigerant during the condition 1 of nominal heat flux ($T_{\text{sat}} = 105.5^{\circ}\text{F}$ or 41°C) and condition 2 of increased heat flux ($T_{\text{sat}} = 120.2^{\circ}\text{F}$ or 49°C) are shown in Figure 6-9. The refrigerant circulating in the BPHE A1 with a soft corrugation angle of 30° was subjected to practically no sub-cooling at the outlet refrigerant port, suggesting that refrigerant exits the BPHE A1 in two-phase liquid and vapor mixture form if the heat flux is close to nominal design value. The refrigerant in the plate A2 with hard corrugation angle of 63° had about 15 to 35°F (8 to 19°C) of sub-cooling at the outlet refrigerant port for the heat flux conditions 1 and 2, respectively. While the refrigerant was always sub-cooled at the outlet port for the plate A2, the degree of sub-cooling was quite different for the fouling tests of the plate A1. At increased heat flux condition of $T_{\text{sat}} = 120.2^{\circ}\text{F}$ (49°C) the refrigerant in the A1 plate had initially about 8.5°F (~4.7°C) degree of sub-cooling and it became saturated after about 25 days of run. The water entering temperature and leaving temperature of the condenser was measured experimentally. However, the water temperature entering and leaving the saturated region ($T_{w,1}$ and $T_{w,2}$ in Figure 5-2) is not known, thus the impact of neglecting the refrigerant degree of sub-cooling would not be able to evaluated in this thesis work.

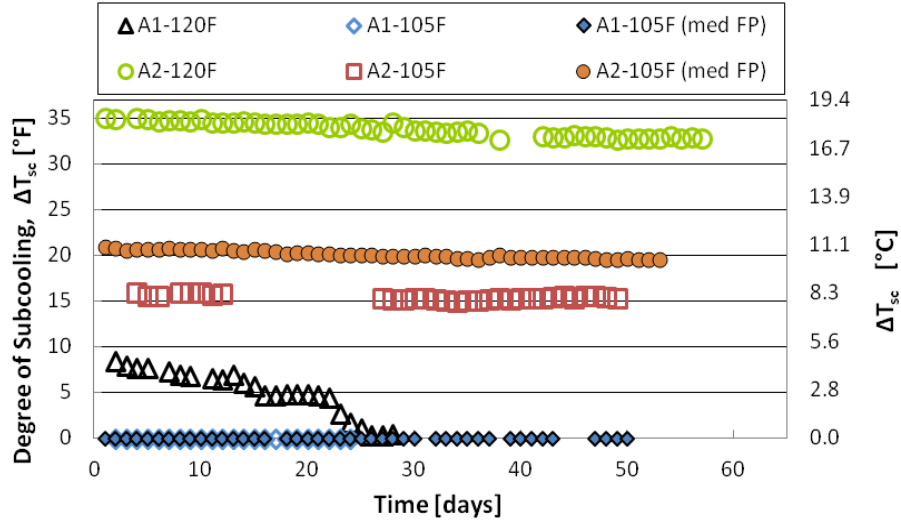


Figure 6-9 Degree of sub-cooling of the refrigerant for the BPHEs in fouling tests

Table 6-1 comparison of measured fouling from approximated LMDT and comprehensive LMDT method

Heat exchanger	Fouling resistance from Approximated method [hr-°F-ft ² /Btu]	Fouling resistance from comprehensive method [hr-°F-ft ² /Btu]	Ratio between comprehensive method & approximated method
BPHE-A2	1.02E-04	8.72E-04	8.55
	7.37E-05	1.08E-03	14.65
	9.47E-05	1.24E-03	13.41
	1.20E-04	1.44E-03	12
	3.11E-04	2.95E-03	9.48
BPHE-A1	5.49E-04	3.41E-03	6.21
	7.35E-04	3.83E-03	5.21
	1.09E-03	5.52E-03	5.06
	1.31E-03	6.00E-03	4.58
	2.72E-03	6.64E-03	2.44
Tube-in-tube	2.09E-05	5.00E-05	2.39
	4.00E-05	1.54E-04	3.85
	3.03E-04	1.22E-03	4.02
	1.74E-04	4.84E-04	2.78
	4.42E-04	1.45E-03	3.28

The hydraulic performance of the BPHE is presented in the form of pressure drop penalty factors (PDPF) in Figure 6-10. These PDPFs were calculated according to Eq. (5-12) and they represent the ratio of the waterside pressure drops measured in fouled conditions to the corresponding ones measured in clean conditions. The pressure drops in clean conditions are also shown in legend area in Figure 6-10. BPHE

A1 with a soft corrugation angle of 30° experienced a large pressure drop during the fouling tests, shown as diamond points in Figure 6-10. An increase of the refrigerant saturation temperature ultimately led to warmer plates and promoted local precipitation and particulate fouling on the heat transfer surface. The effect of particulate fouling is visible in the triangles data points shown in Figure 6-10, which were measured in high water fouling potential, corrugation angle of 30° , and high refrigerant saturation temperature of $T_{\text{sat}} = 120.2^\circ\text{F}$ (49°C). This condition was the most severe water scaling conditions during the experiments. The PDPF increases by about 50% during the first 10 days and by more than 11 times with respect to clean conditions in only 30 days of fouling operation of the BPHE A1. The authors speculate that this pressure drop behavior in Figure 6-10 was due to severe localized flow blockages of the mini channels generated within the plates stack inside the BPHE A1. After 20 days of fouling operation, the particulate fouling mechanism accelerated the flow blockage and the pressure drop increased drastically until it exceeded the maximum pumping head of the test set up in about 31 days during the fouling experiment. For the BPHE A2, the increase of the refrigerant saturation temperature from 105.5 to 120.2°F (41 to 49°C) produced a measurable effect on the waterside pressure drop and the pressure drop across the condenser doubled in fouled conditions with respect to initial pressure drop in clean conditions. From the data in Figure 6-10 one could observe that particulate fouling blocked the flow in between the mini channels of the BPHE A2 and small but finite increments of the pressure drop were recorded during the fouling tests. However, the flow blockage of the mini channels inside BPHE A2 was not as severe as the one that occurred for the BPHE A1.

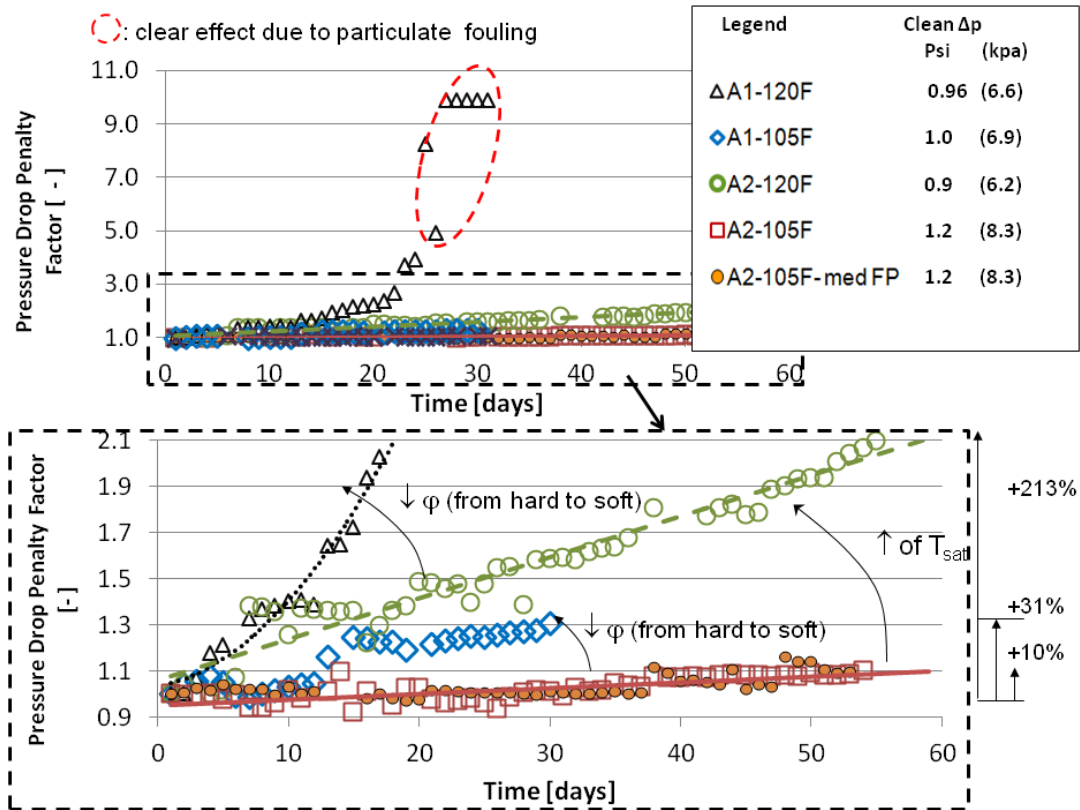


Figure 6-10 Effect of refrigerant temperature and water quality on pressure drop

The heat transfer rate degradation can also be analyzed from the water temperature difference across BPHE condenser. Figure 6-11 shows the water temperature difference versus time, in days, during the fouling tests. Since the entering water temperature and the water flow rate were controlled to be constant for all tests, a decrease of water leaving temperature is equivalent to a decrease in the heat flux in the heat exchanger due to fouling. BPHE-A1 with high fouling potential water showed a sharp temperature drop for increased heat flux conditions (see triangle points in Figure 6-11). The average heat fluxes in clean conditions were about $3,424 \text{ Btu/hr-ft}^2$ ($\sim 11 \text{ kW/m}^2$) at increased heat flux conditions, and after 30 days of fouling operation, the heat fluxes decreased by 28%. Similar trend was observed for the A1 plate with nominal heat flux condition (see solid and hollow diamond data points in Figure 6-11). The BPHE-A2, with a hard corrugation angle of 63° , also experienced a small decrease in the heat flux across the plate and in fouled conditions; the heat flux degradation was within 5% with respect to heat flux in clean

conditions. Both fouling experiments at nominal and increased heat flux conditions showed similar behaviors and the leaving water temperature from the A2 plate decreased by no more than 0.5°F (~0.3°C) in 60 days of fouling operation with both medium and high fouling potential of the cooling tower water.

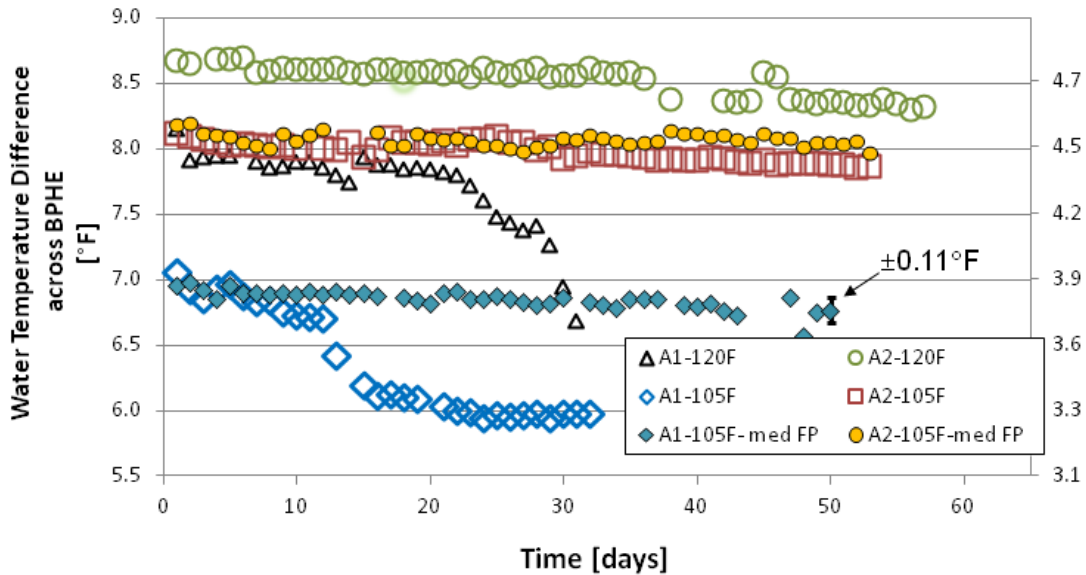


Figure 6-11 Reduction of water leaving temperature in the condenser due to fouling

From the heat transfer data of Figure 6-11 and the waterside pressure drop data previously discussed in Figure 6-10, the authors concluded that the fouling phenomenon is more of a localized type and it impaired the water flow to the channels of the BPHEs rather than the heat transfer rate across the plates. The localized fouling deposit is more likely to occur at the water outlet region of the condenser, where the water is warmer and the surface is hotter. However, this hypothesis could not be confirmed at this time since it was not possible to take a cross section of the BPHEs without destroying the internal stack of plates and removing the deposit material on the surfaces.

The asymptotic fouling resistances were calculated using the following expression, which was originally proposed by Grandgeorge *et al.* (1998)

$$R_f(t) = R_{f,\infty} \cdot \left(1 - e^{-\frac{t}{\tau_c}}\right) \quad (6-2)$$

where R_f is the fouling resistance at time t , $R_{f,\infty}$ is the asymptotic fouling resistance, and τ_c is the time constant. The asymptotic fouling resistances were calculated from the measured fouling resistances and were plotted in Figure 6-12 and Figure 6-13; the values were given in Table 6-2 and Table 6-3, respectively.

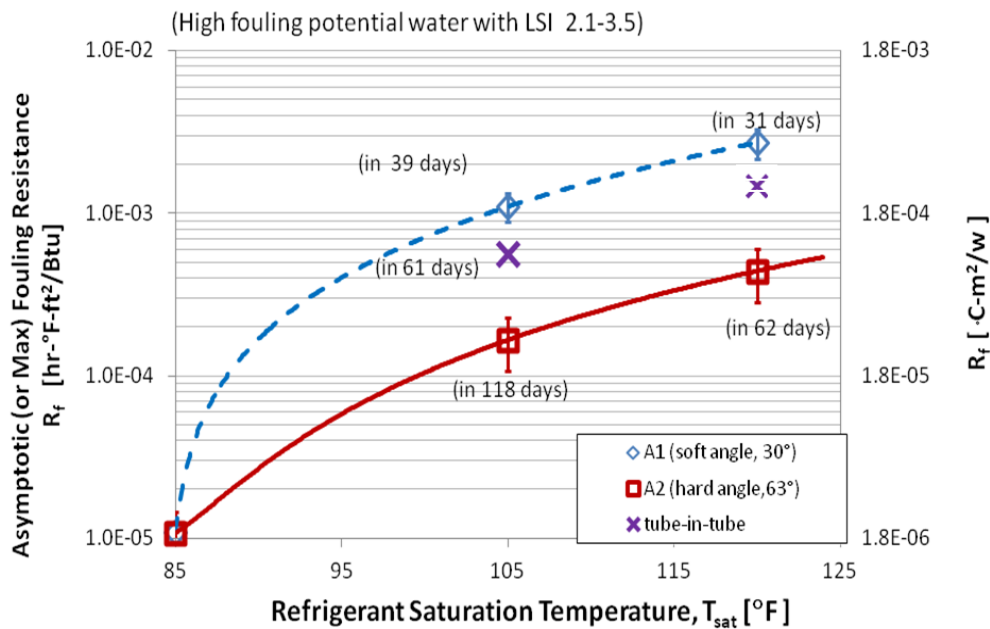


Figure 6-12 Effect of refrigerant saturation temperature on asymptotic fouling resistance (high water fouling potential LSI 2.1 to 3.5)

Figure 6-12 shows the impact of refrigerant saturation temperature on the asymptotic fouling resistance of the BPHEs A1, A2 and the tube-in-tube heat exchanger. All the data presented in Figure 6-12 were obtained from tests with high fouling potential water; the diamond points indicate data collected for BPHE A1, whereas the square data shows the data for BPHE A2 and cross points for the tube. Our instrumentation allowed to measure fouling resistances greater than or at least 1.0×10^{-5} hr-°F-ft²/Btu (1.8×10^{-6} °C-m²/W) and we assumed that this value was the lower limit of fouling resistance in case of little or no scaling occurred.

In Figure 6-12, asymptotic values of the fouling resistance in the case of 105.5°F (41°C) condensing temperature were estimated to be 1.1×10^{-3} hr-°F-ft²/Btu (1.9×10^{-4} °C- m²/W) and about 1.7×10^{-4} hr-°F-ft²/Btu (2.9×10^{-5} °C- m²/W) for BPHEs A1 and A2 with soft and hard corrugation angles, respectively. These asymptotic values would be achieved after about 39 days for the BPHE A1 and after about 118 days for the BPHE A2. The measured fouling resistances at the end of our tests represented about 85% of these asymptotic values. An increase of refrigerant temperature from 105.5 to 120.2°F (41 to 49°C) produced an increase of the asymptotic fouling resistance to 4.5×10^{-4} hr-°F-ft²/Btu (8.0×10^{-5} °C- m²/W) for the A2 plate and this asymptotic value would be achieved in only 62 days instead of 118 days. The asymptotic fouling resistance for the plate A1 at high saturation temperature of 120.2°F (49°C) was taken to be the maximum value of the resistance measured during the fouling test at heat flux condition 2 since the trend for this case was not of asymptotic type. The A1 plate reached a 2.72×10^{-3} hr-°F-ft²/Btu (4.8×10^{-4} °C- m²/W) in about 31 days of operations. The asymptotic fouling resistance of the tube-in-tube heat exchanger was 5.8×10^{-4} hr-°F-ft²/Btu (1.04×10^{-4} °C- m²/W), which is in between BPHE A1 and A2. In this work, the fouling resistance of the tube was experimentally measured at nominal heat flux condition while the fouling resistance at increased heat flux condition was extrapolated from the data based on the results with A1 and A2 plates. This extrapolation point of the fouling resistance for the tubular condenser at increased heat flux condition was shown as the dashed cross in Figure 6-12. It should be noted that the high fouling potential water represent severe scaling conditions which should be avoided by proper water treatment of the cooling tower water.

Table 6-2 Effect of refrigerant saturation temperature on asymptotic fouling resistance

Heat exchanger	BPHE A1($\varphi = 30^\circ$)		BPHE A2($\varphi = 63^\circ$)		TTHE	
	105°F (41°C)	120°F (49°C)	105°F (41°C)	120°F (49°C)	105°F (41°C)	120°F (49°C)
Asymptotic fouling resistance R_f [hr-°F-ft ² /Btu] (m ² -°C/w)	1.1×10^{-3} (1.9×10^{-4})	--	1.7×10^{-4} (3.1×10^{-5})	4.5×10^{-4} (8.1×10^{-5})	5.8×10^{-4} (1.1×10^{-4})	1.5×10^{-3} (3.2×10^{-4})
Time constant, τ_c [days]	39	--	118	62	61	--

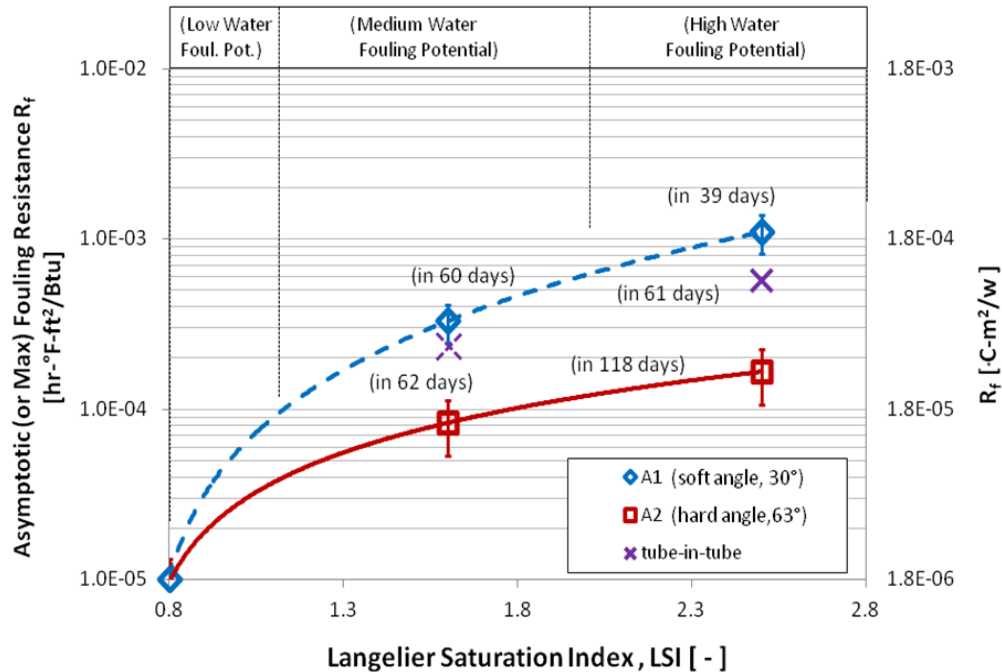


Figure 6-13 Effect of water quality on asymptotic fouling resistance with refrigerant saturation temperature of 1.5.5 °F(41°C)

Figure 6-13 shows the trends of the asymptotic fouling resistances for the two BPHEs A1, A2 and the tube-in-tube heat exchanger with the case of nominal heat flux condition 1 at refrigerant saturation temperature of 105.5°F (~41°C). For the plate A1, an increase of the fouling potential tripled the asymptotic fouling resistance, that is, from 3.3×10^{-4} hr-°F-ft²/Btu (5.8×10^{-5} °C- m²/W) to 1.1×10^{-3} hr-°F-ft²/Btu (1.9×10^{-4} °C- m²/W) for medium and high fouling potential, respectively. For the plate A2 with hard corrugation angle, the asymptotic fouling resistance at medium fouling potential was about 8.5×10^{-5} hr-°F-ft²/Btu (1.5×10^{-5} °C- m²/W); an increase of water fouling potential from medium to high level doubled the fouling resistance. In this thesis, the authors experimentally measured the TTHE performance at high fouling potential water while the fouling resistance at medium fouling potential was extrapolated from the data based on the results with A1 and A2 plates. This extrapolation point of the fouling resistance for the TTHE condenser at medium fouling potential is shown as the dashed cross in Figure

6-13. The trends indicate that water fouling potential has a measurable effect on the fouling performance both for the brazed plate-type condensers and tubular type condenser.

Table 6-3 Effects of water quality on asymptotic fouling resistance

Heat exchanger	BPHE A1($\phi = 30^\circ$)		BPHE A2($\phi = 63^\circ$)		TTHE	
	Med FP	High FP	Med FP	High FP	Med FP	High FP
Asymptotic fouling resistance R_f [hr-°F-ft ² /Btu] (m ² -°C/w)	3.3×10^{-4} (5.9×10^{-5})	1.1×10^{-3} (1.9×10^{-4})	8.5×10^{-5} (1.5×10^{-5})	1.7×10^{-4} (3.1×10^{-5})	2.3×10^{-4} (4.1×10^{-5})	5.8×10^{-4} (1.1×10^{-4})
Time constant, τ_c [days]	60	39	62	118	--	61

6.3 Water loss in cooling tower due to fouling

Fouling formation inside the heat exchangers are strongly dependent on the water quality in cooling tower systems, which is related to the water consumption since fresh make-up water is usually added to dilute the recycled water coming from the cooling tower. The mixing procedure reduces the fouling potential of the water circulating through the condenser.

Fouling tests were conducted on BPHEs A1 and A2 with two corrugation angles and a smooth TTHE that operated as refrigerant condensers. Water with low fouling potential was used in the initial stage of the tests and charged to the system as make-up water. Because of the water evaporation in the cooling tower, water in the system reached medium and high water fouling potentials in 1 to 2 weeks, see Figure 5-1. For the case of high fouling potential (high FP) water, the water loss due to evaporation at the cooling tower was about 88% of the entire water (the total amount of fresh make-up water and reclaimed water) consumed in the cooling tower system at the end of two month period, as shown in Figure 6-14,. The actual water losses in the system ranged from 84% to 93% depending on the geometry of the heat exchanger and refrigerant saturation temperature in the condensers. For the case of medium fouling potential (med FP) water, the water losses were about 83% of the entire water consumed in the cooling tower system and this value was practically independent from the fouling formation. This can be explained with the fact that, in medium fouling potential water application, the impact of fouling thermal

resistance on the water-side cooling capacity was not as significant as for the case of high fouling potential water. In our tests, about 100 gallon of water were initially charged in the cooling tower system and the evaporation rate was about 10 gal/day for medium fouling potential case and 15 gal/day for the case of high fouling potential water. Due to evaporation in the cooling tower loop, minerals contained in recycled water become concentrated and reached the solubility limits.

For the fouling test on a smooth TTBE condenser at high fouling potential water, due to water evaporation in the cooling tower, the amount of Ca^{2+} in the water loop practically increased linearly with time, shown in Figure 6-15. In two weeks without any water treatment, the Ca^{2+} concentration doubled, and the water losses exceed 50% of the total water consumption in the system. After two months of continuous operation, water losses due to evaporation reached about 85% of the total water consumption and the Ca^{2+} concentration increased by more than 6 times. A dilution of the recycled water with more fresh water might have relieved the fouling issues but it would have increased the fresh water usage. Cycle of concentration provides a measure of the accumulation of dissolved minerals in the circulating cooling water. It is defined in Eq. (6-3) and it is practically the ratio of concentration of chlorides in the circulating water and in the make-up water (Beychok, 1952). High cycles of concentration mean high fraction of recycled water from the cooling tower in the main stream that flows through the condenser.

$$cycle = \frac{[Cl^-]_{circulate}}{[Cl^-]_{makeup}} \quad (6-3)$$

In the present fouling experiments on BPHEs and on TTBE, in the case of condensation saturation temperature of 105°F (41°C), the concentration cycles ranged from 4 to 7.3. An increase of condensation temperature from 105°F to 120°F (41°C to 49°C) augmented the cycles of concentration to 14~16.1, because the evaporation rate in the cooling tower was higher when the water temperature entering the cooling tower increased.

In actual cooling tower loops, water treatment plants and filter systems help mitigating the mineral precipitation and particulate fouling, thus the time required to achieve medium or high fouling potential water is usually longer than two months. It was reported that cooling tower could operate at 5 cycles of concentration if fouling inhibitors are used (Betz, 1991). Cycles greater than 5 are sometimes used in regions with water shortages. The cycles of concentration increase yields to higher propensity to mineral precipitation on the heat transfer surfaces where the solubility limits are reached. In order to balance the water consumption and fouling formation in the cooling tower systems, Cho *et al.*, (2006) examined the effect of electronic antifouling technology with a solenoid coil on fouling mitigation in cooling tower systems at high cycles of concentration and they reported that the physical water treatment was able to reduce the fouling resistance by 70% at 5 cycles and by 60% at 10 cycles. Their work was an example of using high cycles of concentration in cooling tower applications and preventing fouling with physical water treatment technology.

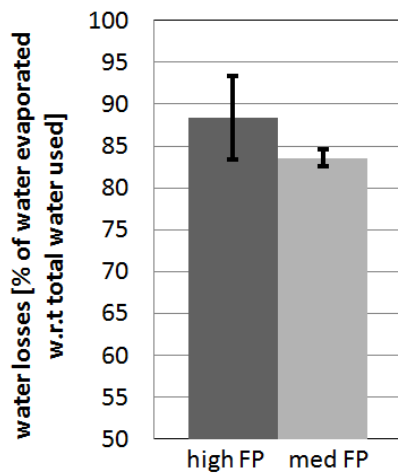


Figure 6-14 Summary of water losses in cooling tower

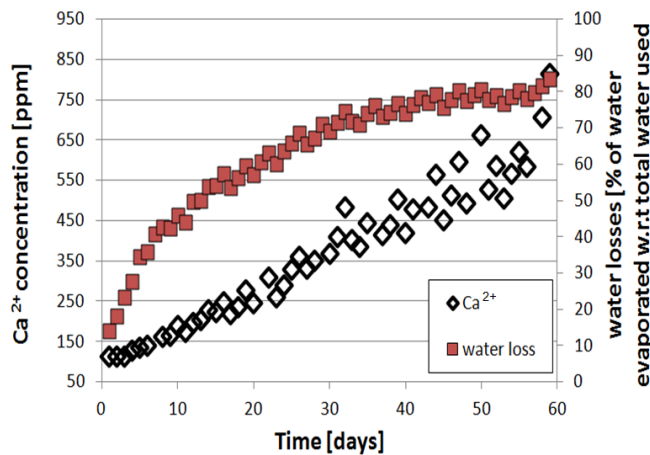


Figure 6-15 Ca²⁺ accumulate due to water loss in smooth tubes

6.4 Application and improvement of existing fouling model

Among the different fouling model approaches in the open literature, a common linear correlation with the format of $R_f = a_0 + a_1x_1 + a_2x_2 + a_3x_3 + \dots + a_nx_n$ was proposed to predict fouling resistance inside heat

exchangers (Wen, *et al.*, 2013; Xu, *et al.*, 2011; Zhang & Wang, 2010), in which $x_1, x_2, x_3, \dots, x_n$ represent parameters such as water chemistry, water velocity, water temperature, etc. The linear correlation proposed in the literature was verified against the experimental work presented in this thesis, and comparison results by applying (Xu, *et al.*, 2011) are shown in Table 6-4. The linear approach tended to overestimate the fouling resistance significantly and it would not capture the asymptotic trend of the fouling formation inside heat exchangers. The model verification proved that the linear correlation does not represent the fouling formation in a general case.

Table 6-4 Fouling model verification of linear correlation

Heat exchanger	Measured $R_f \times 1E4$ ($m^2 \cdot ^\circ C/w$)	Simulated $R_f \times 1E4$ ($m^2 \cdot ^\circ C/w$)	$R_{f_simulated}/R_{f_measured}$
Tube-in-tube	0.209	116.12	555.6
	1.7	266.94	157
	3.27	552.35	168.9
	4.35	675.91	155.4
BPHE A2 (hard angle, 63°)	0.531	164.93	310.6
	0.45	193.08	429.1
	0.761	469.73	617.3
	0.841	529.32	629.4
BPHE A1 (soft angle, 30°)	1.54	73.72	47.9
	1.32	172.1	130.4
	1.98	313.98	158.6
	2.13	484.13	227.3

Another type of semi-empirical fouling model in the literature which considered the chemical dissociation, heat and mass transfer by applying the first principle equations in fouling formation was further verified against our experimental work. The model, which was adapted from the Hasson-Quan model (Hasson, *et al.*, 1978; Quan, *et al.*, 2008), considers the chemical dissociation and the mass transfer processes when a water solution with mineral dissolved is heated and the temperature increases beyond the critical temperature of the solubility limits. The present model was specifically developed for refrigerant condensers used in chiller applications (Wu & Cremaschi, 2013).

In agreement with Kern & Seaton (1959), the governing equation of fouling process is given in Eq. (6-4), where R_f is the fouling resistance, in $m^2\text{-K/W}$, m_d and m_r are the mass of fouling deposited and removed on the heat transfer surface, respectively, in $g/m^2\text{-s}$; and ρ_f and λ_f are the density and thermal conductivity of fouling deposit.

$$\frac{dR_f}{dt} = \frac{m_d - m_r}{\rho_f \lambda_f} \quad (6-4)$$

Hasson *et al.*, (1978) conducted a chemical reaction analysis in acid and alkaline solution to predict the mass of fouling deposit. Since medium and high fouling potential water have pH that ranged from 8.4 to 9.6, the fouling deposit rate in alkaline solutions from (Hasson, *et al.*, 1978) was applied in this model and it yielded to Eq. (6-5). k_{sp} is the solubility product of calcium carbonate and it has a magnitude of $10^{-9} \text{ mol}^2/\text{L}^2$. The precipitation rate coefficient, k_R is temperature dependent and specific to fouling minerals. In section 6.1, a chemical composition analysis was discussed on the fouling deposit. Samples of fouling deposits were taken from the inner surfaces of the TTHE at the end of the experiment and the chemical analysis indicated that more than 85% of the fouling deposit was calcium carbonate while the amount of magnesium, iron, copper, zinc and other elements were less than 5% (Wu & Cremaschi, 2012). Therefore in the present model, calcium carbonate was assumed to be the only chemical species present in the fouling deposit, and it was calculated from Eq (6-6). where R_g is universal gas constant, (1.986 cal/K-mol) and T is water bulk temperature, in K.

$$m_d = k_D [CO_3^{2-}] \frac{1 - \frac{k_{sp}}{[Ca^{2+}][CO_3^{2-}]}}{1 + \frac{k_D}{k_R [CO_3^{2-}]} + \frac{[CO_3^{2-}]}{[Ca^{2+}]}} \quad (6-5)$$

$$\ln k_R = 38.74 - \frac{20700}{R_g T} \quad (6-6)$$

k_D in Eq. (6-5) is the convective diffusion coefficient of calcium carbonate, which was estimated by using Eq. (6-7) from (Quan, *et al.*, 2008), where v is the flow velocity inside the heat exchanger and Re and Sc are Reynolds number and Schmidt number.

$$k_D = 0.023 \cdot v \cdot Re^{-0.17} \cdot Sc^{-0.67} \quad (6-7)$$

In agreement with Quan's model (Quan, *et al.*, 2008) the removal rate of fouling can be expressed by a proportionality law shown in Eq. (6-8), where δ_f is the thickness of fouling deposit.

$$m_r = c_r \rho_f \delta_f^{1.5} \quad (6-8)$$

Since the thickness of fouling is unknown in each test, and $\rho_f \delta_f^{1.5}$ describes the instantaneous mass of fouling deposit, Eq. (6-8) was simplified with Eq. (6-9), where the removal coefficient c_r is shown in Eq. (6-10) and ψ is the deposition strength factor.

$$m_r = c_r m_d \quad (6-9)$$

$$c_r = \frac{0.00212v^2}{\lambda_f^{0.5}\psi} \quad (6-10)$$

Based on the analysis above, by integrating Eq. (6-4) in time, the fouling thermal resistance was predicted. Comparison between the predicted fouling resistance and the experimental data in this thesis are shown in Figure 6-16 to Figure 6-18, in which the fouling tests were conducted on a smooth TTHE and BPHEs with corrugation angle of 63° and 30°, respectively.

Figure 6-16 shows the comparison between experimental data and predicted results in a smooth tube-in-tube heat exchanger, with high fouling potential water. The deposition strength factor is not known and a sensitivity study was conducted by considering that in the experiments the fouling thermal resistance increased asymptotically. Thus, the overall amount of fouling deposited increased but the removal process slowed its rate of increase with time. This means that in Eq. (6-10), the removal coefficient c_r must be in the range of $0 < c_r < 1$. In addition, the fouling thermal resistance must always be greater than zero. These

constraints provided a range of investigation for the deposition strength factor. ψ had a minimum value of 0.002 and while the maximum value has no theoretical constraints, by assessing the root mean square (RMS) error it was found that $\psi = 1$ provided better accuracy of the model, shown in Table 6-5.

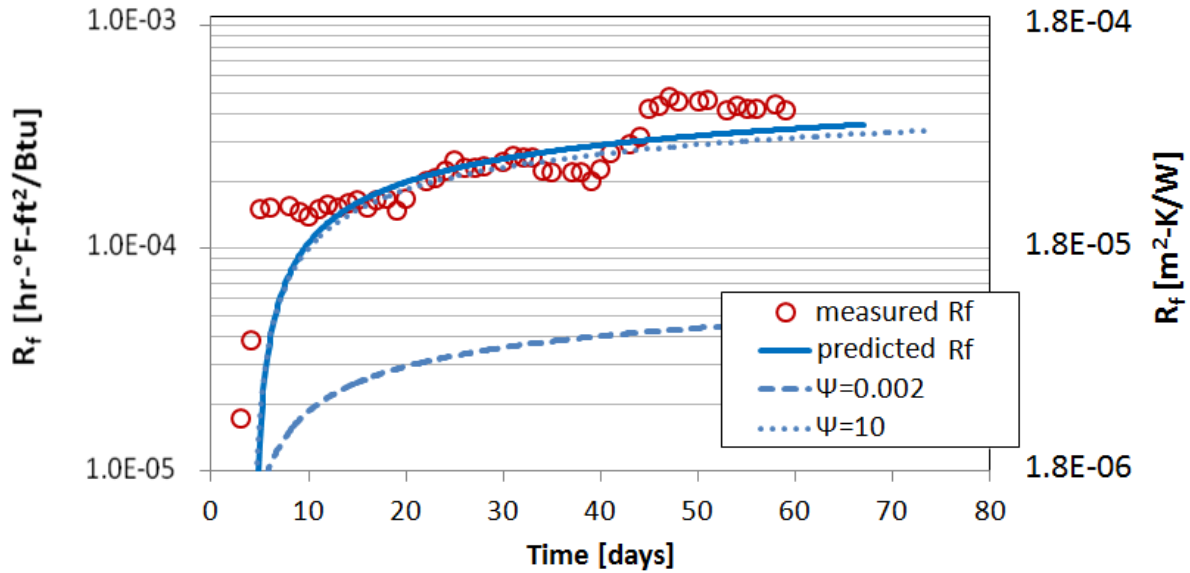


Figure 6-16 Fouling model verification in a smooth tube-in-tube heat exchanger

Table 6-5 Sensitivity analysis of R_f with respect to Ψ

ψ	RMS error $\times 10^5$
0.02	1.5329
1	1.3787
10	1.3795
Correlation in Eq. (6-11)	1.3782

To improve the accuracy further, the authors proposed that the deposition strength factor changed with the deposition thickness because this parameter describes the level of aggregation of the precipitate on the heat transfer surface. In this thesis, the correlation (6-11) was proposed and the corresponding predicted thermal fouling resistance is shown as solid line in Figure 6-16. Then, the same correlation was applied to

all the other cases, that is, for predicting the thermal fouling resistance in BHPEs and for the experimental data from literature.

$$\begin{aligned} \psi(t) &= 1 & t &= 1 \\ \psi(t) &= 0.99 \psi(t - 1) & t &> 1 \end{aligned} \quad (6-11)$$

In Figure 6-16, it is evident that during the first two weeks, the simulation results under predicted the fouling resistance, whereas the simulations and the test data are in good agreement thereafter. It should be noted that, our experiment was designed to initially circulate low fouling potential water in the cooling tower water loop and progressively concentrate the water to high fouling potential in about two weeks. We monitored the water chemistry once a week, and $[Ca^{2+}]$ and $[CO_3^{2-}]$ data between one week and the next one were assumed to vary linearly. Since water chemistry changed rapidly in the first two weeks and then remained fairly constant once it reached high fouling potential condition, it is possible that the assumption of linear variation of the mineral concentration during the first two weeks is not representative. Another observation is that, the present model only considers fouling formation due to precipitation and it did not take into account the particulate fouling. However, as discussed in Figure 6-7, in the first week of fouling test on TTHE, the water side pressure drop across the TTHE increased suddenly, which might have been a sign of localized flow blockage due to particulate fouling. Since the present model did not include particulate fouling, the fact that the simulation results under-predict the fouling resistance data can be expected.

Figure 6-17 shows the comparison of the simulation results with the data for the fouling tests on BPHE with hard corrugation angle of 63° in medium fouling potential water. With respect to the BPHEs with soft corrugation angle of 30° , the tested BPHE with hard corrugation angle had lower propensity to foul, and was less sensitive to mineral particles clogging the channels. The current model under predicted slightly the fouling thermal resistance in the first week. This might be due to the estimation of $[Ca^{2+}]$ and $[CO_3^{2-}]$ during the concentration phase of the circulating water or it might be due to under estimation of ψ

in the initial stage of fouling formation in the model. It is also possible that, the fouling deposition strength factor depends on surfaces energy, particles type and shape, and local flow velocity and shear stress near the wall (Zettler *et al.*, 2005); all these variables were not included in the present model for ψ .

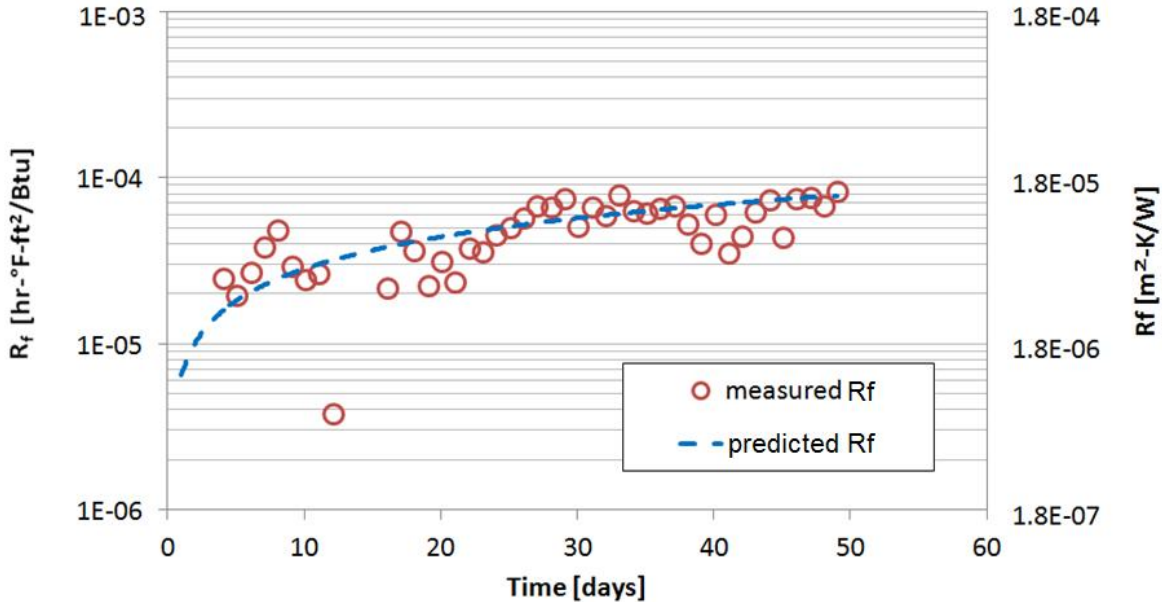


Figure 6-17 Fouling model verification in BPHE ($\varphi=63^\circ$)

Figure 6-18 shows the comparison of the simulation results with the data for the fouling tests on BPHE with a soft corrugation angle of 30° in high fouling potential water. As discussed in Figure 6-12 and Figure 6-13, BPHE A1 with a corrugation angle of 30° had more potential to foul than BPHE A2 with a corrugation angle of 63° , the precipitation fouling blocked the mini channels inside the BPHE or created a barrier for the water flow, so the water velocity increased and shear stress increased accordingly. Once the shear stress is high enough to carry particles away from the fouling deposit, floating particles would appear in the water stream, which is visually observed in this fouling test. The high precipitation rate and removal process promoted the chance of particle attachment and detachment on the heat transfer surface, and lead to severe particulate fouling, so the fouling mechanism in this test is a combination of precipitation fouling and particulate fouling. However, the current model does not taken into account the

particulate fouling and the model tended to under predicted the fouling thermal resistance in the case of severe particulate fouling appearance.

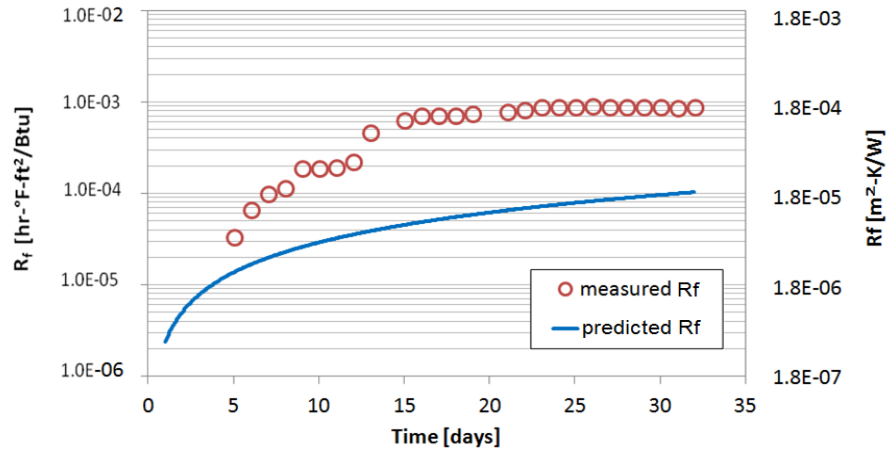


Figure 6-18 Fouling model verification in BPHE ($\varphi=30^\circ$)

Further comparison of the present model was made by considering the fouling test data from the open literature. Figure 6-19 shows the comparison of simulation results and experimental data of Karabelas *et al.*,(1997) in which a BPHE with corrugation angle of 30° was tested in high fouling potential water. Due to the high concentration of Ca^{2+} , the fouling tests only lasted for 220 hours before asymptotic fouling resistance was reached.

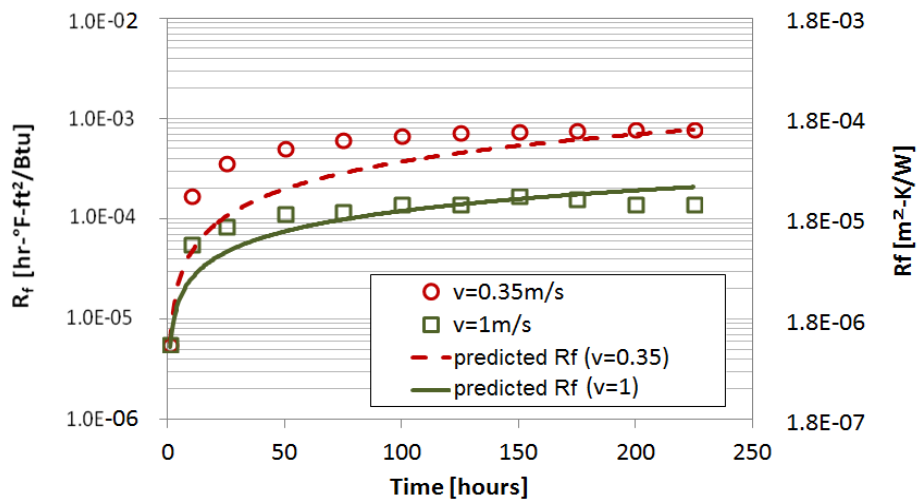


Figure 6-19 Fouling model verification in BPHE ($\varphi=30^\circ$) from literature

In Figure 6-19, the model predicted the asymptotic fouling resistance at different flow velocity and followed similar trends as indicated in the experimental data. Due to limited water chemistry information in the experimental data of Karabelas *et al.*, work, some assumptions on the water chemistry were made and the model underestimated the fouling resistance at the beginning of the fouling tests.

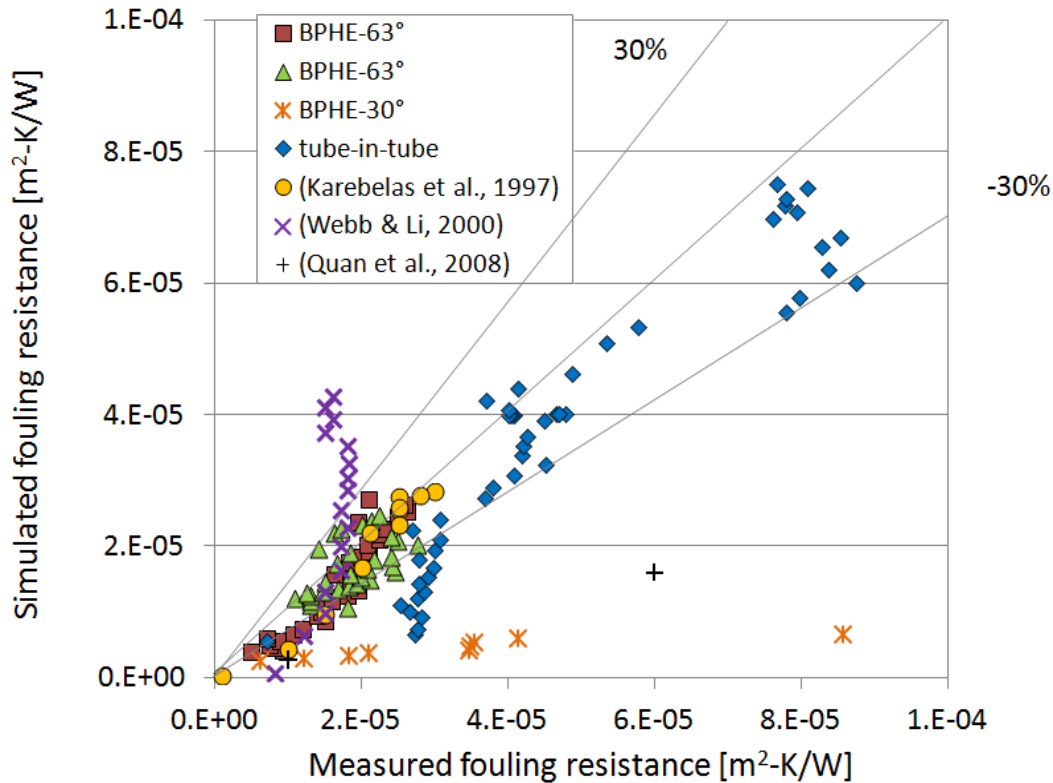


Figure 6-20 Fouling model verification with experimental data

In addition, experimental data on smooth tube in medium fouling potential water from the work of Webb and Li (2000) was also applied to compare the modified Hasson-Quan model, and similar fouling trends were observed, which is the “x” point shown in Figure 6-20. However, since the water chemistry information was limited, the author assumed the mineral concentration remained the same throughout the entire fouling test, due to the inaccurate estimation of the mineral concentration change during the fouling test, the model over predicted the fouling resistance after three weeks of operation.

The experimental work from (Quan, *et al.*, 2008) was finally included in the present comparison of the predicted thermal fouling resistance by the semi-empirical model with data from the literature. The tested fluid in Quan *et al.* had lower pH values and the fouling deposition model based on alkaline solution in the present model tended to under estimate the fouling resistance by 30% to 50% in the first 10 hours and over predicted the fouling resistance thereafter. The overall comparison between the simulation results of the present model and the experiment data from the experimental work in this thesis and from the literature is summarized in Figure 6-20. The present model predicted the fouling thermal resistance within 30% error in average. It generally under-predicted the fouling thermal resistance at the beginning stage of fouling formation and in the case of severe particulate fouling. More detailed information on water chemistry, type of mineral precipitation and local flow velocity near the wall of the heat exchangers might help to improve the accuracy of the present model and further work is needed to incorporate particulate fouling approach and more enhanced geometry into this model.

CHAPTER VII

7 CONCLUSION

7.1 Conclusion from this thesis work

Brazed plate heat exchangers (BPHEs) and tube-in-tube heat exchangers (TTHEs) are commonly used in the refrigeration, air conditioning, and food industry as refrigerant-to-water condensers and they often suffer from severe fouling issues.

In this thesis, two BPHEs with different corrugation angles and a smooth TTHE with the same heat transfer area were experimentally investigated in a small scale 3 ton cooling tower system operating in controlled environmental conditions in a laboratory. Their thermal and hydraulic performance in fouling operating conditions was compared under similar operating conditions. The following conclusions could be drawn from the experimental work discussed in this thesis.

- i. Fouling resistance in BPHEs varies with different corrugation angles and this was due to different local velocity and internal turbulence intensity of the water stream inside the plates. Under the same test condition, the fouling resistance in TTHE was higher than BPHE with a hard corrugation angle but lower than BPHEs with a soft corrugation angle. The hydraulic performance of TTHE is more close to BPHEs with a hard corrugation angle of 63° .
- ii. Fouling deposits on the TTHE was sampled and chemical analysis revealed that more than 85% of the fouling was calcium carbonate while the amount of iron, copper and zinc were within 5%. The mineral precipitation mass flux was practically the same for the entire

system and the analysis provided an order of magnitude of the mineral precipitation mass flux for the case of high water fouling potential.

- iii. The effects of refrigerant condensation were experimentally investigated and asymptotic values of the fouling resistance were determined. Two refrigerant saturation temperatures of 105.5 and 120.2°F (~41 and ~49°C) were set in extensive controlled laboratory fouling experiments and they were representative of two heat flux conditions across the plates of the brazed-plate type condensers. Both heat flux and wall plate surface temperature were responsible for mineral scaling and particulate fouling of the BPHEs. Soft corrugation angles (30°) of the plates were quite sensitive to these factors and an increase of the condensation temperature critically impaired the operation. For BPHE with hard corrugation angles (63°), the fouling resistance was still a function of refrigerant saturation temperature but the degradation of the heat flux was only a few percents. We observed that the fouling of the BPHEs affected the waterside pressure drops and might cause a severe flow blockage of the mini channels formed within the plate stacked inside the heat exchanger. Measured pressure drops in fouled conditions were from 10% to 11 times higher than the corresponding pressure drops in clean conditions.
- iv. Water quality, measured by the Langelier saturation index to define a fouling potential of the cooling tower water, had a measurable effect on the fouling resistance of the BPHEs. High fouling potential water, which is representative of strong to severe scaling conditions, increased the asymptotic fouling resistance by as much as three times compared to asymptotic fouling resistance derived for the cases of medium fouling potential of the cooling tower water.

Fouling models in the literature were studied and verified against the experimental work in this thesis. One common approach to predict fouling formation proposed in literature was applying linear correlation with the format of $R_f = a_0 + a_1x_1 + a_2x_2 + a_3x_3 + \dots + a_nx_n$, in which x_1, x_2, x_3, \dots represent water

chemistry information, water temperature, water velocity, etc. The model validation proved that this type of linear correlation does not represent fouling formation inside heat exchangers in the general case.

A semi-empirical model for the species dissociation and mineral precipitation on the heat transfer surfaces in the literature was further verified against the experimental work in this thesis as well as in the literature. Since mineral solubility varies according to the pH of the solution, the chemical reaction in the fouling model needs to be properly considered. Information on the type of mineral precipitation and local flow velocity near the internal walls of the heat exchanger are keys to obtain an accurate prediction on fouling resistance, thus this information needs to be intensively monitored, documented, and reported in future fouling experiments.

Deposition strength factor is a parameter in computing the fouling removal rates in the present fouling model. Very limited work exists in the literature and this parameter was estimated from one test in the present work. By applying the same fouling deposition strength factor to all the other tests in this thesis as well as in the literature, the semi-empirical model would be able to predict the fouling thermal resistance with an average error of 30%. The present model can be considered simple but accurate enough for engineering application. However, this model was not verified against more enhanced geometries in tubular heat exchangers, and it tended to under estimate the fouling resistance in the case of severe particulate fouling since it did not include particulate fouling approach in fouling formation, thus these factors should be incorporated into the model in future work.

7.2 Recommendations for future work

During the fouling tests in this thesis work, floating particles were visually observed in the cooling tower water loop. And the author speculated that the sudden increase in the measured fouling resistance and pressure drop is due to severe particulate fouling and particle blockage inside the mini channels. In order to verify this speculation, we can measure the size of the floating particles in the water stream,

and inject particles with similar size into low fouling potential water for future fouling studies. Since slight or no precipitation fouling is expected in low fouling potential water, if the sudden increase in fouling resistance and pressure drop could be replicated, the speculation would be verified. In addition, for the test conducted on BPHEs with a hard corrugation angle of 63° with high fouling potential water, a lot of scattered data was observed in the pressure drop for the first 20 days of operation, and some of the pressure drop data was even lower than the initial value. The author speculated that it might be due to the high uncertainty in the measurement or due to particle contamination coming from the rest of the test set up at the beginning of the fouling test. Thus, its measured pressure drop in clean conditions might have been a worst case estimate. For future reference, pressure drop measurement by applying a differential pressure transducer with a smaller working range and better accuracy might help to confirm this speculation.

Based on the experiences with the current fouling tests and results, some recommendations on the experimental procedures are proposed. On the one hand, the procedure of fouling deposition mass flux measurement needs to be improved. By assessing the amount of fouling deposit on the surface of the cap located at the end of the smooth tube, the fouling precipitation mass flux inside the test heat exchanger was estimated in this thesis. However, the cap is not heated up by refrigerant directly; the fouling precipitation rate on the cap could be lower than that inside the heat exchanger. In future work, it is suggested to weigh the test heat exchanger, water pumps, heaters, water tanks, copper pipes and other necessary components in the cooling tower water loop before and after the fouling tests to determine the amount of fouling deposition in each component.

On the other hand, more intensive monitor on the mineral concentration contained in the water is required. During the fouling tests conducted in this thesis work, water was sample once a week to measure the change of mineral concentration, and this information was applied as input values in fouling model verification. Particularly, the mineral concentration change from one week to the next

was assumed to be linear and this assumption is not accurate enough in fouling resistance prediction. So, it is recommended that the measurement of mineral concentration in future fouling tests should be more intensive and the change of mineral concentration during the fouling tests needs to be reported together with the data measurement.

In this thesis, LSI is applied to evaluate water fouling potential, which is a function of total dissolved solid, water temperature, concentration of calcium ions and alkalinity. An observation was made during the fouling tests: inside the cooling tower, due to aeration effect, more carbon dioxide was introduced and the concentration of carbonate ions increased, leading to a localized increase in the fouling deposition. However, the quantification of the carbonate concentration was not included in the current water quality evaluation, and needs to be incorporated in the future work. Another short coming of LSI is that, it uses total dissolved solid to represent the total amount of elemental ions dissolved in the water solution instead of referring to the specific ions. If the LSI can be more specific to the involving ions, it would be helpful to determine the corresponding anti-fouling agent, such as phosphate in the case of calcium precipitation. In addition, water with and without corresponding anti-fouling agents could be applied as control groups for future fouling tests to investigate the effect of fouling inhibitors.

Researchers proposed that the precipitation fouling has an induction period of 3-4 days, in which crystal nucleation sites start to establish before mineral precipitation (Webb & Li, 2000; Zan, *et al.*, 2009). And the induction period is affected by the roughness of the surface (Hasson, 1997). Since the fouling mechanism in the current work is a combination of precipitation and particulate fouling, no apparent effects of induction period was observed in the fouling curve. In future fouling studies, the employment of filtration system, might help to isolate precipitation fouling and particulate fouling; applying different surface materials with and without coating would help determine the role of the surface on the precipitation process.

Counter flow is commonly applied inside heat exchangers in industry to increase heat transfer rate. However, the promotion of heat transfer rate would lead to a higher water temperature, which ultimately leads to more fouling deposition. In future fouling studies, parallel flow can be included in the control group, to seek a balance in heat transfer rate and fouling formation inside the heat exchangers.

REFERENCE

- AHRI. 1997. AHRI Guideline E - Fouling Factors: A Survey of Their Application in Today's Air Conditioning and Refrigeration Industry. Arlington, VA, USA: Air-Conditioning, Heating and Refrigeration Institute.
- AHRI. 2007. AHRI Standard 450 - Performance rating of water-cooled refrigerant condensers. Arlington, VA, United States.
- Al-Rawajfeh, A. E., & Al-Shamaileh, E. M., 2007. Assessment of tap water resources quality and its potential of scale formation and corrosivity in Tafila Province, South Jordan. *Desalination*, 206(1-3), 322-332.
- Andritsos, N., & Karabelas, A. J., 2003. Calcium carbonate scaling in a plate heat exchanger in the presence of particles. *International Journal of Heat and Mass Transfer*, 46(Compendex), 4613-4627.
- ASHRAE. 2007. 1345-RFP, *Waterside fouling performance of brazed-plate type condensers in cooling tower applications - Request for Proposal: ASHRAE*.
- Awad, M. M., Gad, H. E., & Yousef, A., 2009. *Effect of surface temperature on particulate and crystalline fouling*. In: Proceedings of 13th Int. Water Technology Conference. vol. 1, Hurghada, Egypt, 1431-1442.
- Ayub, Z. H., 2003. Plate heat exchanger literature survey and new heat transfer and pressure drop correlations for refrigerant evaporators. *Heat Transfer Engineering*, v(24), 3-16.
- Bansal, B., & Mueller-Steinhagen, H., 1993. Crystallization fouling in plate heat exchangers. *Journal of Heat Transfer, Transactions ASME*, v(115), 584-591.
- Bansal, B., Muller-Steinhagen, H., & Chen, X. D., 1997. Effect of suspended particles on crystallization fouling in plate heat exchangers. *Journal of Heat Transfer*, 119(Compendex), 568-574.
- Bansal, B., Muller-Steinhagen, H., & Chen, X. D., 2001. Comparison of crystallization fouling in plate and double-pipe heat exchangers. *Heat Transfer Engineering*, v(22), 13-25.
- Benzinger, W., Brandner, J. J., Schygulla, U., & Schubert, K., 2007. *Influence of different surface materials on the fouling process in a microstructured heat exchanger under laminar regime*. In: Proceedings of Heat Exchanger Fouling and Cleaning conference, July 1-6, 2007, Tomar, Portugal.
- Betz. 1991. Handbook of industrial water conditioning, 9th ed. Trevese, PA, USA.
- Beychok, M. R., 1952. How to calculate cooling tower control variables. *Petroleum Processing*, v(7), 1452-1456.
- Brahi, F., Augustin, W., & Bohnet, M., 2003. *Numerical simulation of the fouling on structured heat transfer surfaces*. In: Proceedings of Heat Exchanger Fouling and Cleaning conference, June 5-10, 2005, Kloster Irsee, Germany.
- Chamra, L. M., 2007. *Waterside Fouling Inside Smooth and Augmented Copper-Alloy Condenser Tubes in Cooling Tower Water Applications (1205-TRP)*: Mississippi State University.
- Chamra, L. M., & Webb, R. L., 1993. Effect of particle size and size distribution on particulate fouling in enhanced tubes. *Journal of Enhanced Heat Transfer*, 1(1), 65-75.
- Chamra, L. M., & Webb, R. L., 1994. Modeling liquid-side particulate fouling in enhanced tubes. *International Journal of Heat and Mass Transfer*, v(37), 571-579.
- Cho, Y. I., Kim, W. T., & Cho, D., 2006. Fouling mitigation in a heat exchanger: High cycles of concentration for a cooling-tower application. *Experimental Heat Transfer*, 19(2), 113-128.

- Cho, Y. I., Lee, S., & Kim, W., 2003. *Physical water treatment for the mitigation of mineral fouling in cooling-tower water applications*. In: Proceedings of 2003 ASHRAE Winter Meeting Technical paper, January 26, 2003 - January 29, 2003, Chicago, IL, United states.
- Cremaschi, L., Barve, A., & Wu, X., 2012. Effect of condensation temperature and water quality on fouling of brazed-plate heat exchangers. *ASHRAE Transactions*, 118(PART 1), 1086-1100.
- Cremaschi, L., Spitler, J. D., Lim, E., & Ramesh, A., 2011. Waterside fouling performance in brazed-plate-type condensers for cooling tower applications. *HVAC & R Research*, 17(2), 198-217.
- Flynn, D. J., & Nalco, C. (2009). The Nalco water handbook. from <http://www.knovel.com/knovel2/Toc.jsp?BookID=2799>
- Focke, W. W., Zachariades, J., & Olivier, I., 1985. Effect of the corrugation inclination angle on the thermohydraulic performance of plate heat exchangers. *International Journal of Heat and Mass Transfer*, v(28), 1469-1479.
- Geddert, T., Bialuch, I., Augustin, W., & Scholl, S., 2009. Extending the induction period of crystallization fouling through surface coating. *Heat Transfer Engineering*, 30(10-11), 868-875.
- Grace, S. 2007. *The effect of orthophosphate as a copper corrosion inhibitor in high alkalinity drinking water systems (No. AFIT/GES/ENV/07-M2)*. . Air Force Inst of Tech Wright-Patterson AFB OH School of Engineering and Management.
- Grandgeorge, S., Jallut, C., & Thonon, B., 1998. Particulate fouling of corrugated plate heat exchangers. Global kinetic and equilibrium studies. *Chemical Engineering Science*, 53(17), 3050-3071.
- Haider, S. I., Webb, R. L., & Meitz, A. K., 1991. *Survey of water quality and its effect on fouling in flooded water chiller evaporators*. In: Proceedings of ASHRAE Winter Meeting - Technical Papers, January 19, 1991 - January 23, 1991, New York, NY, USA.
- Hasson, D., 1997. *Progress in precipitation fouling research -- a review*. In: Proceedings of International Conference of Fouling Mitigation of Industrial Heat-Exchange Equipment, Begell House.
- Hasson, D., Sherman, H., & Biton, M., 1978. Prediction of Calcium Carbonate Scaling Rates. v(2), 193-199.
- Hasson, D., & Zahavi, J., 1970. Mechanism of Calcium Sulfate Scale Deposition on Heat-Transfer Surfaces. v(9), 1-10.
- Izadi, M. 2011. *Experimental and numerical investigation of fouling in heat exchangers*. Clarkson University.
- Karabelas, A. J., Yiantsios, S. G., Thonon, B., & Grillot, J. M., 1997. Liquid-side fouling of heat exchangers. An integrated R D approach for conventional and novel designs. *Applied Thermal Engineering*, v(17), 727-737.
- Kern, D. Q., & Seaton, R. E., 1959. A theoretical analysis of thermal surface fouling. *British Chemical Engineering*, 4(5), 258-262.
- Kim, N.-H., & Webb, R. L., 1991. Particulate fouling of water in tubes having a two-dimensional roughness geometry. *International Journal of Heat and Mass Transfer*, 34(11), 2727-2738.
- Knudsen, J. G., & Story, M., 1978. Effect of Heat Transfer Surface Temperature on the Scaling Behavior of Simulated Cooling Tower Water. *AIChE Symposium Series*, v(74), 25-30.
- Langelier, W. F., 1936. The analytical control of anti-corrosion water treatment. *Journal of American Water Works Association*, 28(10), 1500-1521.
- Lim, E. 2010. *A preliminary investigation of fouling in brazed plate heat exchangers*. Unpublished Master Thesis, Oklahoma State University, Stillwater, Oklahoma, US.
- Luan, Z., Zhang, G., Tian, M., & Fan, M., 2008. Flow resistance and heat transfer characteristics of a new-type plate heat exchanger. *Journal of Hydrodynamics*, 20, 524-529.

- Morse, R. W., & Knudsen, J. G., 1977. Effect of alkalinity on the scaling of simulated cooling tower water. *Canadian Journal of Chemical Engineering*, v(55), 272-278.
- Muller-Steinhagen, H. M., & Branch, C. A., 1988. Influence of thermal boundary conditions on calcium carbonate fouling in double pipe heat exchangers. *Chemical engineering and processing*, v 24, 65-73.
- Mwaba, M. G., Golriz, M. R., & Gu, J., 2006a. A semi-empirical correlation for crystallization fouling on heat exchange surfaces. *Applied Thermal Engineering*, 26(4), 440-447.
- Mwaba, M. G., Rindt, C. C. M., Van Steenhoven, A. A., & Vorstman, M. A. G., 2006b. Validated numerical analysis of CaSO₄ fouling. [Jour]. *Heat Transfer Engineering*, 27(7), 50-62.
- Noda, S., Saito, T., Miya, K., Furukawa, S., Clarke, S. M., & Wilson, D. I., 2013. *The influence of phosphate on calcium carbonate formation in hard water*. In: Proceedings of 2013 Heat Exchanger Fouling and Cleaning Conference, June 09- June 16, 2013, Budapest, Hungary.
- Ojamiemi, U., Manninen, M., Pattikangas, T., & Riihimaki, M., 2013. *Effects of turbulence and thermophoresis on particulate fouling in heat exchangers modelled with CFD*. In: Proceedings of 2013 Heat Exchanger Fouling and Cleaning Conference, June 09- June 16, 2013, Budapest, Hungary.
- Palm, B., & Claesson, J., 2006. *Plate heat exchangers: Calculation methods for single and two-phase flow*. In: Proceedings of.
- Pearson. 2003. *Basic Water Treatment Training Material*. Goldsboro, NC: Southeastern Laboratory, Inc.
- Quan, Z. H., Chen, Y. C., & Ma, C. F., 2008. Heat mass transfer model of fouling process of calcium carbonate on heat transfer surface. *Science in China Series E-Technological Sciences*, 51(7), 882-889.
- Ramesh, A. 2010. *An experimental facility to measure fouling resistance in condensers*. Unpublished Master Thesis, Oklahoma State University, Stillwater, OK, US.
- Rother, H. J., Kuron, D., & Storp, S., 1985. *Comparative investigations of corrosion inhibitors for copper*. In: Proceedings of 6th European Symposium on Corrosion Inhibitors, 133rd Manifestation of the European Federation of Corrosion, Proceedings., Ferrara, Italy.
- Somerscales, E. F. C., 1990. Fouling of heat transfer surfaces: an historical review. *Heat Transfer Engineering*, v(11), 19-36.
- Stasiak, J., Collins, M. W., Ciofalo, M., & Chew, P. E., 1996. Investigation of flow and heat transfer in corrugated passages—I. Experimental results. *International Journal of Heat and Mass Transfer*, 39(1), 149-164.
- Taborek, J., Aoki, T., Ritter, R. B., Palen, J. W., & Knudsen, J. G., 1972a. Fouling. The major unresolved problem in heat transfer. *Chemical Engineering Progress*, 68(Compendex), 59-67.
- Taborek, J., Aoki, T., Ritter, R. B., Palen, J. W., & Knudsen, J. G., 1972b. Predictive methods for fouling behavior. *Chemical Engineering progress*, 68(7), 69-78.
- Taylor, B. N., & Kuyatt, C. E., 1994. *Guidelines for evaluating and expressing the uncertainty of NIST measurements results*. Washington, D. C.: National Institute of Standards and Technology.
- TEMA. 2007. TEMA Standards 9th Edition - Tubular Exchanger Manufacturers Association, Recommended Good Practice - T-2 Fouling. Tarrytown, NY: TEMA.
- Thonon, B., Grandgeorge, S., & Jallut, C., 1999. Effect of geometry and flow conditions on particulate fouling in plate heat exchangers. *Heat Transfer Engineering*, v(20), 12-24.
- Walker, R., 1976. Corrosion Inhibition of Copper by Tolyriazole. *Corrosion*, v(32), 339-341.
- Webb, R. L., 1994. *Principles of heat transfer*. New York, N.Y: Wiley & Sons.
- Webb, R. L., & Li, W., 2000. Fouling in enhanced tubes using cooling tower water Part I: Long-term fouling data. *International Journal of Heat and Mass Transfer*, v(43), 3567-3578.

- Webb, R. L., Narayanamurthy, R., & Thors, P., 2000. Heat transfer and friction characteristics of internal helical-rib roughness. *Journal of Heat Transfer-Transactions of the Asme*, 122(1), 134-142.
- Wen, X. Q., Xu, Z. M., Wang, J. G., & Sun, L. F., 2013. Forecasting and discussing of the fouling characteristic of the plain tube. *Advanced Materials Research*, 668(v), 949-953.
- Wu, X., & Cremaschi, L., 2012. *Thermal and chemical analysis of fouling phenomenon in condensers for cooling tower applications*. In: Proceedings of 14th International Refrigeration and Air Conditioning conference at Purdue, Paper No.2198, July 16, 2012 - July 19, 2012, West Lafayette, Indiana, United States
- Wu, X., & Cremaschi, L., 2013. *Effect of fouling on the thermal performance of condensers and on the water consumption in cooling tower systems*. In: Proceedings of 2013 Heat Exchanger Fouling and Cleaning Conference, June 09- June 16, 2013, Budapest, Hungary.
- Xu, D., & Knudsen, J. G., 1986. Functional Correlation of Surface Temperature and Flow Velocity on Fouling of Cooling-Tower Water. *Heat Transfer Engineering*, 7(1-2), 63-71.
- Xu, Z., Wen, X., Zheng, J., Guo, J., & Huang, X., 2011. Cooling water fouling resistance prediction of plate heat exchanger based on partial least-squares regression. *Huagong Xuebao/CIESC Journal*, 62(6), 1531-1536.
- Zan, C., Shi, L., & Ou, H., 2009. Effects of temperature and velocity on fouling by municipal secondary effluent in plate heat exchangers. *Qinghua Daxue Xuebao/Journal of Tsinghua University*, 49(2), 240-243.
- Zdaniuk, G. J., Chamra, L. M., & Mago, P. J., 2008. A survey of cooling tower water quality for condenser tube fouling potential. *Proceedings of the Institution of Mechanical Engineers, Part A: Journal of Power and Energy*, 222, 111-122.
- Zettler, H. U., Wei, M., Zhao, Q., & Muller-Steinhagen, H., 2005. Influence of surface properties and characteristics on fouling in plate heat exchangers. *Heat Transfer Engineering*, 26(2), 3-17.
- Zhang, Y., & Wang, Y., 2010. Prediction of condenser fouling based on locally weighted partial least squares regression algorithm. *Yi Qi Yi Biao Xue Bao/Chinese Journal of Scientific Instrument*, 31(2), 299-304.

APPENDICES

Appendix A Fouling tests results summary

Eight fouling tests were conducted on BPHEs and THE in this thesis, the test matrix is shown in **Error! reference source not found.** and a quick overview of the test results are given below.

Figure A - 1 Summary of fouling tests results

Test No.	Description	Water fouling potential	Ref. saturation temperature [°F] (°C)	Time [days]	Fouling resistance measured [ft ² -°F/Btu] (m ² -°C/w)	Asymptotic fouling resistance [ft ² -°F/Btu] (m ² -°C/w)
1*	A1-105F	High	105 (40)	30	1.0×10 ⁻³ (1.8×10 ⁻⁴)	1.1×10 ⁻³ (1.9×10 ⁻⁴)
2*	A2-105F	High	105 (40)	49	1.3×10 ⁻⁴ (2.4×10 ⁻⁵)	1.7×10 ⁻⁴ (3.1×10 ⁻⁵)
3	A2-120F	High	120 (49)	57	3.6×10 ⁻⁴ (6.5×10 ⁻⁵)	4.5×10 ⁻⁴ (8.1×10 ⁻⁵)
4	A1-120F	High	120 (49)	31	2.7×10 ⁻³ (4.9×10 ⁻⁴)	--
5	A1-105F- med FP	Medium	105 (40)	50	2.4×10 ⁻⁴ (4.3×10 ⁻⁵)	3.3×10 ⁻⁴ (5.9×10 ⁻⁵)
6	A2-105F-med FP	Medium	105 (40)	53	7.5×10 ⁻⁵ (1.4×10 ⁻⁵)	8.5×10 ⁻⁵ (1.5×10 ⁻⁵)
7	A1-105F-repeat	High	105 (40)	32	9.1×10 ⁻⁴ (1.6×10 ⁻⁴)	1.1×10 ⁻³ (2.0×10 ⁻⁴)
8	Tube-in-tube	High	105 (40)	59	4.8×10 ⁻⁴ (8.6×10 ⁻⁵)	5.8×10 ⁻⁴ (1.1×10 ⁻⁴)

*: Tests adapted from (Lim, 2010)

Appendix B water sample report

The water sample report from SWFAL (Soil, Water & Forage Analytical Laboratory) in Oklahoma State University for all the fouling tests were listed below.

Table B - 1 Water sample report for Test No. 1 (A1-105F)

time	Fouling Potential	Total Hardness	Calcium (as CaCO ₃)	Magnesium (as CaCO ₃)	M-Alkalinity (as CaCO ₃)	P-Alkalinity (as CaCO ₃)	Chloride (ppm)	Sulfate (ppm)
Day 1	low	291	71	28	81	4	141	114
Day 5	medium	602	142	60	144	10	357	251
Day 8	medium	291	135	50	172	18	327	228
Day 25	high	433	254	90	262	59	254	418
time	Fouling Potential	Sodium (ppm)	Iron (ppm)	Copper* (ppm)	pH	Total Dissolved Solid (ppm)	EC (µS/cm)	LSI (-)
Day 1	low	63	<0.1	NA	8.4	622	942	0.8
Day 5	medium	134	<0.1	NA	8.4	1272	1927	1.34
Day 8	medium	130	<0.1	NA	8.8	1294	1960	1.99
Day 25	high	211	<0.1	NA	9.0	2369	3590	2.75

Table B - 2 Water sample report for Test No. 2 (A2-105F)

time	Fouling Potential	Total Hardness	Calcium (as CaCO ₃)	Magnesium (as CaCO ₃)	M-Alkalinity (as CaCO ₃)	P-Alkalinity (as CaCO ₃)	Chloride (ppm)	Sulfate (ppm)
Day 1	low	207	47	22	207	13	142	89
Day 10	medium	285	57	35	196	76	208	162
Day 15	medium	260	58	28	233	77	399	339
Day 28	high	567	85	84	204	58	569	422
time	Fouling Potential	Sodium (ppm)	Iron (ppm)	Copper* (ppm)	pH	Total Dissolved Solid (ppm)	EC (µS/cm)	LSI (-)
Day 1	low	44	<0.1	NA	8.6	523	793	0.6
Day 10	medium	87	<0.1	NA	8.5	869	1316	1.78
Day 20	medium	154	<0.1	NA	8.6	1769	2680	1.88
Day 28	high	192	<0.1	NA	9.2	2158	3270	3.23

Table B - 3 Water sample report for Test No. 3 (A2-120F)

time	Fouling Potential	Total Hardness	Calcium (as CaCO ₃)	Magnesium (as CaCO ₃)	M-Alkalinity (as CaCO ₃)	P-Alkalinity (as CaCO ₃)	Chloride (ppm)	Sulfate (ppm)
Day 1	low	200	53	16	68	10	118	64
Day 14	medium	250	13	53	267	33	408	241
Day 35	high	362	40	85	799	156	838	517
Day 47	high	572	40	136	1105	236	1391	828
Day 54	high	698	62	166	1475	328	1652	1009
time	Fouling Potential	Sodium (ppm)	Iron (ppm)	Copper* (ppm)	pH	Total Dissolved Solid (ppm)	EC (µS/cm)	LSI (-)
Day 1	low	50	<0.1	NA	8.2	440	667	0.5
Day 14	medium	169	<0.1	NA	8.8	1670	2530	1.67
Day 35	high	295	<0.1	NA	9.5	3650	5530	2.52
Day 47	high	533	<0.1	NA	9.5	5550	8230	2.61
Day 54	high	674	<0.1	NA	9.5	6957	10290	2.78

Table B - 4 Water sample report for Test No. 4 (A1-120F)

time	Fouling Potential	Total Hardness	Calcium (as CaCO ₃)	Magnesium (as CaCO ₃)	M-Alkalinity (as CaCO ₃)	P-Alkalinity (as CaCO ₃)	Chloride (ppm)	Sulfate (ppm)
Day 3	medium	759	8	180	1371	330	1716	1054
Day 9	high	647	55	154	1350	350	1656	974
Day 15	high	765	70	182	1813	348	1947	1167
Day 25	high	687	80	162	1814	417	1900	1094
time	Fouling Potential	Sodium (ppm)	Iron (ppm)	Copper* (ppm)	pH	Total Dissolved Solid (ppm)	EC (µS/cm)	LSI (-)
Day 1	medium	684	<0.1	NA	9.3	6869	10130	1.81
Day 9	high	649	<0.1	NA	9.6	6640	10060	2.1
Day 15	high	740	<0.1	NA	9.3	7971	11690	2.5
Day 25	high	717	<0.1	NA	9.5	7900	11030	2.6

Table B - 5 Water sample report for Test No. 5 (A1-105F-med)

time	Fouling Potential	Total Hardness	Calcium (as CaCO ₃)	Magnesium (as CaCO ₃)	M-Alkalinity (as CaCO ₃)	P-Alkalinity (as CaCO ₃)	Chloride (ppm)	Sulfate (ppm)
Day 4	Low	347	92	28	91	10	211	100
Day 7	medium	345	67	43	160	7	364	198
Day 20	medium	533	97	71	226	23	522	405
Day 33	medium	772	130	109	289	28	837	586
Day 47	medium	802	115	126	315	23	884	603
time	Fouling Potential	Sodium (ppm)	Iron (ppm)	Copper* (ppm)	pH	Total Dissolved Solid (ppm)	EC (μS/cm)	LSI (-)
Day 4	Low	77	<0.1	NA	8.3	643	974	0.5
Day 7	medium	150	<0.1	NA	8.6	1251	1895	1.1
Day 20	medium	231	<0.1	NA	8.6	1947	2950	1.53
Day 33	medium	328	<0.1	NA	8.5	2746	4160	1.84
Day 47	medium	373	<0.1	NA	8.4	2896	4360	1.85

Table B - 6 Water sample report for Test No. 6 (A2-105F-med)

time	Fouling Potential	Total Hardness	Calcium (as CaCO ₃)	Magnesium (as CaCO ₃)	M-Alkalinity (as CaCO ₃)	P-Alkalinity (as CaCO ₃)	Chloride (ppm)	Sulfate (ppm)
Day 2	Low	234	58	22	76	10	102	89
Day 9	medium	519	122	52	120	15	312	176
Day 16	medium	590	123	69	133	17	354	207
Day 29	medium	980	205	114	176	21	619	363
Day 44	medium	1159	236	139	221	22	752	482
Day 51	medium	1231	265	138	214	24	871	490
time	Fouling Potential	Sodium (ppm)	Iron (ppm)	Copper* (ppm)	pH	Total Dissolved Solid (ppm)	EC (μS/cm)	LSI (-)
Day 2	Low	43	<0.1	NA	8.3	438	663	0.31
Day 9	medium	98	<0.1	NA	8.5	1034	1567	0.51
Day 16	medium	117	<0.1	NA	8.6	1139	1726	1.1
Day 29	medium	198	<0.1	NA	8.6	1763	2660	1.38
Day 44	medium	277	<0.1	NA	8.6	2277	3450	1.6
Day 51	medium	295	<0.1	NA	8.6	2554	3870	1.64

Table B - 7 Water sample report for Test No. 7 (A1-105F-repeat)

time	Fouling Potential	Total Hardness	Calcium (as CaCO3)	Magnesium (as CaCO3)	M-Alkalinity (as CaCO3)	P-Alkalinity (as CaCO3)	Chloride (ppm)	Sulfate (ppm)
Day 1	Low	234	55	23	91	10	126	89
Day 9	medium	246	42	34	170	28	220	139
Day 24	high	343	71	77	408	75	491	319
Day 32	high	461	117	102	427	102	672	427
time	Fouling Potential	Sodium (ppm)	Iron (ppm)	Copper* (ppm)	pH	Total Dissolved Solid (ppm)	EC (µS/cm)	LSI (-)
Day 1	Low	62	<0.1	NA	8.3	491	744	0.38
Day 9	medium	103	<0.1	NA	8.8	826	1252	1.42
Day 24	high	238	<0.1	NA	9.3	2000	3030	2.5
Day 32	high	307	<0.1	NA	9.3	2528	3830	2.7

Table B - 8 Water sample report for Test No. 8 (tube-in-tube)

time	Fouling Potential	Total Hardness	Calcium (as CaCO3)	Magnesium (as CaCO3)	M-Alkalinity (as CaCO3)	P-Alkalinity (as CaCO3)	Chloride (ppm)	Sulfate (ppm)
Day 2	Low	358	83	37	128	15	258	133
Day 9	medium	424	90	49	164	14	336	215
Day 17	medium	526	99	68	215	27	462	342
Day 24	high	670	107	98	272	45	780	504
Day 44	high	756	89	130	473	157	969	631
Day 59	high	711	129	155	568	158	1225	769
time	Fouling Potential	Sodium (ppm)	Iron (ppm)	Copper* (ppm)	pH	Total Dissolved Solid (ppm)	EC (µS/cm)	LSI (-)
Day 1	Low	93	<0.1	NA	8.7	897	1359	0.9
Day 9	medium	140	<0.1	NA	8.5	1142	1727	1.3
Day 17	medium	205	<0.1	NA	8.6	1670	2530	1.47
Day 24	high	313	<0.1	NA	9.0	2470	3640	2.21
Day 44	high	394	<0.1	NA	9.3	3256	4890	3.03
Day 59	high	496	<0.1	NA	9.0	4070	6110	3.18

Appendix C LSI computation

LSI is defined as the difference between actual pH of the water sample and its computed saturation pH, pH_{sat} , which is the pH at which the calcium concentration in a given water sample is in equilibrium with the total alkalinity. In the current work, the saturation pH values were approximated using Eq (2-2) and (2-3).

LSI calculation for each test is listed below. It should be noted that, the water chemistry data were obtained from the SWFAL one time every week, as shown in Table B - 1 to Table B - 8. During the sampling intervals, the daily amounts of Calcium and Magnesium in the cooling tower water loop were calculated from such lab measurements and by estimating the evaporation of water in the loop. This was achieved by directly measuring the daily volumes of water in the tanks in the water loop. The water pH values were measured every day by using an electronic pH meter. All these values were used for the calculation of the daily LSI during the fouling tests and are listed in Table C - 1 to Table C - 8.

Table C - 1 LSI computation for Test No. 1 (A1-105F)

Day	Added Volume (gal)	Added Volume (liter)	Total Volume (gal)	Total Volume (liter)	Added Calcium (mg)	Calcium (ppm)	Added Magnesium (mg)	Magnesium (ppm)	pH	LSI
3	17	64.26	63	238.14	4562.46	109.32	1799.28	43.11	9.31	2.16
4	17	64.26	60	226.8	4562.46	134.90	1799.28	53.20	8.32	1.26
5	18	68.04	65	245.7	4830.84	144.18	1905.12	56.86	9.17	2.14
6	12.5	47.25	60	226.8	3354.75	170.99	1323	67.43	9.36	2.4
7	17.5	66.15	60	226.8	4696.65	191.70	1852.2	75.60	9.28	2.45
8	20	75.6	65	245.7	5367.6	198.80	2116.8	78.40	9.1	2.29
9	17	64.26	63	238.14	4562.46	224.27	1799.28	88.44	9.2	2.44
10	21	79.38	66	249.48	5635.98	236.67	2222.64	93.33	9.5	2.76
11	20	75.6	67	253.26	5367.6	254.33	2116.8	100.30	9.26	2.55
12	22	83.16	67	253.26	5904.36	277.64	2328.48	109.49	9.02	2.31
13	21.5	81.27	67	253.26	5770.17	300.43	2275.56	118.48	9.24	2.61
14	21	79.38	67.5	255.15	5635.98	320.29	2222.64	126.31	9.2	2.59
15	35	132.3	87.5	330.75	9393.3	275.48	3704.4	108.64	9.4	2.73
16	40	151.2	87.5	330.75	10735.2	307.94	4233.6	121.44	8.9	2.28
17	18.5	69.93	67.5	255.15	4965.03	418.64	1958.04	165.10	9.05	2.56
18	32	120.96	69	260.82	8588.16	442.46	3386.88	174.49	9.4	2.69
19	24	90.72	72	272.16	6441.12	447.69	2540.16	176.56	9.05	2.69
20	40	151.2	70	264.6	10735.2	501.06	4233.6	197.60	9	2.74
21	25	94.5	70	264.6	6709.5	526.41	2646	207.6	9.22	2.99

Day	Added Volume (gal)	Added Volume (liter)	Total Volume (gal)	Total Volume (liter)	Added Calcium (mg)	Calcium (ppm)	Added Magnesium (mg)	Magnesium (ppm)	pH	LSI
22	20	75.6	70	264.6	5367.6	546.70	2116.8	215.60	9.29	3.07
23	0	0	50	189	0	765.38	0	301.84	9.1	3.03
24	0	0	48.8	184.464	0	784.20	0	309.26	8.9	2.84
25	0	0	47.6	179.928	0	803.97	0	317.06	8.8	2.75
26	0	0	46.4	175.392	0	824.76	0	325.26	9.1	3.06
27	0	0	45.2	170.856	0	846.66	0	333.89	9.31	3.28
28	0	0	44	166.32	0	869.75	0	343.00	9.2	3.18

Table C - 2 LSI computation for Test No. 2 (A2-105F)

Day	Added Volume (gal)	Added Volume (liter)	Total Volume (gal)	Total Volume (liter)	Added Calcium (mg)	Calcium (ppm)	Added Magnesium (mg)	Magnesium (ppm)	pH	LSI
1	0	0	84	317.52	0	47.00	0	22.00	9.2	1.3
2	0	0	64	241.92	0	61.69	0	28.88	9.3	1.42
3	44.5	168.21	83.5	315.63	7905.87	72.33	3700.62	33.86	9.28	1.59
5	42	158.76	82.5	311.85	7461.72	97.13	3492.72	45.47	9.24	1.68
7	35	132.3	80	302.4	6218.1	120.73	2910.6	56.51	9.21	1.74
9	60	226.8	96.5	364.77	10659.6	129.31	4989.6	60.53	9.5	2.06
12	47.5	179.55	101	381.78	8438.85	145.65	3950.1	68.18	9.4	2.01
14	44.5	168.21	103	389.34	7905.87	163.13	3700.62	76.36	9.6	2.26
17	36	136.08	79	298.62	6395.76	234.11	2993.76	109.58	9.05	2.3
19	56	211.68	100	378	9948.96	211.27	4656.96	98.89	9.22	2.43
21	44	166.32	93	351.54	7817.04	249.40	3659.04	116.74	9.6	2.88
22	0	0	91.8	347.004	0	252.66	0	118.27	9.3	2.84
23	52	196.56	90.6	342.468	9238.32	282.99	4324.32	132.46	9.1	2.75
24	0	0	69	260.82	0	371.57	0	173.93	9.1	3.06
25	40	151.2	82	309.96	7106.4	335.59	3326.4	157.09	9.31	3.28
27	43	162.54	92	347.76	7639.38	321.08	3575.88	150.29	9.66	3.54
29	40	151.2	88	332.64	7106.4	357.04	3326.4	167.13	9.43	3.36
31	31	117.18	86	325.08	5507.46	382.28	2577.96	178.94	9.2	3.16
33	40	151.2	89	336.42	7106.4	390.52	3326.4	182.80	9	2.97
35	38	143.64	90	340.2	6751.08	406.03	3160.08	190.06	9	2.98
37	42	158.76	91	343.98	7461.72	423.26	3492.72	198.12	9.25	3.25
39	38	143.64	90	340.2	6751.08	447.81	3160.08	209.61	9.5	3.53
41	41	154.98	91	343.98	7284.06	464.06	3409.56	217.22	9.3	3.34
43	41	154.98	91	343.98	7284.06	485.24	3409.56	227.13	9.35	3.41
44	34	128.52	91	343.98	6040.44	502.80	2827.44	235.35	9.41	3.49
46	38	143.64	91	343.98	6751.08	522.42	3160.08	244.54	9.38	3.47
48	36	136.08	91	343.98	6395.76	541.02	2993.76	253.24	9.4	3.49
50	41	154.98	91	343.98	7284.06	562.19	3409.56	263.15	9.4	3.51
51	28	105.84	91	343.98	4974.48	576.65	2328.48	269.92	9.43	3.54
53	39	147.42	91	343.98	6928.74	596.80	3243.24	279.35	9.38	3.53

Table C - 3 LSI computation for Test No. 3 (A2-120F)

Day	Added Volume (gal)	Added Volume (liter)	Total Volume (gal)	Total Volume (liter)	Added Calcium (mg)	Calcium (ppm)	Added Magnesium (mg)	Magnesium (ppm)	pH	LSI
1	50	189	97	366.66	2457	19.70	10017	80.32	9.35	1.31
2	0	0	82	309.96	0	23.30	0	95.01	9.46	1.5
3	0	0	67	253.26	0	28.52	0	116.28	9.55	1.67
4	0	0	55	207.9	0	34.75	0	141.65	9.65	1.86
5	43.5	164.43	96.5	364.77	2137.59	25.66	8714.79	104.63	9.56	1.64
6	0	0	95.5	360.99	0	25.93	0	105.72	9.7	1.78
7	0	0	82	309.96	0	30.20	0	123.13	9.42	1.57
8	0	0	65	245.7	0	38.10	0	155.33	9.68	1.93
9	46	173.88	100	378	2260.44	30.75	9215.64	125.35	9.46	1.62
10	0	0	84	317.52	0	36.60	0	149.22	9.32	1.55
11	0	0	78	294.84	0	39.42	0	160.70	9.72	1.98
12	0	0	67	253.26	0	45.89	0	187.08	9.32	1.65
13	45	170.1	97	366.66	2211.3	37.73	9015.3	153.81	9.28	1.53
14	0	0	87	328.86	0	42.06	0	171.49	9.38	1.67
15	0	0	77	291.06	0	47.53	0	193.76	9.37	1.79
16	0	0	62	234.36	0	59.02	0	240.64	9.3	1.81
17	51	192.78	99	374.22	2506.14	43.66	10217.34	178.01	9.35	1.77
18	0	0	90	340.2	0	48.03	0	195.81	9.37	1.82
19	0	0	77	291.06	0	56.14	0	228.86	9.36	1.85
21	0	0	62	234.36	0	69.72	0	284.23	9.33	1.91
22	41	154.98	85	321.3	2014.74	57.12	8213.94	232.89	9.35	1.85
23	0	0	75.5	285.39	0	64.31	0	262.19	9.36	1.91
24	0	0	59.5	224.91	0	81.61	0	332.70	9.33	1.98
25	42	158.76	85	321.3	2063.88	63.55	8414.28	259.08	9.37	1.95
26	0	0	72	272.16	0	75.02	0	305.85	9.33	1.97
27	0	0	59.5	224.91	0	90.78	0	370.11	9.33	2.03
28	66	249.48	103	389.34	3243.24	60.77	13222.44	247.76	9.49	2.01
29	0	0	92	347.76	0	68.04	0	277.39	9.45	2.38
30	0	0	72	272.16	0	86.94	0	354.44	9.42	2.46
31	0	0	59	223.02	0	106.09	0	432.53	9.48	2.61
32	0	0	45	170.1	0	139.10	0	567.10	9.33	2.57
33	57.5	217.35	87	328.86	2825.55	80.54	11519.55	328.36	9.38	2.39
34	0	0	72	272.16	0	97.32	0	396.76	9.38	2.47
35	0	0	57	215.46	0	122.93	0	501.18	9.33	2.52
36	47	177.66	91	343.98	2309.58	83.71	9415.98	341.30	9.4	2.42
38	20	75.6	90	340.2	982.8	87.53	4006.8	356.87	9.32	2.37
42	0	0	87	328.86	0	90.55	0	369.17	9.34	2.53
43	30	113.4	95	359.1	1474.2	87.03	6010.2	354.82	9.32	2.37
44	30	113.4	102	385.56	1474.2	84.88	6010.2	346.06	9.34	2.41
45	25	94.5	107	404.46	1228.5	83.95	5008.5	342.27	9.31	2.35
46	20	75.6	88	332.64	982.8	105.03	4006.8	428.22	9.35	2.48
47	20	75.6	91	343.98	982.8	104.43	4006.8	425.75	9.32	2.61
48	20	75.6	109	412.02	982.8	89.57	4006.8	365.17	9.32	2.51
49	40	151.2	105	396.9	1965.6	97.93	8013.6	399.27	9.32	2.55

Day	Added Volume (gal)	Added Volume (liter)	Total Volume (gal)	Total Volume (liter)	Added Calcium (mg)	Calcium (ppm)	Added Magnesium (mg)	Magnesium (ppm)	pH	LSI
50	15	56.7	105	396.9	737.1	99.79	3005.1	406.84	9.32	2.55
51	20	75.6	105	396.9	982.8	102.27	4006.8	416.93	9.35	2.59
52	0	0	83	313.74	0	129.37	0	527.45	9.32	2.66
53	40	151.2	107	404.46	1965.6	105.21	8013.6	428.95	9.34	2.71
54	0	0	90	340.2	0	125.09	0	509.98	9.33	2.78
55	40	151.2	111	419.58	1965.6	106.11	8013.6	432.59	9.3	2.68
56	0	0	92	347.76	0	128.02	0	521.93	9.32	2.78
57	40	151.2	113	427.14	1965.6	108.83	8013.6	443.70	9.3	2.69

Table C - 4 LSI computation for Test No. 4 (A1-120F)

Day	Added Volume (gal)	Added Volume (liter)	Total Volume (gal)	Total Volume (liter)	Added Calcium (mg)	Calcium (ppm)	Added Magnesium (mg)	Magnesium (ppm)	pH	LSI
1	40	151.2	113	427.14	1965.6	13.23	8013.6	53.94	9.3	1.74
2	0	0	82	309.96	0	18.23	0	74.33	9.31	1.89
3	40	151.2	67	253.26	1965.6	30.07	8013.6	122.61	9.36	2.11
4	0	0	55	207.9	0	36.64	0	149.36	9.35	2.29
5	20	75.6	96.5	364.77	982.8	23.58	4006.8	96.11	9.35	2
6	0	0	95.5	360.99	0	23.82	0	97.12	9.35	2.01
7	0	0	82	309.96	0	27.74	0	113.11	9.33	2.09
8	0	0	79	298.62	0	28.80	0	117.41	9.37	2.14
9	40	151.2	109	412.02	1965.6	25.64	8013.6	104.54	9.33	2.05
10	0	0	100	378	0	27.95	0	113.95	9.32	2.08
11	10	37.8	90	340.2	491.4	32.50	2003.4	132.50	9.35	2.18
12	0	0	75	283.5	0	39.00	0	159.00	9.38	2.28
13	0	0	72	272.16	0	40.63	0	165.63	9.38	2.3
14	40	151.2	100	378	1965.6	34.45	8013.6	140.45	9.32	2.17
15	40	151.2	116	438.48	1965.6	34.18	8013.6	139.35	9.37	2.29
16	0	0	108	408.24	0	36.71	0	149.68	9.31	2.27
17	0	0	89	336.42	0	44.55	0	181.63	9.33	2.37
18	40	151.2	78	294.84	1965.6	57.50	8013.6	234.42	9.32	2.47
19	0	0	102	385.56	0	43.97	0	179.26	9.3	2.33
20	0	0	90	340.2	0	49.83	0	203.17	9.3	2.39
21	40	151.2	80	302.4	1965.6	62.56	8013.6	255.06	9.35	2.54
22	0	0	109	412.02	0	45.92	0	187.20	9.33	2.43
23	0	0	97	366.66	0	51.60	0	210.36	9.3	2.45
24	20	75.6	102	385.56	982.8	51.62	4006.8	210.44	9.37	2.52
25	20	75.6	111	419.58	982.8	49.77	4006.8	202.93	9.33	2.46
26	0	0	94	355.32	0	58.78	0	239.63	9.33	2.54
27	20	75.6	107	404.46	982.8	54.07	4006.8	220.42	9.31	2.5
28	0	0	97	366.66	0	59.64	0	243.14	9.32	2.53
29	25	94.5	105	396.9	1228.5	58.19	5008.5	237.24	9.33	2.53
30	0	0	95	359.1	0	64.32	0	262.21	9.34	2.59
31	0	0	82	309.96	0	74.51	0	303.78	9.33	2.64

Table C - 5 LSI computation for Test No. 5 (A1-105F-med FP)

Day	Added Volume (gal)	Added Volume (liter)	Total Volume (gal)	Total Volume (liter)	Added Calcium (mg)	Calcium (ppm)	Added Magnesium (mg)	Magnesium (ppm)	pH	LSI
1	28	105.84	123	464.94	9737.28	92.00	2963.52	28.00	8.6	0.81
2	0	0	112	423.36	0	101.04	0	30.75	8.62	0.87
3	0	0	104	393.12	0	108.81	0	33.12	9	1.28
4	0	0	92	347.76	0	123.00	0	37.43	8.72	1.05
5	0	0	88	332.64	0	128.59	0	39.14	8.66	1.01
6	35	132.3	77	291.06	12171.6	188.78	3704.4	57.45	8.68	1.2
7	0	0	100	378	0	145.36	0	44.24	8.67	1.08
8	40	151.2	88	332.64	13910.4	207.00	4233.6	63.00	8.66	1.12
9	0	0	112	423.36	0	162.64	0	49.50	8.62	1.07
10	0	0	98	370.44	0	185.88	0	56.57	8.61	1.12
11	20	75.6	107	404.46	6955.2	187.44	2116.8	57.05	8.67	1.41
12	20	75.6	112	423.36	6955.2	195.50	2116.8	59.50	8.61	1.36
13	0	0	99	374.22	0	221.17	0	67.31	8.62	1.43
14	20	75.6	102	385.56	6955.2	232.71	2116.8	70.82	8.63	1.46
15	40	151.2	123	464.94	13910.4	222.89	4233.6	67.84	8.63	1.44
16	0	0	117	442.26	0	234.32	0	71.32	8.62	1.45
17	0	0	106	400.68	0	258.64	0	78.72	8.63	1.53
18	20	75.6	86	325.08	6955.2	340.19	2116.8	103.53	8.62	1.61
19	0	0	96	362.88	0	304.75	0	92.75	8.63	1.58
20	40	151.2	119	449.82	13910.4	276.77	4233.6	84.24	8.61	1.53
21	0	0	105	396.9	0	313.68	0	95.47	8.61	1.57
22	40	151.2	132	498.96	13910.4	277.39	4233.6	84.42	8.62	1.53
23	0	0	116	438.48	0	315.66	0	96.07	8.67	1.63
24	0	0	101	381.78	0	362.53	0	110.34	8.63	1.65
25	20	75.6	110	415.8	6955.2	349.60	2116.8	106.40	8.62	1.75
26	0	0	98	370.44	0	392.41	0	119.43	8.63	1.81
27	20	75.6	104	393.12	6955.2	387.46	2116.8	117.92	8.61	1.79
28	20	75.6	109	412.02	6955.2	386.57	2116.8	117.65	8.61	1.79
29	0	0	98	370.44	0	429.96	0	130.86	8.63	1.85
30	40	151.2	122	461.16	13910.4	375.54	4233.6	114.30	8.62	1.88
31	0	0	110	415.8	0	416.51	0	126.76	8.64	1.94
32	0	0	98	370.44	0	467.51	0	142.29	8.62	1.97
33	20	75.6	108	408.24	6955.2	441.26	2116.8	134.30	8.61	1.94
34	0	0	99	374.22	0	481.37	0	146.51	8.61	1.97
35	40	151.2	122	461.16	13910.4	420.79	4233.6	128.07	8.63	1.94
36	0	0	118	446.04	0	435.05	0	132.41	8.62	1.94
37	0	0	112	423.36	0	458.36	0	139.50	8.62	1.96
38	0	0	109	412.02	0	470.97	0	143.34	8.61	1.97
39	0	0	107	404.46	0	479.78	0	146.02	8.63	1.99
40	0	0	103	389.34	0	498.41	0	151.69	8.62	1.99
41	0	0	98	370.44	0	523.84	0	159.43	8.61	2.02
42	0	0	94	355.32	0	546.13	0	166.21	8.63	2.03
43	20	75.6	106	400.68	6955.2	501.66	2116.8	152.68	8.61	2
44	0	0	111	419.58	0	479.06	0	145.80	8.61	2.01

Day	Added Volume (gal)	Added Volume (liter)	Total Volume (gal)	Total Volume (liter)	Added Calcium (mg)	Calcium (ppm)	Added Magnesium (mg)	Magnesium (ppm)	pH	LSI
45	0	0	95	359.1	0	559.75	0	170.36	8.6	2.07
46	40	151.2	122	461.16	13910.4	466.03	4233.6	141.84	8.6	1.99
47	0	0	110	415.8	0	516.87	0	157.31	8.62	2.05
48	0	0	87	328.86	0	653.52	0	198.90	8.6	2.13
49	40	151.2	114	430.92	13910.4	531.02	4233.6	161.61	8.6	2.04
50	0	0	108	408.24	0	560.52	0	170.59	8.6	2.07

Table C - 6 LSI computation for Test No. 6 (A2-105F-med FP)

Day	Added Volume (gal)	Added Volume (liter)	Total Volume (gal)	Total Volume (liter)	Added Calcium (mg)	Calcium (ppm)	Added Magnesium (mg)	Magnesium (ppm)	pH	LSI
1	0	0	113	427.14	0	48.76	0	18.50	8.94	0.81
2	0	0	101	381.78	0	54.55	0	20.69	8.78	0.7
3	0	0	93	351.54	0	59.25	0	22.47	8.66	0.61
4	30	113.4	114	430.92	6577.2	63.60	2494.8	24.12	8.63	0.62
5	0	0	104	393.12	0	69.71	0	26.44	8.65	0.68
6	0	0	90	340.2	0	80.56	0	30.56	8.62	0.71
7	30	113.4	111	419.58	6577.2	80.99	2494.8	30.72	8.61	0.7
8	0	0	99	374.22	0	90.81	0	34.44	8.61	0.75
9	0	0	89	336.42	0	101.01	0	38.31	8.6	0.79
10	30	113.4	109	412.02	6577.2	98.44	2494.8	37.34	8.6	0.94
11	0	0	98	370.44	0	109.49	0	41.53	8.6	1.11
12	70	264.6	160	604.8	15346.8	92.44	5821.2	35.06	8.69	1.17
13	0	0	153	578.34	0	96.67	0	36.67	8.65	1.1
14	0	0	144	544.32	0	102.71	0	38.96	8.61	0.96
15	0	0	139	525.42	0	106.40	0	40.36	8.62	1.03
16	0	0	138	521.64	0	107.17	0	40.65	8.61	1.02
17	0	0	125	472.5	0	118.32	0	44.88	8.63	1.09
18	0	0	114	430.92	0	129.74	0	49.21	8.63	1.13
19	10	37.8	119	449.82	2192.4	129.16	831.6	48.99	8.62	1.15
20	0	0	110	415.8	0	139.73	0	53.00	8.62	1.15
21	10	37.8	99	374.22	2192.4	161.11	831.6	61.11	8.63	1.22
22	30	113.4	120	453.6	6577.2	147.42	2494.8	55.92	8.62	1.25
23	0	0	109	412.02	0	162.29	0	61.56	8.62	1.29
24	0	0	95	359.1	0	186.21	0	70.63	8.61	1.34
25	30	113.4	121	457.38	6577.2	160.58	2494.8	60.91	8.62	1.35
26	0	0	110	415.8	0	176.64	0	67.00	8.63	1.34
27	0	0	99	374.22	0	196.26	0	74.44	8.61	1.37
28	30	113.4	117	442.26	6577.2	180.94	2494.8	68.63	8.6	1.32
29	0	0	107	404.46	0	197.85	0	75.05	8.6	1.38
30	0	0	97	366.66	0	218.25	0	82.78	8.6	1.43
31	30	113.4	117	442.26	6577.2	195.81	2494.8	74.27	8.61	1.39
32	0	0	107	404.46	0	214.11	0	81.21	8.6	1.42
33	30	113.4	126	476.28	6577.2	195.63	2494.8	74.21	8.6	1.46

Day	Added Volume (gal)	Added Volume (liter)	Total Volume (gal)	Total Volume (liter)	Added Calcium (mg)	Calcium (ppm)	Added Magnesium (mg)	Magnesium (ppm)	pH	LSI
34	0	0	115	434.7	0	214.35	0	81.30	8.6	1.42
35	0	0	105	396.9	0	234.76	0	89.05	8.6	1.46
36	30	113.4	123	464.94	6577.2	214.55	2494.8	81.38	8.6	1.44
37	0	0	113	427.14	0	233.54	0	88.58	8.6	1.48
38	0	0	107	404.46	0	246.64	0	93.55	8.62	1.53
39	0	0	96	362.88	0	274.90	0	104.27	8.62	1.57
40	30	113.4	116	438.48	6577.2	242.50	2494.8	91.98	8.61	1.51
41	0	0	105	396.9	0	267.90	0	101.62	8.6	1.54
42	0	0	91	343.98	0	309.12	0	117.25	8.61	1.61
43	40	151.2	127	480.06	8769.6	239.76	3326.4	90.94	8.61	1.56
44	0	0	117	442.26	0	260.26	0	98.72	8.61	1.6
45	0	0	110	415.8	0	276.82	0	105.00	8.61	1.63
46	0	0	101	381.78	0	301.49	0	114.36	8.61	1.66
47	30	113.4	119	449.82	6577.2	270.50	2494.8	102.61	8.61	1.62
48	0	0	112	423.36	0	287.41	0	109.02	8.61	1.64
49	0	0	110	415.8	0	292.64	0	111.00	8.61	1.65
50	0	0	101	381.78	0	318.71	0	120.89	8.61	1.67
51	30	113.4	119	449.82	6577.2	285.13	2494.8	108.15	8.61	1.64
52	0	0	110	415.8	0	308.45	0	117.00	8.61	1.67
53	0	0	103	389.34	0	329.42	0	124.95	8.61	1.7

Table C - 7 LSI computation for Test No. 7 (A1-105F-repeat)

Day	Added Volume (gal)	Added Volume (liter)	Total Volume (gal)	Total Volume (liter)	Added Calcium (mg)	Calcium (ppm)	Added Magnesium (mg)	Magnesium (ppm)	pH	LSI
1	0	0	127	480.06	0	55.00	0	23.00	9.38	1.38
2	0	0	115	434.7	0	60.74	0	25.40	9.31	1.35
3	30	113.4	134	506.52	6237	64.44	2608.2	26.95	9.3	1.36
4	30	113.4	125	472.5	6237	82.28	2608.2	34.41	9.38	1.55
5	0	0	115	434.7	0	89.43	0	37.40	9.34	1.55
6	30	113.4	129	487.62	6237	92.52	2608.2	38.69	9.24	1.46
7	0	0	115	434.7	0	103.78	0	43.40	9.33	1.6
8	0	0	106	400.68	0	112.59	0	47.08	9.34	1.9
9	30	113.4	126	476.28	6237	107.82	2608.2	45.09	9.38	1.92
10	0	0	112	423.36	0	121.29	0	50.72	9.31	1.9
11	30	113.4	129	487.62	6237	118.10	2608.2	49.39	9.3	1.88
12	0	0	118	446.04	0	129.11	0	53.99	9.33	1.94
13	0	0	102	385.56	0	149.36	0	62.46	9.32	2.0
14	0	0	95.5	360.99	0	159.53	0	66.71	9.38	2.09
15	0	0	89	336.42	0	171.18	0	71.58	9.35	2.09
16	40	151.2	122	461.16	8316	142.91	3477.6	59.76	9.31	2.19
17	0	0	109	412.02	0	159.95	0	66.89	9.34	2.27
18	0	0	97	366.66	0	179.74	0	75.16	9.32	2.3
19	40	151.2	114	430.92	8316	172.24	3477.6	72.03	9.43	2.39

Day	Added Volume (gal)	Added Volume (liter)	Total Volume (gal)	Total Volume (liter)	Added Calcium (mg)	Calcium (ppm)	Added Magnesium (mg)	Magnesium (ppm)	pH	LSI
21	40	151.2	121	457.38	8316	180.45	3477.6	75.46	9.38	2.36
22	0	0	116	438.48	0	188.23	0	78.72	9.31	2.31
23	0	0	100	378	0	218.35	0	91.31	9.34	2.4
24	30	113.4	110	415.8	6237	213.50	2608.2	89.28	9.32	2.57
25	0	0	102	385.56	0	230.25	0	96.28	9.36	2.64
26	40	151.2	120	453.6	8316	214.04	3477.6	89.51	9.34	2.59
27	0	0	103	389.34	0	249.37	0	104.28	9.35	2.66
28	0	0	89	336.42	0	288.60	0	120.69	9.42	2.8
29	0	0	80	302.4	0	321.06	0	134.26	9.39	2.81
30	60	226.8	126	476.28	12474	230.04	5216.4	96.20	9.32	2.6
31	0	0	117	442.26	0	247.74	0	103.60	9.36	2.67
32	0	0	103	389.34	0	281.41	0	117.68	9.33	2.7

Table C - 8 LSI computation for Test No. 8 (Tube-in-tube)

Day	Added Volume (gal)	Added Volume (liter)	Total Volume (gal)	Total Volume (liter)	Added Calcium (mg)	Calcium (ppm)	Added Magnesium (mg)	Magnesium (ppm)	pH	LSI
2	25	94.5	107	404.46	7843.5	112.48	3496.5	50.14	9.3	1.73
3	30	113.4	128	483.84	9412.2	113.48	4195.8	50.59	9.39	1.82
4	0	0	115	434.7	0	126.30	0	56.30	9.37	1.85
5	0	0	107	404.46	0	135.75	0	60.51	9.3	1.81
6	20	75.6	116	438.48	6274.8	139.53	2797.2	62.20	9.35	1.87
8	20	75.6	110	415.8	6274.8	162.23	2797.2	72.32	9.31	1.9
9	20	75.6	118	446.04	6274.8	165.30	2797.2	73.69	9.31	2
10	0	0	104	393.12	0	187.55	0	83.61	9.3	2.05
11	40	151.2	132	498.96	12549.6	172.92	5594.4	77.08	9.3	2.01
12	0	0	116	438.48	0	196.77	0	87.72	9.31	2.07
13	20	75.6	120	453.6	6274.8	204.04	2797.2	90.96	9.3	2.08
14	0	0	108	408.24	0	226.71	0	101.06	9.31	2.14
15	20	75.6	117	442.26	6274.8	223.46	2797.2	99.62	9.35	2.17
16	0	0	106	400.68	0	246.65	0	109.95	9.34	2.21
17	40	151.2	135	510.3	12549.6	218.26	5594.4	97.30	9.33	2.24
18	0	0	125	472.5	0	235.72	0	105.08	9.34	2.28
19	0	0	106	400.68	0	277.97	0	123.92	9.37	2.39
20	40	151.2	134	506.52	12549.6	244.66	5594.4	109.07	9.34	9.34
22	0	0	106	400.68	0	309.29	0	137.88	9.32	2.39
23	43	162.54	140	529.2	13490.82	259.67	6013.98	115.76	9.34	2.33
24	0	0	126	476.28	0	288.52	0	128.62	9.33	2.44
25	0	0	111	419.58	0	327.51	0	146.00	9.33	2.49
26	0	0	101	381.78	0	359.94	0	160.46	9.37	2.57
27	35	132.3	119	449.82	10980.9	329.91	4895.1	147.07	9.37	2.54
28	0	0	112	423.36	0	350.53	0	156.26	9.38	2.57

Day	Added Volume (gal)	Added Volume (liter)	Total Volume (gal)	Total Volume (liter)	Added Calcium (mg)	Calcium (ppm)	Added Magnesium (mg)	Magnesium (ppm)	pH	LSI
30	40	151.2	116	438.48	12549.6	367.06	5594.4	163.63	9.37	2.58
31	0	0	104	393.12	0	409.41	0	182.51	9.31	2.57
32	0	0	88	332.64	0	483.85	0	215.69	9.37	2.72
33	40	151.2	114	430.92	12549.6	402.62	5594.4	179.48	9.38	2.65
34	30	113.4	126	476.28	9412.2	384.04	4195.8	171.20	9.38	2.63
35	0	0	109	412.02	0	443.94	0	197.90	9.37	2.68
37	40	151.2	125	472.5	12549.6	413.67	5594.4	184.41	9.38	2.66
38	0	0	118	446.04	0	438.21	0	195.35	9.37	2.67
39	0	0	103	389.34	0	502.03	0	223.80		
40	40	151.2	131	495.18	12549.6	420.07	5594.4	187.26	9.3	2.58
41	0	0	115	434.7	0	478.51	0	213.31	9.3	2.63
43	30	113.4	119	449.82	9412.2	483.35	4195.8	215.47	9.33	2.67
44	0	0	102	385.56	0	563.91	0	251.38	9.39	3.03
45	40	151.2	135	510.3	12549.6	450.66	5594.4	200.90	9.39	2.93
46	0	0	119	449.82	0	511.25	0	227.91	9.35	2.95
47	0	0	102	385.56	0	596.46	0	265.89	9.34	3
48	40	151.2	130	491.4	12549.6	493.53	5594.4	220.01	9.31	2.89
50	0	0	97	366.66	0	661.43	0	294.86	9.34	3.05
51	40	151.2	128	483.84	12549.6	527.18	5594.4	235.01	9.39	3
52	0	0	115	434.7	0	586.77	0	261.57	9.38	3.04
53	40	151.2	140	529.2	12549.6	505.71	5594.4	225.44	9.3	2.89
54	0	0	125	472.5	0	566.39	0	252.49	9.31	2.99
55	0	0	114	430.92	0	621.04	0	276.85	9.39	3.11
56	40	151.2	127	480.06	12549.6	583.61	5594.4	260.17	9.4	3.09
58	0	0	105	396.9	0	705.90	0	314.68	9.34	3.12
59	0	0	91	343.98	0	814.49	0	363.09	9.31	3.18

VITA

Xiaoxiao Wu

Candidate for the Degree of

Master of Science

Thesis: EXPERIMENTAL AND THEORETICAL STUDY OF WATER SIDE
FOULING THERMAL PERFORMANCE OF REFRIGERANT TO WATER CONDENSERS

Major Field: Mechanical and Aerospace Engineering

Biographical: From the city of Changchun, China; daughter of Yi Wu and Xiaojuan Li

Education:

Completed the requirements for the Master of Science in Mechanical & Aerospace Engineering at Oklahoma State University, Stillwater, Oklahoma in December, 2013

Completed the requirements for the Master of Engineering in Heating, Ventilation & Air Conditioning at Donghua University, Shanghai, China in March, 2010

Completed the requirements for the Bachelor of Sciences in Heating, Ventilation & Air Conditioning at Donghua University, Shanghai, China in July, 2007

Experience:

- Worked in Mechanical & Aerospace Engineering department at Oklahoma State University as a graduate research assistant and teaching assistant
- Worked in Environmental Science & Engineering department at Donghua University as graduate research assistant and counseling assistant
- Worked in Shanghai Research Institute of Building Science as engineering intern

Professional Memberships:

- American Society of Heating, Refrigeration and Air-conditioning (ASHRAE) student member